

AN ABSTRACT OF THE THESIS OF

Jennifer DiGiulio for the degree of Master of Science in Geology presented on November 19, 2015

Title: Reconstructing the Physical Record of a Four-Million-Year Volcanic System: Geochemistry, Thermobarometry, and Geologic Map of the Mount Jefferson Area, Oregon

Abstract approved:

Adam J.R. Kent

Volcanic and sedimentary deposits of the Mount Jefferson area (MJA) record a four-million-year history of arc-related volcanism related to the subduction of the Juan de Fuca plate beneath North America. 171 mapped stratigraphic units over an area of 150 km² reveal four periods of volcanic activity resulting in diverse composition lavas ranging from ~48 to 72 wt% SiO₂. Eruptive periods are divided into (1) ~4.0 – 0.78 Ma; (2) 0.78 – 0.3 Ma; (3) 0.3 – 0.02 Ma; and (4) eruptions of the past 13,000 years. Repeated glaciations over the past 800,000 years have sculpted the landscape of the MJA and include the Pleistocene glaciations of Jack Creek (early Wisconsin) and Cabot Creek (late Wisconsin), and the Holocene glaciation of Jefferson Park. Anomalously glassy lava flows, columnar jointing, and streamlined shapes are lithologic evidence of intraglacial eruptions in numerous units, including the andesite of Whitewater Creek (*Qawc*), andesite and dacite of Park Butte (*Qapb*; *Qdpb*), and the basaltic andesite of Whiskey Creek (*Qbawh*).

Mineral compositions and textures are highly variable among the four units. Patchy to oscillatory zoning in plagioclase and dissolution cores and partially resorbed rims in amphiboles indicate pervasive disequilibrium conditions. Feldspar ($\sim\text{An}_{35-98}$) and amphibole ($\sim 1.1-1.5 \text{ IVAl}$) compositions are relatively continuous across a broad range, and pyroxene compositions are typically $\sim\text{En}_{42-49}$ and En_{65-74} .

Phenocryst assemblages of units *Qawc*, *Qapb*, *Qdpb*, and *Qbawh* were probed to assess pressure and temperature conditions of pre-eruptive magmas in the MJA. Estimates from amphiboles, feldspars, and pyroxenes indicate temperatures ranging from ~ 650 to $1100 \text{ }^\circ\text{C}$. Pressure estimates indicate crystallization depths of ~ 3 to 25 km , with the majority of crystallization occurring between ~ 15 and 25 km . Pyroxene temperatures (Putirka model) are always the highest, ($\sim 950-1150 \text{ }^\circ\text{C}$) and plagioclase-amphibole pair (HBAS model) temperatures are the lowest ($\sim 650-875 \text{ }^\circ\text{C}$), with amphibole temperatures (Ridolfi model) falling in between those ranges. Calculated partition coefficients of Sr and Ba from this study range from 1.5 to 6.75 and 0.12 to 1.00 , respectively, in close agreement with calculated partition coefficients of Bindeman et al. (1998) and Dohmen and Blundy (2014). Reconstructed Sr concentrations range from 227 to $799 \text{ } \mu\text{g/g}$, which is inconsistent with the melting of a Sr-rich andesite end-member produced at $30-40 \text{ km}$ depth as proposed by Conrey et al. (2001). The diverse spread of data reported here suggests complex petrologic mixing processes predominantly occurring in the mid- to upper crust beneath the MJA and contributes to the understanding of pre-eruptive magmatic conditions in the Cascade volcanic arc.

© Copyright by Jennifer DiGiulio
November 19, 2015
All Rights Reserved

Reconstructing the Physical Record of a Four-Million-Year Volcanic System: Geochemistry,
Thermobarometry, and Geologic Map of the Mount Jefferson Area, Oregon

by
Jennifer DiGiulio

A THESIS

Submitted to

Oregon State University

in partial fulfillment of
the requirements for the
degree of

Master of Science

Presented November 19, 2015
Commencement June 2016

Master of Science thesis of Jennifer DiGiulio presented on November 19, 2015

APPROVED:

Major Professor, representing Geology

Dean of the College of Earth, Ocean, and Atmospheric Sciences

Dean of the Graduate School

I understand that my thesis will become part of the permanent collection of Oregon State University libraries. My signature below authorizes release of my thesis to any reader upon request.

Jennifer DiGiulio, Author

ACKNOWLEDGMENTS

Though each and every person experiences a unique set of personal and professional challenges as a graduate student, I believe there is one thing we can all agree on whole-heartedly, and that is that we did not do it alone. There are so many people I would like to thank for making my time here at Oregon State University a success. First and foremost, I would like to profoundly thank my advisor and mentor, Dr. Adam Kent. It has been almost exactly a year since Adam welcomed me into his research group and the guidance he has provided me in that time has been invaluable. He is a bottomless well of geochemical knowledge and his encouragement has been a constant source of strength to me in both my thesis- and career-related goals.

I would next like to thank Dr. David Sherrod of the U.S. Geological Survey. Though Dave knew little about me as a scientist or person, he promptly agreed to collaborate with me in construction of a geologic map and accompanying paper of the Mount Jefferson area, what I now realize to be a several-year commitment. The vast amount of geologic knowledge I have gained through working with Dave cannot be easily expressed in this short acknowledgment. It also goes without saying that none of the work completed here would have been possible without Dr. Richard Conrey, the scientist who completed the 171-unit geologic map and detailed geochemical investigation of Mount Jefferson on which this study is based. Rick has been constantly supportive of my work on Mount Jefferson and freely provides me any materials I may need from geochemical analyses to driving directions. Dr. Anita Grunder has also been incredibly supportive of me over this past year, lending her advice generously in all matters of graduate student life. Thank you also Dr. Frank Tepley for serving on my committee and entrusting me with the honored task of electron microprobe technician my first summer at OSU. Never again will I take for granted a well-calibrated analysis or precisely carbon-coated thin

section. Thank you also Dale Burns, for spending nearly 9 months training me on the electron microprobe and imparting general nuggets of wisdom upon me when I least expected it. Also many thanks to Dr. Michael Olsen, my graduate council representative. Mike went above and beyond the duties of any GCR. Finally, thank you Roger Nielsen for sparking my interest in Mount Jefferson and guiding the early stages of this project.

I deeply thank the organizations that provided me funding to complete my work including Oregon State University, the Geological Society of America, and Mazamas Mountaineering. Hearty thanks to Lori Hartline, Robert Allan, and the CEOAS staff for the seemingly never-ending stream of mirth and produce. An especial thank you to Melinda Jensen for the dozens of times I borrowed her keys after locking mine in my office. I would like to impart a particularly molten thank you to the entire VIPER research group for the intellectually stimulating weekly discussions, strong sense of community, stylish snake patches, and *Volcano Zombies* movie nights. Thank you to the Oregon State Cartography and Geovisualization Group, Kuuipo Walsh, and Mike Sepp for your assistance and your patience while I was learning the powerful, but frustrating, ArcGIS.

Thank you also Matt Loewen, my Mount Jefferson field sherpa, and my fearless field assistants Carlie Duda, Danny Azzopardi, and Allan Lerner. My time here would not have been complete without Jacob Petersen-Perlman, Kyle Krawl, Beth Rutila, and Jessie Peirson, who transformed a windowless office into a place of laughter and learning. I am also grateful to my roommates, Rachel Boren and Liz King, who are always ready with some outrageous story to brighten my day. I honestly would not have made it through these past few months without the special nights we spent laughing together.

I attribute a great deal of my success in the unshakable friendships I have formed since living in Corvallis. The adventures I've had with these friends have been hilarious and heart-warming, and truly built on a foundation of love. You know who you are, and I sincerely thank you.

I also want to thank Vaclav Kuna, who came into my life just in the nick of the time, providing a shoulder to lean on, a confidant to laugh with, and a home-cooked dinner almost every night in the weeks leading up to my defense.

A HUGE thank you to my loving family, who have always provided me with unconditional support and encouragement to follow my dreams (even when it means moving 1,000 miles away). You hold me up.

And finally, thank you Julie Kurtz! For your exceptional patience through this whole thesis-submittal process.

CONTRIBUTION OF AUTHORS

Adam Kent's participation in this project was unconditional. In his mentorship he offered insight, focused the project, and sparked ideas. He also provided thorough (and speedy!) review of Chapters 1-4 several times over. David Sherrod was also a major contributor to this project. His discussions were an inspiration for much of the content and several of the figures in this thesis. He compiled the regional geochemistry and ages, completed additional geologic mapping in the summer of 2015, and accomplished countless other tasks related to this project. He also played a significant role in the reviewing and editing of Chapter 2. Richard Conrey completed the geologic mapping of the Mount Jefferson area between 1983 and 1990. He has allowed me access to all data associated with his initial study and is now involved in the publication of the Mount Jefferson area map and accompanying pamphlet. Rick additionally analyzed the majority of geochemical analyses in the Mount Jefferson area at the Geoanalytical Laboratory at WSU. Anita Grunder added extremely valuable insight and interpretation with respect to mineral data, thermobarometric methods, and interpretation of Chapter 3 results. Frank Tepley helped acquire much of the electron microprobe data presented in Chapter 4. His discussions were also valuable.

TABLE OF CONTENTS

	<u>Page</u>
1 GENERAL INTRODUCTION.....	1
1.1 Argument.....	1
1.2 Tectonic context of the Mount Jefferson area	3
1.3 The Mount Jefferson area.....	5
1.4 Organization	5
2 GEOLOGIC MAP OF THE MOUNT JEFFERSON AREA	7
2.1 Introduction	7
2.1.1 Physiography and Access.....	8
2.1.2 Methods.....	9
2.1.3 Geologic and Tectonic Setting.....	11
2.2 Eruptive History of the Mount Jefferson Area	13
2.2.1 Rocks emplaced between 4.0 and 0.78 Ma	18
2.2.2 Rocks emplaced between~0.78 and 0.3 Ma.....	20
2.2.3 Rocks emplaced between 0.3 and 0.02 Ma: Construction of Mount Jefferson volcano and scattered along-arc volcanism to north and south	22
2.2.4 Eruptions of the past 13,000 years (Holocene)	28
2.3 Glacial History.....	29
2.3.1 Cabot Creek Glaciation, Late Wisconsin.....	30
2.3.2 Jack Creek Glaciation, Early Wisconsin.....	31
2.3.3 Jefferson Park Advance, Holocene	32
2.4 Evidence of Ice-Magma Interactions.....	32
2.5 Summary.....	37
3 MAGMATIC EVOLUTION OF A FOUR MILLION YEAR VOLCANIC SYSTEM: GEO THERMOMETRY, GEOBAROMETRY, AND RECONSTRUCTIONS OF EQUILIBRIUM COMPOSITION MAGMAS IN THE MOUNT JEFFERSON AREA	38
3.1 Introduction	38
3.2 Study Area	43
3.3 Summary of Geologic Units	45
3.3.1 Andesite of Whitewater Creek.....	45

TABLE OF CONTENTS (Continued)

	<u>Page</u>
3.3.2 Andesite of Park Butte	46
3.3.3 Basaltic andesite of Whiskey Creek.....	50
3.4 Methods	51
3.4.1 Field Work and Sample Selection:.....	51
3.4.2 Analytical Approach:	52
3.5 Petrography.....	57
3.5.1 Andesite of Whitewater Creek.....	57
3.5.2 Andesite of Park Butte	62
3.5.3 Basaltic Andesite of Whiskey Creek.....	64
3.6 Geochemistry.....	65
3.6.1 Andesite of Whitewater Creek.....	65
3.6.2 Andesite of Park Butte	65
3.6.3 Basaltic Andesite of Whiskey Creek.....	66
3.7 Thermobarometry	73
3.8 Plagioclase-Melt Partitioning Model.....	82
3.9 Discussion.....	89
3.9.1 Thermobarometric Considerations.....	89
3.9.2 Reconstructed Melt Composition Considerations.....	95
3.9.1 Synthesis: Model for Diversity of MJA Magma Compositions.....	99
3.10 Conclusion.....	102
4 GENERAL CONCLUSION	104
REFERENCES	106
DIGITAL APPENDICES	

LIST OF FIGURES

<u>Figure</u>	<u>Page</u>
Figure 1.1. Index map showing geographic locations, physiographic provinces and subdivisions, and some faults and lithologic units mentions in text.	4
Figure 2.1. Geographic location of the Mount Jefferson area (MJA).	9
Figure 2.2. Silica variation diagram of MJA.	14
Figure 2.3. Generalized geologic map of MJA, divided into four main phases of volcanism.	15
Figure 2.4. Andesite of Skyline Trail (Qdst) spires exposed in Cathedral Rocks.	22
Figure 2.5. Middle member of the dacite of Whitewater Glacier (Qdw2) photographed looking south from Jefferson Park.	26
Figure 2.6. Andesite of Whitewater Creek (Qawc).	28
Figure 2.7. Andesite of Goat Peak (Qagp), a plagioclase-rich cinder cone remnant eroded by glaciation.	34
Figure 2.8. North (Qant), Middle (Qamt), and South (Qast) Tables photographed looking south from Goat Peak.	36
Figure 3.1. Generalized schematic of magma production.	39
Figure 3.2. Model crustal cross section beneath MJA.	42
Figure 3.3. Study area.	44
Figure 3.4. Photographs of andesite of Whitewater Creek (Qawc).	46
Figure 3.5. Jefferson Park and Mount Jefferson volcano photographed looking south from Park Butte. Incised drainage at center of shot is Russell Creek.	48
Figure 3.6. Typical of Park Butte andesite (Qapb, a) and atypical inclusions (b-d) collected from drainage of off Pacific Crest Scenic Trail.	49
Figure 3.7. Dacite of Park Butte (Qdpb) outcrop (left) and amphibole-rich phenocryst assemblage (right).	49
Figure 3.8. Basaltic andesite of Whiskey Creek (Qbawh) lava dome.	51
Figure 3.9. Photomicrographs of MJA thin-sections.	61
Figure 3.10. Total alkali silica (TAS) diagram.	67
Figure 3.11. Major element variation diagrams from representative units in the MJA.	68
Figure 3.12. Trace element variation diagrams for representative units.	70
Figure 3.13. Compositions of MJA feldspars.	72

LIST OF FIGURES (Continued)

<u>Figure</u>	<u>Page</u>
Figure 3.14. Compositions of MJA pyroxenes.	72
Figure 3.15. Compositions of MJA amphiboles.	73
Figure 3.16. All crystallization pressures and temperatures of Mount Jefferson amphibole data.	75
Figure 3.17. Pressure vs temperature as calculated using plagioclase-amphibole pairs.	76
Figure 3.18. Backscattered electron images of selected plagioclase-amphibole pairs.....	77
Figure 3.19. Pressure and temperature solutions calculated from Ridolfi et al. (2010) plotted against solutions calculated from Holland and Blundy (1994) and Anderson and Smith (1995). .	78
Figure 3.20. Temperature solutions calculated from the Ridolfi and HBAS models plotted against solutions calculated from Putirka (2008).....	79
Figure 3.21. Backscattered electron images of selected 2-pyroxene pairs.....	80
Figure 3.22. Pressure vs temperature as calculated using two-pyroxene pairs. Holland and Blundy and Ridolfi fields as shown.	81
Figure 3.23. Mount Jefferson thermometry data for individual mineral systems. Each spot represents a single electron probe analysis.....	82
Figure 3.24. Measured trace element contents of Sr and Ba in the host feldspar phase ([Sr], [Ba]) for units Qawc, Qapb, Qdpb, and Qbawh.	86
Figure 3.25. Calculated trace element contents of Sr and Ba in the primary melt ([Sr] _{melt} , [Ba] _{melt}) in units Qawc, Qapb, Qdpb, and Qbawh.	87
Figure 3.26. [Sr] _{melt} versus [Sr/Ba] _{melt} for units Qawc, Qapb, Qdpb, and Qbawh.....	88
Figure 3.27. Calculated partition coefficients ($D_{\text{calculated}}$) versus measured partition coefficients (D_{measured})	112
Figure 3.28. [Sr/Ba] _{melt} versus temperature in kelvin. Notes that higher [Sr/Ba] _{melt} values tend to associate with lower temperatures.....	113
Figure 3.29. Temperature (K) versus anorthite content (XAn).	114
Figure 3.30. Sr concentrations in units Qawc, Qapb, Qdpb, and Qbawh.....	116
Figure 3.31. Synthesize depth model.....	117

LIST OF TABLES

<u>Table</u>	<u>Page</u>
Table 2.1. K-Ar and $^{40}\text{Ar}/^{39}\text{Ar}$ ages for units across the MJA.	16
Table 2.2. Types of analysis completed on each sample in the MJA.	57
Table 3.1. Mount Jefferson samples used in this study.	83
Table 3.2. Calculated plagioclase-melt partition coefficients.....	84

LIST OF DIGITAL APPENDICES

Digital Appendix I. Sampling locations and rock descriptions	
Digital Appendix II. Instrument parameters and standards of LA-ICP-MS	
Digital Appendix III. Instrument parameters and standards of EMP	
Digital Appendix IV. Petrographic descriptions of units Qawc, Qapb, Qdpb, and Qbawh	
Digital Appendix V. Whole rock major and trace element geochemistry of representative units	
Digital Appendix VI. EMP major element geochemistry of representative units	
Digital Appendix VII. LA-ICP-MS trace element concentration data of representative units.....	
Digital Appendix VIII. Summary thermobarometry table: Ridolfi, HBAS, and Putirka estimates ..	
Digital Appendix IX. Summary melt reconstruction parameters and estimates.....	

1 GENERAL INTRODUCTION

1.1 Argument

Volcanic systems represent some of the most dynamic environments on earth. Significant hazards to human life and infrastructure are associated with volcanic systems (Blong, 1996; Myers et al., 1997; Tilling, 1989). In addition, volcanism and the underlying magma plumbing system play an important role in crustal differentiation and ore deposit formation; (Hildreth and Moorbath, 1988). Although numerous hazards are associated with active and dormant volcanoes (e.g., lahars, debris avalanches), a wide a range of hazardous events are specifically associated with eruption (e.g., lava flows, pyroclastic flows, tephra fall, acid rain). Determining the likelihood of a given event for a specific volcanic system and estimating possible timing of future events is a primary goal of volcanology. An important aspect of this is gaining and understanding of the processes that result in production of magmas, and the nature of subvolcanic magma storage. Specifically, whether an eruption results in highly destructive pyroclastic explosions or low-impact effusive discharges depends greatly on magma composition and the physical conditions of the pre-eruptive magmatic reservoir (Hildreth, 1981; Marsh, 1981; Hildreth and Moorbath, 1988; Hildreth, 2004; Bachmann and Bergantz, 2008).

There are several approaches for gauging the physical conditions of magmatic reservoirs, which vary based on eruptive style. For example, intrusive magmatic reservoirs, called plutons, are the physical fossil specimens of a magmatic system and, when exposed, their mineral assemblages, radiometric ages, and textures provide a time-integrated, spatial perspective into the long-term processes of crustal magmatism. However, intact plutons are rarely exposed at the earth's surface, instead residing tens of kilometers within the earth's crust or as exposures in

deeply eroded mountains. Plutonic rocks also experience a long period of subsolidus cooling which may mask critical chemical and textural features. As a result, and because the long-term processes shaping intrusive magmatic systems can rarely be observed directly, studies of volcanic rocks are also particularly important. Once erupted, volcanic mixtures of crystals and liquid cool rapidly, preserving and providing a snapshot of magma reservoir conditions leading up to the time of a given eruption (Bachmann and Bergantz, 2008).

Understanding magma reservoir conditions is particularly important in long-lived magmatic systems (Walker et al., 2007; Grunder et al., 2008), where repeated injections of mafic magma rejuvenate the magmatic reservoir and drive the evolution of magma. In many cases, our understanding of rejuvenation is based on large-volume centers like Yellowstone (Girard and Stix, 2009; Watts et al., 2012), Toba (Vazquez and Reid, 2004), or Fish Canyon Tuff (Bachmann et al., 2002) in which the injected magma affects only a portion of the large-volume intrusive body, and only localized evidence of rejuvenation is preserved (Paterson, 2009; Memeti et al., 2010). In other cases, our understanding is based on studies of smaller volcanic systems like Mount Hood (Darr, 2006; Kent et al., 2010, Cooper and Kent, 2014) or Mount Lassen (Klemetti and Clynne, 2014), where the evidence of rejuvenation is more inclusive and often manifests itself as homogeneously or heterogeneously mixed magmas of intermediate composition (Anderson, 1976; Eichelberger, 1978; Reubi and Blundy, 2009).

In both types of systems, the degree of heterogeneity of erupted magmas, and also the nature of individual eruptions themselves, is dependent upon several physical factors including compositions of the injected magma and crustal reservoir, depth at which injection takes place, and the pressure and temperature of the magma immediately preceding eruption (Marsh, 1981). Observation of crystal chemistry, estimation of intensive parameters, and calculation of melt

compositions can improve our understanding of pre-eruptive magmatic conditions and provide perspective on the evolution and organization of long-lived volcanic systems.

1.2 Tectonic context of the Mount Jefferson area

The Mount Jefferson area (MJA) is situated at 44°40' N along the axis of the Cascade Range in central Oregon. Subduction magmatism along the west coast of North America has been ongoing nearly continuously since the middle Eocene (Silver, 1971; Couch and Riddihough, 1989). Between 5 and 45 Ma, plutons of the Western Cascades subprovince were emplaced at the latitude of the MJA (Verplanck and Duncan, 1987). To the east resides the active volcanic arc, called the High Cascades subprovince (Peck et al., 1964; Lux, 1982; Verplanck and Duncan, 1987; Walker and Duncan, 1988; Priest et al., 1983; Sherrod and Smith, 2000; **fig. 1.1**). Around 4-5 Ma, subsidence and erosion associated with rifting began in the central Oregon volcanic arc, leading to a structural feature called the High Cascades graben beginning around the latitude of Three Sisters and terminating slightly south of Mount Jefferson (Smith and Taylor, 1983; Smith, 1986; Smith et al., 1989a; Conrey et al., 2004; Sherrod et al., 2004). Back-arc processes are also influenced the Basin and Range extensional province, whose northwestern margin diffusely terminates just southeast of the MJA (Trench et al., 2012).

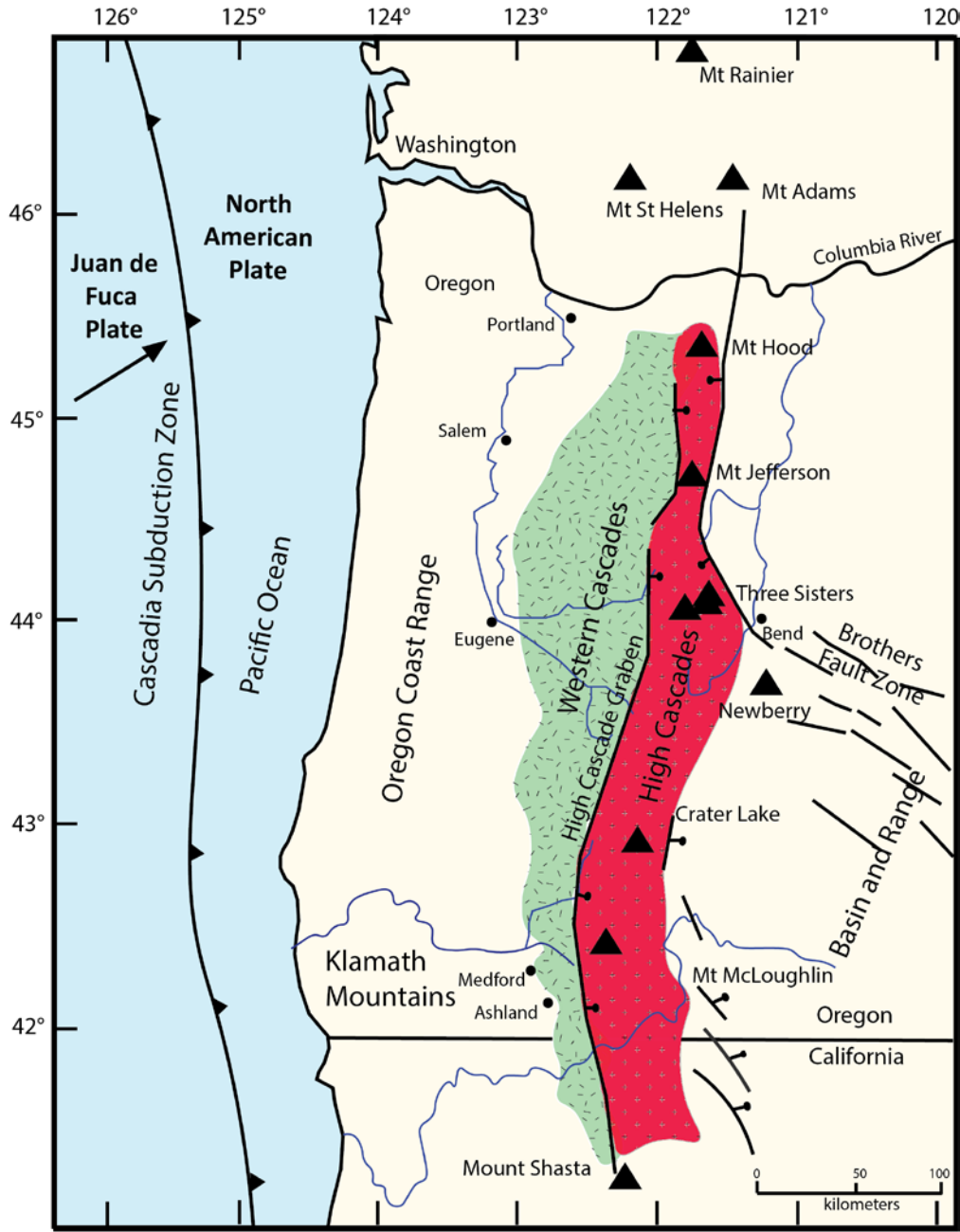


Figure 1.1. Index map showing geographic locations, physiographic subprovinces, and some faults and lithologic units mentions in text. Approximate extent of Western and High Cascades shown for Oregon and northern California. High Cascades. High Cascades graben, Cascadia subduction zone, and Juan de Fuca plate (JdF) also shown. Modified from Sherrod and Smith (2000).

1.3 The Mount Jefferson area

Deposits of the MJA consist of basaltic andesite to rhyodacite lava flows, scoria cones, pyroclastic flows, and near-vent tuff breccias clustered over an area of 150 km². Dozens of mapped volcanic deposits occur, with an eruptive history spanning the last 4 million years. Four main phases of MJA volcanism are identified herein based on the work of Conrey (1991): 1) rocks emplaced between 4.0 and 0.78 Ma, 2) 0.78 and 0.3 Ma, 3) 0.3 and 0.02 Ma, and 4) eruptions of the past 13,000 years. The majority of the MJA eruptive history is characterized by widespread, mafic eruption, transitioning to more focused intermediate and silicic eruptive products in only the past 300,000 years (Conrey, 1991). Consequently, basaltic andesite and basaltic composition rocks tend to belong to older eruptive sequences buried at the periphery of the volcanic field, and andesite and dacite typically form the central stratocone. Scott (1977) identified the moraines of three major glaciations in the MJA in the past 800,000 years: the Jack Creek (early Wisconsin), Cabot Creek (late Wisconsin), and Jefferson Park (Holocene) glaciations, and evidence of intraglacial eruptions is abundant. The detailed history of the MJA is discussed in Chapter 2.

1.4 Organization

The second chapter of this thesis describes a broad overview of the volcanic and glacial history of the Mount Jefferson area. It is a preliminary version of text incorporated into the explanatory pamphlet for a geologic map currently undergoing technical review at the USGS. Digitization and attribution of the Mount Jefferson area map has also been part of the work completed towards this thesis. The chemistry, spatial distribution, and ages (absolute and relative) of 171 units are investigated to examine the temporal evolution of the MJA. Several examples of ice-magma interactions and an in-depth discussion of the tectonic setting of the

MJA are also included in Chapter 2. The third chapter explores the structure of the magmatic system beneath Mount Jefferson using an array of petrological geothermobarometers to constrain the temperature and depth at which phenocryst phases in the MJA were crystallizing. These data provide 1) estimates of pre-eruptive conditions of magma crystallization and storage from the MJA and 2) a framework on which to build a petrologic model of the magmatic system beneath the MJA. The fourth chapter summarizes the general conclusions of this thesis and provides recommendations for future work.

2 GEOLOGIC MAP OF THE MOUNT JEFFERSON AREA

2.1 Introduction

The Mount Jefferson area (MJA) is located along the axis of the Cascade Range in central Oregon. Prominent is Mount Jefferson itself, a composite volcano with a summit rising 3,199 m (10,497 ft) above the surrounding landscape. The map area includes a surrounding 150 km² of lava flows, domes, shield volcanoes, and scoria cones. To the north lies Mount Hood; to the south, the Three Sisters and Crater Lake, other major volcanic centers of the Oregon Cascade Range. Unlike Mount Hood, whose eruptive products display little geochemical variation (58–66 weight percent SiO₂; Kent et al., 2010), the lava of Mount Jefferson is diverse, with compositions ranging from basalt to rhyolite (48–72 percent SiO₂, Conrey, 1991).

Rocks and deposits in the map area record a four-million-year history of volcanic and glacial activity. But Mount Jefferson volcano achieved its present stratocone form only in the past 300,000 years (Conrey, 1991). Summit eruptions, including some whose ash fallout are reported from as far away as central Idaho, have been lacking since before the last glacial maximum about 15,000 years ago. In the map area but beyond the limit of Mount Jefferson, the most recent eruption was about 1,000 years ago, when basalt scoria and lava issued from a vent on the south flank of South Cinder Peak (Scott, 1977).

Several lava flows and domes in the map area display evidence of volcano-ice interaction owing to extrusion during at least two major glaciations. Presently, the glacially scoured slopes of the volcano boast five glaciers, the largest of which blankets nearly the entire upper east flank of the volcano. Despite its lengthy quiescence, Mount Jefferson is regarded as potentially active on the basis of history at similar Cascade Range volcanoes (Walder et al., 1999).

2.1.1 Physiography and Access

The Mount Jefferson area is located at the junction of Marion, Wasco, and Jefferson Counties (**fig. 2.1**). The entire map area is in forested land under the jurisdiction of the Mount Hood, Deschutes, and Willamette National Forests. Most of the area is roadless, and about one-half lies within the Mount Jefferson Wilderness. Backcountry access throughout the area is simplified by a well-maintained trail system, including the Pacific Crest National Scenic Trail. Several trailheads provide access from graveled forest roads on nearly all sides of the area. The northeastern part of the map area lies within the Warm Springs Indian Reservation, where a permit must be obtained for access. The field season varies depending on annual snowpack, but trails are typically snow free from June to October.

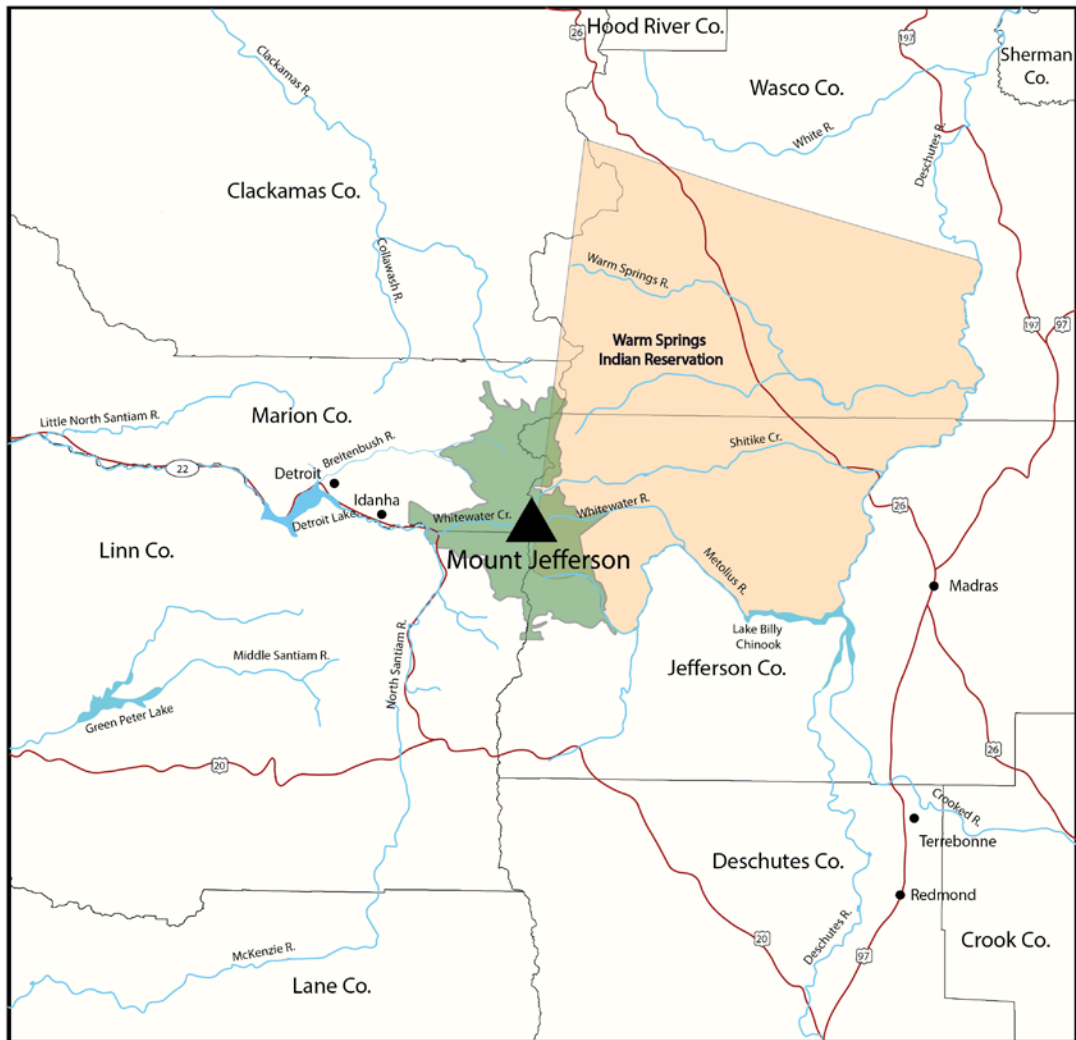


Figure 2.1. Geographic location of the Mount Jefferson area (MJA), shown in green. Major highways are shown in red, rivers in blue, and county lines in black. Warm Springs Indian Reservation denoted in orange.

2.1.2 Methods

Detailed geologic mapping of 171 volcanic, sedimentary, and glacial units was completed during the field seasons of 1983–90 by Conrey (1991) with the goal of deciphering the volcanic and glacial history of the Mount Jefferson area. Stratigraphic units were distinguished in the field by lithologic aspect, chiefly phenocryst abundance and estimated silica content in hand sample.

The rock compositional assignments are substantiated by 867 whole-rock chemical analyses (Conrey, 1991).

Absolute ages for the map units are known from 48 K-Ar and $^{40}\text{Ar}/^{39}\text{Ar}$ ages. A fuller description of sources and methodology is compiled in **digital appendix I**. Analytical error is reported as two-sigma (2σ), which has become the standard in recent years. Readers comparing previously published ages should be aware of the consequent doubling of our reported analytical error as we convert from 1σ to 2σ . For undated units, relative ages are estimated on the basis of morphology, weathering characteristics, and magnetic polarity (Scott, 1977; Conrey, 1991). Ages for the three Holocene eruptions in the map area are based on a report that used tephrostratigraphy and averaged sedimentation rates from lake cores to establish approximate absolute ages (Scott, 1977).

Magnetic polarity, normal or reversed, was determined at many sites using a portable fluxgate magnetometer (Conrey, 1991). In most places, capping strata are younger than 0.78 Ma and possess normal-polarity magnetization, characteristic of rocks emplaced in the Brunhes Normal-Polarity Chron (time since 0.78 Ma). The first magnetic reversal found when sampling downsection is presumed to correspond to volcanic rocks emplaced in the Matuyama Reversed-Polarity Chron—older than 0.78 Ma. This age-polarity aspect was substantiated in the map area by radiometric dating and forms the basis for age assignments of several undated units (Conrey, 1991).

Geologic mapping was undertaken at 1:24,000 scale, then compiled at 1:62,500 scale (map plate in Conrey, 1991). For our planned publication version (1:40,000), the legacy map was scanned, georeferenced, and digitized using ArcGIS 10.2.2. Line-node density is suitable for

presentation at 1:24,000 scale because many GIS users will choose to display the map on modern topographic map base.

In a few instances, similar or identical geographic place names may cause confusion. For example, Whitewater Creek drains the northwest flank of Mount Jefferson, whereas Whitewater River drains the northeast flank (**fig. 2.1**). The name Milk Creek is applied to streams on the west and east flanks.

2.1.3 Geologic and Tectonic Setting

The Cascade Range is a 1,200-km long volcanic arc resulting from N. 50° E. oblique subduction of the Juan de Fuca plate beneath North America (Silver, 1971; Couch and Riddihough, 1989). The volcanic front is thought to have migrated eastward through time (Peck et al., 1964; Priest, 1990; Wells, 2014).

The present-day crest of the central Oregon Cascades is situated approximately 250–300 km east of the forearc trench (**fig. 1.1**). The range-crest volcanoes from Mount Jefferson to the Three Sisters lie atop 44-km-thick accreted crust (Leaver et al., 1984; Hildreth et al., 2012) that likely ranges in age from Late Mesozoic to Eocene, the youngest part of which includes oceanic plateau lava and forearc sediment of the Siletz terrane (Wells et al., 1984; Wells, 2014). The subducting slab pitches from 10° to 15° beneath the forearc (Trehu et al., 1994) and as steep as 60°–80° beneath the arc front (Rasmussen and Humphreys, 1988). Though seemingly aseismic (the last large earthquake was 1700 C.E.; for example, Atwater et al., 2005), the subduction zone is now known to have frequent seismic tremor associated with episodic transient slip. Deformation studies (West and McCrumb, 1988; Kelsey, 1990; Mitchell et al., 1994) have long recognized ongoing uplift of the Coast Range, another indication of a dynamic subduction zone.

Sometime between about 8 and 5 Ma, uplift and erosion in the western part of the range throughout Oregon led to a moderately incised terrain, what was described as the Western Cascades subprovince of the Cascade Range by Dicken (1965). At the latitude of the map area, the Western Cascades encompasses deeply dissected volcanic strata ranging in age from ~45 to 5 Ma (Peck et al., 1964; Lux, 1982; Verplanck and Duncan, 1987; Walker and Duncan, 1988; Sherrod and Smith, 2000). Adjacent on the east is the High Cascades subprovince, encompassing the active volcanic arc, where volcanic construction has kept pace with erosion in most places (Priest et al., 1983; Sherrod and Smith, 2000).

Beginning about 4–5 Ma, the volcanic arc in central Oregon underwent an episode of subsidence and extension which led to a structural rift called the High Cascades graben (Smith and Taylor, 1983; Smith, 1986; Smith et al., 1989a; Conrey et al., 2004; Sherrod et al., 2004). This graben is 50 km long and 30 km wide, initiating at the latitude of Three Sisters and terminating just south of Mount Jefferson (**fig. 1.1**). The 1.2-km-high Green Ridge escarpment southeast of Mount Jefferson marks the eastern boundary of the graben (Conrey, 1985); whereas the Horse Creek fault west of the South Sister and Mount Jefferson, with 600 m of displacement, defines the western margin. Locally the graben margin is characterized by numerous discontinuous faults typically less than 10 km in length and striking N. 30° W. (Conrey et al., 2004; Sherrod et al., 2004). The graben is widest at its southern extent and narrows northward where it transitions into a half-graben connecting with the Hood River fault (Conrey et al., 2004). Few intragaben faults have been mapped, but scattered north-trending lineaments of small scoria cones are the shallow expression of regional tectonic controls (Taylor, 1981, 1990; Conrey et al., 2004; Schmidt et al., 2008).

The relation between tectonics and volcanism in the central Oregon Cascades is complicated by behind-the-arc processes (Wells et al., 1984; Hughes and Taylor, 1986; Conrey et al., 2002, 2004). The northwestern margin of the Basin and Range, a broad extensional province, terminates just southeast of Mount Jefferson at the Brothers fault zone, an extensional breakaway in which the northwestern Basin and Range is separating from an undeformed block to the northeast (Blue Mountains) (Trench et al., 2012). Buoyant mantle that rises beneath the western Basin and Range province (Jones et al., 1996) promotes back-arc extension as great as 4 ± 2 mm/yr (Pezzopane and Weldon, 1993). Clockwise rotation of the forearc block at rate of 1.5° per m.y. contributes to intra- and back-arc rifting (Magill and Cox, 1980; Wells et al., 1998; Wells, 2014). Intra-arc extension is estimated to be about 1 mm/yr (Wells et al., 1998; McCaffrey et al., 2007; McCaffrey et al., 2013).

2.2 Eruptive History of the Mount Jefferson Area

Rocks exposed in the Mount Jefferson area are as old as about 4 Ma (**table 2.1**). Rocks of more mafic composition tend to belong to older eruptive sequences at the periphery of the volcanic field and in the lower parts of canyon walls, whereas andesite and dacite typically form younger, more central stratigraphic units and ridge-capping lava flows.

Volcanic rocks in the Mount Jefferson area range in composition from basalt to rhyodacite (48–72 weight percent SiO_2). To judge solely from the number of mapped units, the most abundant composition is basaltic andesite (n=54) followed by andesite (n=50). Fewer dacite

(n=35) and rhyodacite (n=11) units are mapped in the Mount Jefferson area, and basalt (n=3) is the least abundant composition (**fig. 2.2**).

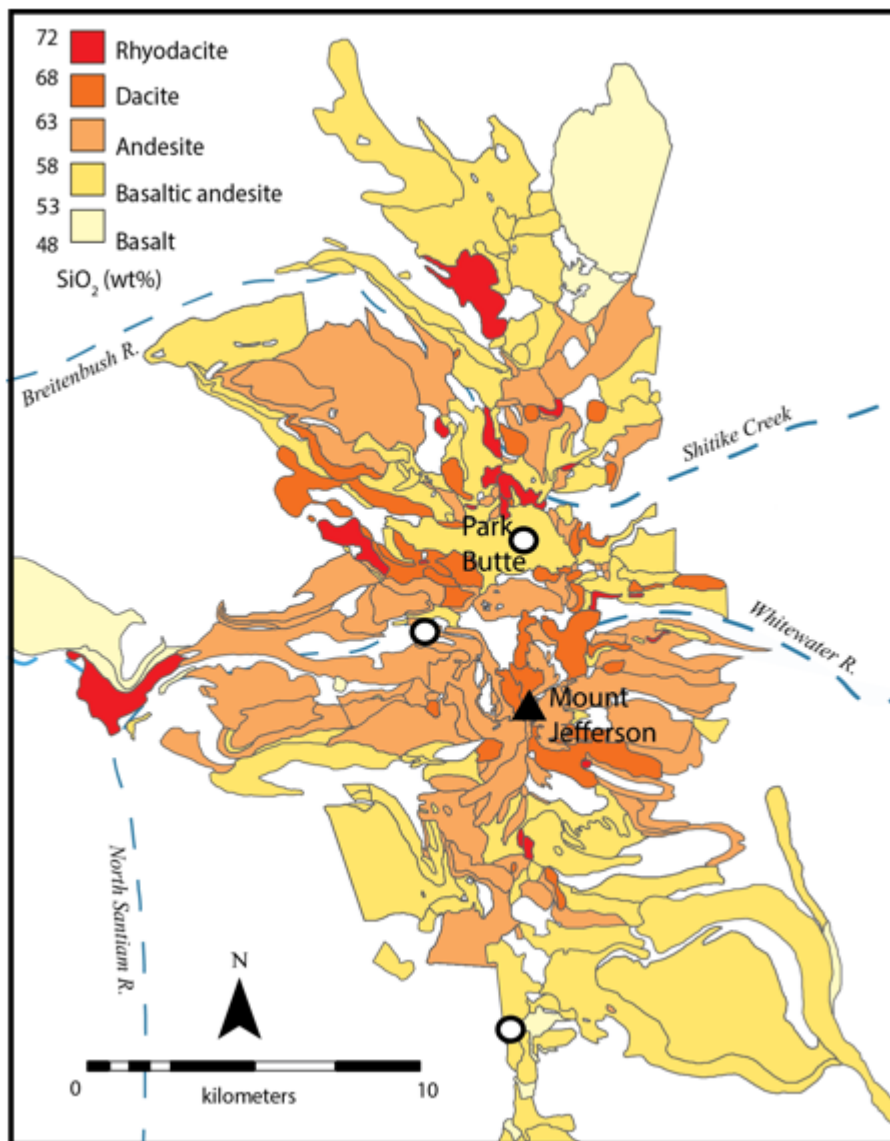


Figure 2.2. Silica variation diagram of MJA. Note that silica content is lowest around the periphery of the map area (oldest units) and increases toward the center (relatively young stratocone).

For descriptive purposes, the following discussion divides the volcanic history into four time periods. They are: (1) ~4.0 – 0.78 Ma, early eruptive products in the map area, ending with the last major magnetic reversal; (2) 0.78 – 0.3 Ma, older rocks on the flanks and along the crest

of the Cascade Range; (3) 0.3 – 0.02 Ma, coincident with the construction of the Mount Jefferson volcano and including the end of the last major glaciation; and (4) eruptions of the past 13,000 year (Holocene) (fig. 2.3).

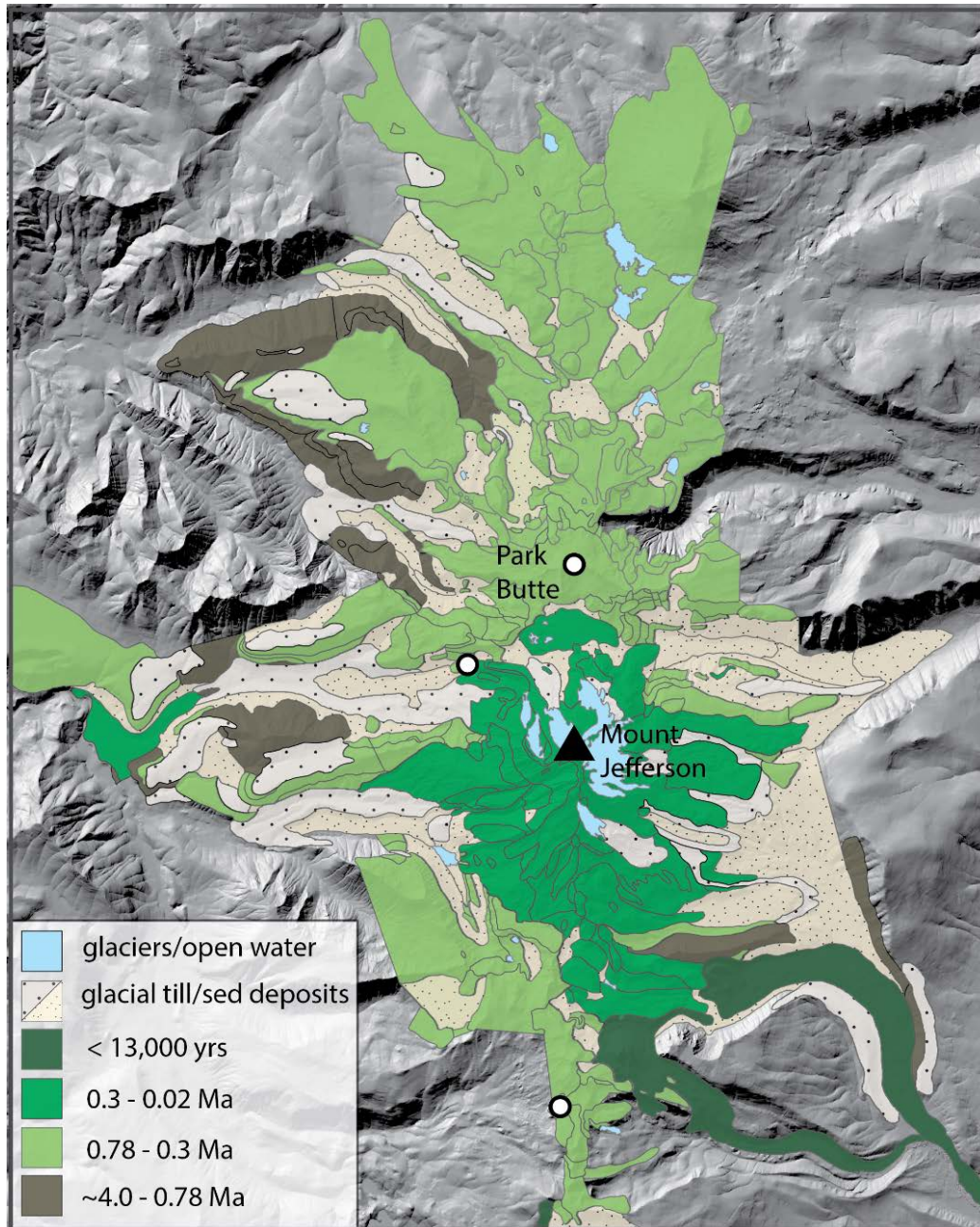


Figure 2.3. Generalized geologic map of MJA, divided into four time periods of volcanism. Present-day glaciers, tills, and sedimentary deposits are also indicated.

Table 2.1. K-Ar and $^{40}\text{Ar}/^{39}\text{Ar}$ ages for units across the MJA (D. Sherrod, written commun., 2015).

Map No.	Map unit	Sample	Age \pm 2σ error, Ma	Method	Material	Longitude (WGS 84)	Latitude (WGS 84)	Reference
1	Qdw3	WSJ-7R	0.017 \pm 0.015	K-Ar		-121.732309	44.679968	E. Layman, 1993
2	Qdw3	RCMJ-270	0.039 \pm 0.033	K-Ar		-121.798026	44.703445	Conrey, 1991
3	Qdw1	RCMJ-268	0.031 \pm 0.020	$^{40}\text{Ar}/^{39}\text{Ar}$ -integrated age	Plagioclase	-121.801344	44.706655	M. Lanphere, 1999
4	Qaw	RCMJ-243	0.032 \pm 0.004	$^{40}\text{Ar}/^{39}\text{Ar}$ -integrated age	Plagioclase	-121.817088	44.695574	M. Lanphere, 1999
5	Qrdse	RCMJ-#035	0.032 \pm 0.020	K-Ar		-121.961518	44.675243	Conrey, 1991
6	Qrdp	WSJ-13R	0.033 \pm 0.011	K-Ar		-121.776042	44.664722	E. Layman, 1993
7	Qamc	RCMJ-S16	0.064 \pm 0.017	K-Ar		-121.822890	44.665579	Conrey, 1991
8	Qamj	RCMJ-254	0.071 \pm 0.024	K-Ar		-121.813844	44.685435	Conrey, 1991
9	Qdpy	WSJ-1R	0.091 \pm 0.018	K-Ar		-121.798543	44.762601	E. Layman, 1993
10	Qamt	RCMJ-MTBL	0.093 \pm 0.040	K-Ar		-121.793287	44.625273	Conrey, 1991
11	Qdbl	WSJ-16R	0.098 \pm 0.023	K-Ar		-121.804101	44.753555	E. Layman, 1993
12	Qdpb	WSJ-21R	0.118 \pm 0.012	K-Ar		-121.808126	44.733945	E. Layman, 1993
13	Qdmx	RC02-217	0.14 \pm 0.010	Unspiked K-Ar		-121.841220	44.665397	D. Barfod, 2005
14	Qapb	RCMJ-133	0.154 \pm 0.014	K-Ar		-121.824349	44.723804	Conrey, 1991
15	Qdcb	WSJ-2R	0.172 \pm 0.013	K-Ar		-121.778207	44.762287	E. Layman, 1993
16	Qbam	RCMJ-S2	0.280 \pm 0.540	K-Ar		-121.841365	44.665255	Conrey, 1991
17	Qacl?	NS-212	0.29 \pm 0.020	K-Ar		-121.840535	44.652855	Priest et al., 1987
18	Qbast	RCMJ-645	0.299 \pm 0.020	K-Ar		-121.828997	44.622259	Conrey, 1991
19	Qbawc	RCMJ-945	0.348 \pm 0.104	K-Ar		-121.916128	44.669518	Conrey, 1991
20	Qdbc	WSJ-5R	0.370 \pm 0.030	K-Ar		-121.759791	44.715898	E. Layman, 1993
21	Qdhl	WSJ-11R	0.461 \pm 0.028	K-Ar		-121.769236	44.747211	E. Layman, 1993
22	Qawr	RC02-210	0.47 \pm 0.10	Unspiked K-Ar		-121.872218	44.679233	D. Barfod, 2005
23	Qbp	S88-35	0.48 \pm 0.10	K-Ar		-122.051157	44.704916	L.B. Gray, 1990
24	Qbp	PP-2	0.54 \pm 0.10	K-Ar		-121.999155	44.688617	Priest, 1990
25	Qdst	RC02-213	0.58 \pm 0.12	Unspiked K-Ar		-121.845574	44.683927	D. Barfod, 2005
26	Qdss	NS-209	0.57 \pm 0.59	K-Ar		-121.827150	44.708819	Priest et al., 1987

27	Qahl	RCMJ-700	0.626±0.096	K-Ar		-121.766870	44.748728	Conrey, 1991
28	Qask	BHS-23	0.65±0.10	K-Ar		-121.794150	44.758119	Sherrod and Conrey, 1988
29	Qapr	RCMJ-917	0.651±0.056	K-Ar		-121.916652	44.661718	Conrey, 1991
30	Qa	RCMJ-455	0.668±0.096	K-Ar		-121.774041	44.699346	Conrey, 1991
31	Qbagp	NS-217	0.68±0.06	K-Ar		-121.853150	44.643819	Priest et al., 1987
32	QTba	RCBR-66	0.845±0.084	K-Ar		-121.854856	44.781414	Conrey, 1991
33	Qbasf	BHS-20	0.86±0.12	K-Ar		-121.905154	44.761518	Sherrod and Conrey, 1988
34	QTbaj	RCCC-44	1.28±0.40	K-Ar		-121.678202	44.613407	Conrey, 1991
35	QTa	BHS-21	1.47±0.12	K-Ar		-121.874653	44.751485	Sherrod and Conrey, 1988
36	QTba	CT-75	1.49±0.18	K-Ar		-121.839152	44.773118	White, 1980
37	QTba	GWV-2-85	1.54±1.48	K-Ar		-121.878158	45.028116	Sherrod and Conrey, 1988
38	Tbab	WR-311	2.1±0.4	K-Ar		-121.700146	44.653920	Armstrong et al., 1975
39	Tbab	WR-308	2.1±0.4	K-Ar		-121.690145	44.653820	Armstrong et al., 1975
40	--	LH1	2.4±0.10	⁴⁰ Ar/ ³⁹ Ar	WR	-121.701147	44.718120	Smith, 1986
41	QTba	BHS-24	2.31±0.10	K-Ar		-121.839152	44.778918	Sherrod and Conrey, 1988
42	Tbabb	RCMJ-BB1	2.46±0.52	K-Ar		-121.762489	44.631234	Conrey, 1991
43	--	1059	2.6±0.4	K-Ar		-121.681146	44.696520	Yogodzinski, 1985
44	--	NS-225	3.06±0.10	K-Ar		-121.922152	44.625618	Priest et al., 1987
45	Tba	DMS-47	3.70±0.10	K-Ar		-121.920840	44.763649	Sutter, 1978
46	Tba	RCMJ-944	3.93±0.10	K-Ar		-121.907591	44.679366	Conrey, 1991
47	Trd	RCBR-412	3.95±0.10	K-Ar		-121.892872	44.757321	Conrey, 1991
48	--	1065	4.1±1.4	K-Ar		-121.684146	44.713120	Yogodzinski, 1986

2.2.1 Rocks emplaced between 4.0 and 0.78 Ma

The oldest rocks exposed in the Mount Jefferson area are of early Pliocene age. They are found in the steep canyon walls in the eastern and western parts of the map area. The most extensive exposures are at Woodpecker Hill, Breitenbush Mountain, and canyon walls of Whitewater Creek and the South Fork of the Breitenbush River. Eruptions were characterized by the extrusion of thin basaltic andesite lava and sparse interlayered andesite lava (collectively, unit Tba). Small lenses of augite-bearing basaltic andesite (unit Tbca) are mapped separately on the ridges of Breitenbush Mountain and Bear Point. Lava flows and domes of dacite and rhyodacite (unit Trd) were extruded throughout this time period. Ridgetop exposures are generally fresh, whereas rocks deeper in the stratigraphic sequence tend to be altered (Conrey, 1991).

On the west flank of the map area, the stratigraphically lowest dated sample is a basaltic andesite from a roadcut along a forest road on the South Fork of the Breitenbush River, age **3.70±0.10 Ma (table 2.1, unit Tba)**. It is overlain nearby, albeit 250 m upsection, by a rhyodacite with age **3.95±0.10 Ma (table 2.1, unit Trd)**. The discrepancy between stratigraphic position and age is minor; the ages almost overlap at 2σ error. To the south, an age of **3.93±0.10 Ma** was obtained from a basaltic andesite lava (unit Tba) at Woodpecker Ridge. Taken together, these ages indicate a roughly 4-Ma age for the base of the High Cascades in the map area. Farther south on the west flank near Minto Creek, a basaltic andesite lava flow yielded an age of **3.10±0.10 Ma**. (Sample location on map, although in an area not depicted geologically.)

On the east side, a K-Ar age of **4.1±1.4 Ma** was obtained from a basaltic andesite lava at the base of the Whitewater River's north canyon wall (altitude 1,160 m) in an area mapped by Gene Yogodzinski (1985). The analytical error for this sample is large, but some ages

stratigraphically higher lend credence to its value. For example, a dacite lava flow sampled 700 m upsection at the crest of Lionshead (1,860 m altitude) has an $^{40}\text{Ar}/^{39}\text{Ar}$ age of **2.4±0.10 Ma** (Yogodzinski, 1985). And across the canyon, a basaltic andesite lava flow (1,520 m altitude) has an $^{40}\text{Ar}/^{39}\text{Ar}$ age of **2.6±0.04 Ma**. Thus, the oldest of the three lava flows is probably at least 3 Ma. To the south, the basaltic andesite of Bear Butte (unit Tbab) forms the dissected remnant of an 8-10-km-diameter shield volcano erupted from a vent near Hole in the Wall Park. Its age is **2.46±0.52 Ma**.

Younger (2.5–0.8 Ma) rocks are exposed in shield volcanoes across the map area. Although basaltic andesite is predominant, andesitic lava flows (in unit QTa) are exposed at the ridges of Bear Point, Woodpecker Hill, and near the summit of the ridge above the South Fork of the Breitenbush River (**1.47±0.12 Ma**). The basaltic andesite of South Fork Breitenbush River (Qbasf; **0.86±0.12 Ma**) fills a paleovalley cut into the 1.47-Ma andesite lava (unit QTa) and underlying basaltic andesite (unit Tba).

In the southeast corner of the map area is Bald Peter, a late Pliocene basaltic andesite shield volcano (unit Tbab). Similar ages from lava at Bald Peter's base (**2.1±0.4 Ma**) and summit (**2.1±0.4 Ma**) suggest extrusion from a single source. However, variation in chemical data A substantially younger K-Ar age comes from a lava flow that laps onto the southeast flank of Bald Peter (unit QTbaj; **1.28±0.40 Ma**).

To the northwest, lava flows of Pliocene and lower Pleistocene basaltic andesite (unit QTba) crop out in the canyon walls and bench of the North Fork of the Breitenbush River, where they overlie rhyodacite and basaltic andesite (in units Trd and Tba). Radiometric ages from these Plio-Pleistocene lava flows come from three locations: the head of the river (**1.49±0.18 Ma**) and canyon walls (north side, **2.31±0.10 Ma**; and south side, **0.845±0.084 Ma**).

2.2.2 Rocks emplaced between ~0.78 and 0.3 Ma

Rocks of this age form the bulk of stratigraphic units in the map area, with over 110 individual eruptive sequences that span the full compositional spectrum (basalt to rhyodacite). Only a handful of the mapped units are dated. Of those, two are basalt, three are basaltic andesite, five are andesite, and four are dacite.

West and northwest of the volcano, three K-Ar ages come from Woodpecker Ridge. There, the paleocanyon-filling andesite of Pamela Lake Road (unit Qapr; **0.651±0.056 Ma**) forms the lowest exposure in this sequence; it is directly overlain by the andesite of Woodpecker Ridge (unit Qawr; **0.47±0.10 Ma**). A small exposure of basaltic andesite on the southwest flank of Woodpecker Ridge (unit Qbawc; **0.348±0.104 Ma**) caps the sequence. The andesite (Qass) and dacite (Qdss; **0.57±0.28 Ma**) of South Sentinel Hills similarly fill paleocanyons between the South Fork Breitenbush River and Whitewater Creek drainages.

Ten small-volume Pleistocene andesite lava flows (Qa) were erupted from vents north and northeast of Mount Jefferson. Other similar lava flows form small lenses in canyon-wall exposures of the Whitewater River (**0.668±0.096 Ma**). Cirque-like morphology of the canyon's headwall and columnar and platy-jointed exposures of the dacite of Big Cliff (Qdbc; **0.37±0.03 Ma**) perched in the Whitewater River canyon suggest Big Cliff eruptions were intraglacial. Marine oxygen isotope records (for example, Lisiecki and Raymo, 2005) indicate a cold period around 350,000 years (marine oxygen-isotope stage 10), roughly coincident with the K-Ar age from the dacite of Big Cliff.

Potassium-argon ages were obtained from the andesite (Qahl; **0.626±0.096 Ma**) and adjacent dacite (Qdhl; **0.461±0.028 Ma**) of Harvey Lake, located on the bench above Shitike Creek. Sharp-crested moraine morphology and lava ponding observed at ridge-capping units

Qasc and Qbasc on east side of Shitike Creek suggest eruption against glacial ice. Additionally, perched lavas exposed at the head of the Shitike Creek, including the upper and lower units of the basaltic andesite of Hilda Lake (Qbah1 and Qbah2), preserve glassy basal contacts, evidence that these units were erupted when ice was present across the Cascade Range crest.

Similar eruptive products crop out along the Cascade Range crest north and south of Mount Jefferson. The andesite of Skyline Trail (unit Qask; 0.65 ± 0.10 Ma) is exposed in the valleys between the dacite domes of Babe Lake, Pyramid Butte, and Campbell Butte. The Skyline Trail flows are much older than the surrounding ~90 to 170 ka dacite domes, suggesting a local lull in volcanism. Approximately 12 km to the southwest, the dacite of Skyline Trail (Qdst; 0.58 ± 0.12 Ma) crops out where Woodpecker Ridge plunges beneath the base of the Mount Jefferson stratocone. Another 8 km farther south, the thick glassy flows of the basaltic andesite of Skyline Trail (Qbast; 0.299 ± 0.020 Ma; **fig. 2.4**) were extruded from a vent downslope of Cathedral Rocks.

Andesite and dacite eruptive centers diminish in abundance away from the site of present-day Mount Jefferson volcano. In their place, cinder cones, and small shield volcanoes fed basalt and basaltic andesite lava flows south of the volcano and at the farthest northern extent of the map area. The basaltic andesite of Grizzly Peak (Qbagp; 0.68 ± 0.06 Ma) and basaltic andesite of Yogodzinski (Qbay) are two of the largest remnant shield volcanoes active within this time period in the map area. The lavas extruded from the Grizzly Peak center (unit Qbagp) are thin and chemically heterogeneous with multiple intrusions and layered pyroclastic deposits, whereas the discontinuous outcrops of Qbay display homogenous plagioclase-, two-pyroxene, and olivine-phyric lavas.



Figure 2.4. Andesite of Skyline Trail (Qast) spires exposed in Cathedral Rocks.

The basalt of Pigeon Prairie (unit Qbp, 0.54 ± 0.10 Ma and 0.48 ± 0.10 Ma) is the westernmost unit in the map area. Although individual lava flows are a few meters thick, the unit has aggregate thickness as much as 240 m (800 ft). It forms an intracanyon bench along the North Santiam River as far west as Idanha village, 8 km from the Pigeon Prairie vent.

2.2.3 Rocks emplaced between 0.3 and 0.02 Ma: Construction of Mount Jefferson volcano and scattered along-arc volcanism to north and south

It is during the past 300,000 years that volcanism in the map area progressed steadily from widespread, mafic eruptions to more focused intermediate and silicic products of the Mount Jefferson volcano. At Mount Jefferson, activity has been dominated by widespread andesite and

dacite flows near the summit and smaller rhyodacite and andesite domes and flows erupted from vents around the periphery. Mafic eruptive products are rare.

The oldest sequences thought to be part of Mount Jefferson volcano are clustered on the southwest flank of the stratocone; for example, the andesite of Coyote Lake (Qacl; 0.29 ± 0.02 Ma) and basaltic andesite of Milk Creek (Qbam; 0.280 ± 0.54 Ma). The Milk Creek unit crops out as a small dome exposure within the andesite of Coyote Lake and at the base of Milk Creek canyon. A dacite dome (unit Qdmx) exposed at the trail crossing in the Milk Creek canyon has a K-Ar age of 0.14 ± 0.01 Ma; it is mantled to the north, west, and east by the basaltic andesite of Milk Creek (unit Qbam). All three units overlie intracanyon gravel deposits interpreted as glacial outwash by Scott (1977). If Scott's (1977) interpretation is correct, the gravel marks a glaciation occurring before 140,000 years ago and perhaps even before 300,000 years ago.

An apparent 80,000 year hiatus in volcanic activity at Mount Jefferson followed the emplacement of the basaltic andesite of Milk Creek. Eruptions occurred sporadically in surrounding areas, however; for example, the numerous domes and lava flows in the northern part of the map area. A K-Ar age of 0.172 ± 0.03 Ma was obtained from Campbell Butte (Qdcb), a vent-fed dacite dome north of Shitike Creek (**table 2.1**). The andesite of Park Butte (*Qapb*), a large andesitic lava flow overlooking Jefferson Park, has similar age, 0.154 ± 0.03 Ma. The andesite of Park Butte is cut by an array of north-northwest-striking dacite dikes, including a feeder dike for the dacite dome of Park Butte (*Qdpb*; 0.118 ± 0.02 Ma). Palagonitized basal scoria in the andesite of Park Butte, glassy, prismatic jointing in the dacite of Park Butte, and marine oxygen isotope records indicating a cold stage between approximately 100 and 200 ka suggest units *Qapb* and *Qdpb* were erupted during a glacial epoch (oxygen isotope stage 6). A few kilometers to the north, the vent-fed dacite domes of Babe Lake (Qdbl) and Pyramid Butte

(Qdpy) give statistically indistinguishable ages of 0.098 ± 0.05 and 0.091 ± 0.03 Ma. The flat-topped andesite dome of Middle Table (Qamt; 0.093 ± 0.08 Ma) was also likely erupted during the same glacial epoch as the Park Butte units (*Qapb*, *Qdpb*). Ice-contact morphological features at the Middle Table include glassy margins and cordwood jointing.

Stratocone activity resumed beginning around 70,000 years ago with the extrusion of the andesite of Mount Jefferson (Qamj; 0.071 ± 0.05 Ma), which mantles all flanks of the volcano. This stratigraphic unit was erupted from a central vent near the volcano's modern summit. Of similar age is the andesite of Milk Creek (Qamc; 0.064 ± 0.03 Ma), which crops out on the volcano's west slope. The dacite of Milk Creek (Qdmc) forms a 300-m-high dome near the summit of the volcano and lava flows to the north along the west flank of the volcano. Although undated, the dacite of Milk Creek is interbedded with andesites of Mount Jefferson and Milk Creek, indicating coeval eruptions. Together, these units form the bulk of the Mount Jefferson cone.

The dacite of Whitewater Glacier (Qdw) covers much of the eastern slope of Mount Jefferson. The unit's lava flows and domes are divided into three members on the basis of stratigraphic position. The lower member (Qdw1) consists of an elongate flow and dacite dome aligned along north-trending vents between the main vent of the volcano and Jefferson Park. Little of the middle member (Qdw2) is preserved, and it is restricted to a single lava flow on the northeast slope of the volcano. The middle member's lava bifurcated at about 6,600-ft altitude (~2,000 m). One lobe continued northwest toward Jefferson Park (**fig. 2.5**), where it terminated against lava of the lower member, whereas the other lobe descended northeast toward the Whitewater River headwall. Glassy lava flows of the upper member (Qdw3) form steep, well-preserved, digitate lobes on the north, east, and south flanks of the volcano. Two ages were

obtained from unit Qdw3: **0.039±0.07** Ma from the base of a flow on the northern flank **and** **0.017±0.03** Ma from the base of the easternmost lobe exposed in (east-flank) Milk Creek canyon. The continuity of the map unit suggests extrusion from a single vent near the summit of the volcano.

The three members of the dacite of Whitewater Glacier underlie four of Mount Jefferson's five present-day glaciers. Large analytical uncertainty in the dacite ages precludes knowing confidently whether the Whitewater Glacier dacite was erupted within a glacial epoch, but abundant morphological evidence, including steeply truncated lobes, preservation of glassy jointed margins, and confined flows, suggest eruptions took place while ice was present on the volcano. Marine isotope records mark a cold period between about 15 and 30 ka (oxygen isotope stage 2), consistent, within error, with K-Ar ages from the lower and upper members (Qdw1 and Qdw3). A small dacite dome, the rhyodacite of Parker Creek (Qrdp; **0.033±0.02** Ma), crops out about halfway down the southeast flank of the volcano where Qdw3 diverges into two lobes. Morphologically this suggests the rhyodacite of Parker Creek was erupted before the divergent lobe, and that unit Qdw3 is probably less than about 30,000 to 40,000 years old. The youngest extruded unit is from a vent coincident with the summit of the volcano (10,497 ft; 3,199 m). A glassy northern lobe begins at the central vent and is bounded by present-day Russell and



Figure 2.5. Lower (Qdw1), middle (Qdw2), and upper (Qdw3) members of the dacite of Whitewater Glacier (Qdw) photographed looking south from Jefferson Park. The andesite of Whitewater Glacier (Qaw) forms the eastern ridgeline.

Jefferson park glaciers, forming a ridgeline to the headwall of Whitewater Creek.

Exposed approximately 0.5 km downslope beyond the lava flow's terminus is an isolated domelike mass, the andesite of Whitewater Creek (*Q_{awc}*; **fig. 2.6**). This mass is rich in plagioclase phenocrysts, similar to the andesite of Whitewater Glacier, and it may be the now-eroded toe of the northern lobe. Another lobe flowed south down the southwest slope of the volcano, terminating at about 6,400 ft altitude atop the ~300,000 year old Coyote Lake andesite sequence. A third lobe is isolated on the middle of the western slope and is likely derived from a series of radial dikes exposed near the summit. Confined flow margins suggest eruptions were coincident with the last glacial maximum, whose age is about 22–18 ka in the Oregon Cascade Range (Scott et al., 1990).

Elsewhere in the map area, equally youthful volcanic rocks were erupted at Olallie Butte. Olallie Butte is a steep-sided basaltic andesite shield volcano along the Cascade Range crest at the north edge of the map area. Its age is probably in the range 60–30 ka on the basis of having an erosional state similar to Mount Bachelor, a volcano south of the Three Sisters whose age was established on the basis of paleomagnetic directions (Scott and Gardner, 1992). If Olallie Butte had witnessed successively older glacial episodes its flanks would be more deeply scalloped.



Figure 2.6. Andesite of Whitewater Creek (*Qawc*). May represent the eroded northern lobe of the andesite of Whitewater Glacier (*Qaw*).

2.2.4 Eruptions of the past 13,000 years (Holocene)

Only three eruptions have occurred in the map area in Holocene time, all of them south or southeast of Mount Jefferson. Each formed scoria cones and blocky ‘a‘ā lava flows of basaltic andesite. All three eruptions occurred after emplacement of Mazama ash, a widespread silicic tephra erupted about $6,640 \pm 250$ yr BP from Mount Mazama (Crater Lake National Park; Rubin and Alexander, 1960). Though undated radiometrically, approximate ages have been estimated from sedimentation rates and the presence of interbedded ash layers within sediment cored from the bottom of Cabot Lake (Scott, 1977).

The basaltic andesite of Forked Butte (Qyba_f), estimated to be about 6,500–6,400 years in age, is the oldest of the Holocene units. Deposits include plagioclase-, olivine-, and augite-bearing scoria, lava flows, and ash. The nearby basaltic andesite of Jefferson Lake trail (Qyba_j) also comprises lava flows and tephra, similar in composition to the Forked Butte unit. It was erupted from an unnamed scoria cone just south of Bear Butte. Age estimates of the Jefferson Lake trail lava flows are lacking but, stratigraphically, the lava flows override the Forked Butte lava where the flows meet downcanyon (Scott, 1977; Conrey, 1991).

The youngest eruption in the Mount Jefferson area, the basaltic andesite of Swallow Lake (Qyba_s), is estimated to be about ~1,000 years old (Scott, 1977). A scoria cone on the south flank of South Cinder Peak marks the vent, deposits of which are characterized by black scoriaceous ash, lapilli, and bombs. The Swallow Lake lava flows extend 3 km west, reaching to Marion Lake.

2.3 Glacial History

Mount Jefferson and the surrounding area have been glaciated repeatedly during Quaternary time. Evidence includes deeply notched cirques, U-shaped valleys, and extensively eroded cinder cones. In addition, glacial till of lateral and ground moraines blankets large areas (Scott, 1977).

Moraines of at least three major glaciations have been described in the map area. These include the deposits of two Pleistocene glaciations, the older Jack Creek and younger Cabot Creek glaciations, and one Holocene minor advance, the Jefferson Park advance. Deposits are differentiated largely on basis of soil development, thickness of weathering rinds on clasts in soils formed in the deposits, and the sharpness of moraine crests (Scott, 1977). Much of the following discussion is drawn from work by Scott (1977).

2.3.1 Cabot Creek Glaciation, Late Wisconsin

Deposits of the Cabot Creek glaciation are customarily divided into the older Suttle Lake and younger Canyon Creek advances. A mountain ice sheet covered the High Cascades south of latitude 45° N. during the Suttle Lake advance, which is the last major glacial advance in the area. The resulting deposits cover large areas across the map area. The till of the Suttle Lake advance (Qmw) contains boulder-sized clasts within a fine-grained matrix with thin (<1 m), poorly developed B horizon soils. Weathering rinds are scarce and typically have a maximum thickness of about 0.2 mm. Deposits of the Suttle Lake advance are characterized by sharp crested end moraines and successions of smaller recessional moraines typically about 2 km upvalley from the terminal moraine. Deposits of Suttle Lake age are prominent in several major drainages in the western part of the map area including Pamela Creek, Milk Creek, Whitewater Creek, and the North and South Forks of the Breitenbush River. To the east, Suttle Lake outwash surrounds the Jefferson Lake Trail lava flow in the Candle and Indian Creek drainages. Though not dated radiometrically, morphological and weathering features suggest the Suttle Lake advance is correlative with the Evans Creek stage of the Fraser glaciation of Washington, which advanced roughly 18,000 to 22,000 years ago, coincident with marine oxygen isotope stage 2 (Porter et al., 1983; Scott, 1990; Lisiecki and Raymo, 2005).

Waxing and waning of glaciers continued through the late Pleistocene resulting in several smaller glacial advances following the Suttle Lake advance. The landforms built during these short, successive pulses resulted in the deposits of the Canyon Creek advance (Qmc). Deposits of this age are similar to deposits of the Suttle Lake advance but are restricted to cirques and valley heads near the crest of the range. The till of Canyon Creek age is composed of cobbles and boulders in a loosely consolidated matrix of poorly sorted sand. Clasts are relatively fresh with

weathering rinds less than 0.2 mm thick, and soils resemble those of the Suttle Lake advance. Valley head moraines are sharp-crested with slopes up to 28° and extend about 5 to 8 km from the present glacier termini. Outwash of Canyon Creek age grades from poorly sorted boulders and cobbles to well-sorted gravel and sand downstream. Deposits of Canyon Creek age are mapped only on the eastern flank of the volcano and most conspicuous at the headwalls of Milk Creek, Parker Creek, and Jefferson Creek. The Canyon Creek advance is correlated with the Hyak advance of the Fraser glaciation of southern Washington, which occurred between about 12,500 and 11,000 years ago, representing the final stages of marine oxygen isotope stage 2 (Porter et al., 1983; Lisiecki and Raymo, 2005).

2.3.2 Jack Creek Glaciation, Early Wisconsin

The oldest glaciation from which moraines are preserved is the Jack Creek glaciation. Till of the Jack Creek Formation (Qmj) contains boulders and cobbles with weathering rinds 0.5-0.7 mm thick embedded in argillic B horizon soils as deep as 2 m. Mass wasting has modified lateral moraines so that they display broadly rounded crests sloping from 15° (proximal) to 5° (distal). Deposits of Jack Creek age cap numerous ridge crests west of Mount Jefferson volcano, including Woodpecker Ridge, Sentinel Hills, Breitenbush Mountain, and the Olallie Lake area. The age of the Jack Creek glaciation was not determined explicitly by Scott (1977). Stratigraphic evidence suggests it is younger than lavas at the crest of Woodpecker Ridge and older than the main body of andesite erupted in the Mount Jefferson area, bracketing an interval between about 350,000 and 70,000 years. Additional studies suggest the Jack Creek glaciation is correlative with the Hayden Creek and Moss Creek glaciations of southern Washington (Colman and Pierce, 1981; Easterbrook, 1986), which advanced during a glacial epoch about 140,000 years ago, or marine isotope stage 6.

2.3.3 Jefferson Park Advance, Holocene

Two minor glacial episodes, informally called the early and late neoglacial episodes (Scott, 1990), are described within the context of the Jefferson Park advance (Qmw). Deposits of early neoglacial age are characterized by steep, unstable, and bouldery terminal moraines up to 50 m high and are slightly more degraded than those of the late neoglacial (Scott, 1990). Late neoglacial moraines are smaller, steeper (up to 42° slope), and more sharply crested than those of the early neoglacial. Evidence for early neoglacial advances is typically found immediately beyond late neoglacial ice limits; however, much of these deposits were obliterated by subsequent advance and retreat of the younger neoglacial episode. Deposits of both advances consist of poorly sorted stones and boulders. Clasts appear very fresh and lack weathering rinds, and soils are poorly developed. Deposits of Jefferson Park age are generally restricted to the upper 6,000 feet of Mount Jefferson volcano, occurring immediately in front of the waning, present-day glaciers high on the volcano. Deposits of this age postdate ash of the Mazama eruption (6,845 ¹⁴C yr B.P.; Rubin and Alexander, 1960; Sherrod et al., 2004) as well as tephra from the eruption of the cone on the south flank of South Cinder Peak, estimated around 1,000 ¹⁴C yr B.P. (Scott, 1977). Weathering similarities indicate the Jefferson Park advance is correlative with the Garda advance of Mount Rainier, which is estimated to be as young as 450 ¹⁴C yr B.P., coincident with marine oxygen isotope stage 1 (Crandell, 1969; Lisiecki and Raymo, 2005).

2.4 Evidence of Ice-Magma Interactions

Evidence of intraglacial eruptions is abundant in the Mount Jefferson area and can be recognized by several criteria including (1) anomalously glassy lava flows; (2) lava flow sequences with thick, glassy basal flows surmounted by thin flows of normal aspect; (3) perched

lava flows; (4) vertical chilled flow margins; (4) sheet-like, prismatic, or columnar jointing; and (5) streamlined shapes (Conrey, 1991). In the map area, evidence for intraglacial eruptions is most abundant among lava flows thought coincident with marine oxygen isotope stages 2 and 6; thus, the late and early Wisconsin glacial episodes, respectively.

For the Cabot Creek glaciation (oxygen isotope stage 2), excellent examples of thick, glassy lava flows are seen in the dacite of Whitewater Glacier (unit Qdw) near the summit of the volcano. Well-preserved flow surfaces and levees of the upper member (Qdw3) and restricted flows and perched character of the middle member (Qdw2) suggest lava flows were confined by ice. Unusual sheet jointing observed on the surfaces of domes of the lower member (Qdw1) probably resulted from the advance of lava against ice by extrusion of successive overlapping sheets. Similar features were observed in the andesite of the Whitewater Glacier (Qaw; 20.4 ± 3.1 ka). Slightly northwest of the toe of the Qaw lava lobe, an andesite dome, the andesite of Whitewater Creek (*Qawc*), was erupted on the floor of a glacial valley. The dome exhibits vertical chilled margins and columnar joints of unusual height, and length and glassy chilled margins of the dome are preserved on the planar cliff face, which reaches a height of about 130 m (**fig. 2.6**). Closer inspection reveals crude columnar jointing exposed inside the carapace. All evidence indicates the dome was shaped by a mass of ice pressing against it.

Unusually thick (25-50 m) basaltic andesite lavas are perched on the crest of a cirque near Bear Point (Qbabp) with no means of support, unless by glacial ice. The lavas have an anomalously glassy base and typical aa lavas on the upper surface of the flow. Presumably, the upper surface of the body developed in air after the magma breached the surface. The outer glassy rind of the lavas have been stripped off by ice, exposing long columnar joints. Near Goat Peak (**fig 2.7**), thick glassy lava flows erupted from two cinder cone remnants are perched above

Hole-in-the-Wall Park and Jefferson Creek. The perched character of the andesite lavas of Goat Peak (Qagp), as well as the eroded nature of the cinder cones suggest lavas were erupted against a glacier, which supported the lava during cooling and subsequently eroded the cinder cones during retreat. To the south, basaltic andesite lavas of Jefferson Lake (Qbajl) comprise at least two intraglacial flows on the basis of glassy, confined margins and slight sculpting of the cinder cone from which the lavas were erupted. Continuing south, just west of the Pacific Crest Trail, glassy character of four basaltic andesite domes (*Qbawh*) suggests intraglacial eruption.



Figure 2.7. Goat Peak, a plagioclase-rich rhyodacite dome eroded by glaciation. View north from Pacific Crest National Trail.

Evidence for ice-magma interactions from the Jack Creek glaciation, representing oxygen isotope stage 6, is more scant than for stage 2, as much of the evidence has been scoured away by subsequent glaciations. Ice-magma interactions assigned to this glacial episode are mostly present in units immediately north and south of the volcano. The andesite of North (Qant), Middle (Qamt; 0.09 ± 0.04 Ma), and South Table (Qast), collectively referred to as “The Tables,” consists of three flat-topped domes as well as an outlying glassy mass (informally named “The Wall”) about 1 km northwest of Patsy Lake (**fig. 2.8**). The base of The Tables are each glassy in character and display cordwood and sheetlike jointing, whereas the uppermost part of the domes is cryptocrystalline. The eruption was probably subglacial (glassy part of dome) until the dome eventually broke through the ice cap and erupted subaerially (microcrystalline lava). Farther north, several glassy, prismatic jointed blocks are observed at the base of the andesite of Park Butte (*Qapb*; 0.15 ± 0.01 Ma). Additional field evidence, including the presence of thick (up to 70 m) glassy lava flows overlain by thin (less than 10 m) non-glassy lava flows, palagonitized scoria, and oxidation near to the top of the unit suggest eruptions were intraglacial.

Other examples of ice-magma interaction are found within units throughout the map area which are not assigned to a glacial epoch. Several of these lavas are preserved as perched units above canyon walls or within cirque headwalls including the andesite of Carl Lake (*Qacl*; 292 ± 17 ka), basaltic andesite of South Sentinel Hills (*Qbass*), basaltic andesite of Hilda Lake (*Qbah1, 2*), and andesite of Bear Point (*Qabp*). The dacite of Big Cliff (*Qdbc*; 370 ± 17 ka), at the cirque headwall of Whitewater River, is a particularly imposing dome of columnar and platy-jointed lavas perched over 300 m from the valley floor. Several other units are interpreted as intraglacial on the basis of thickness of lava flows. For example, the andesite of Pyramid Lake (*Qap*), the lowest lava flow in the North Fork Breitenbush River, reaches thicknesses of 150 m.

The glassy basal flow is surmounted by thin flows of normal aspect. The criteria suggest that the basal flow encountered ice and either cleared a pathway through the ice for succeeding flows or provided a platform above the icy interface. Still other units provide constraints of magma-ice interaction through interpretation of erosive deposits. For example, the rhyodacite of Whitewater River (Qrdw; 76 ± 34 ka), an ash-flow tuff at the 4800-ft altitude northeast of Mount Jefferson, is interbedded with glaciofluvial deposits and perched on the walls of the Whitewater River canyon, indicating its formative eruption was probably intraglacial.



Figure 2.8. North (Qant), Middle (Qamt), and South (Qast) Tables looking south from Goat Peak. Poor air quality the result of smoke from the nearby County Line 2 fire, which burned on the Warm Springs Indian Reservation during the summer of 2015.

2.5 Summary

The essential geologic features of the Mount Jefferson area have been pieced together by many previous researchers, to which we have added a digital geologic map, detailed eruptive and glacial histories, and a summary of intraglacial evidence in units across the map area. The MJA has been the locus of andesite-dacite volcanism for several million years and records a complex record of arc volcanism extending back to ~4 Ma. Volcanic products of the MJA show a from more dispersed mafic eruptions (basaltic andesite) to increasingly focused felsic (dacite to rhyodacite) eruptions over its 4 million year history, and much of the volcanic construction occurred in the past ~300,000 yrs. The MJA resides within the High Cascades graben and is framed to west and east by the Horse Creek and Green Ridge fault escarpments. The map area encompasses four main phases of volcanism, the moraines of three major glaciations, and abundant evidence of volcano-ice interaction in its 150 km² area. As seen today, Mount Jefferson is a 10,497 ft stratovolcano situated over within the central Oregon Cascade Range. Despite its ~13,000 yr hiatus, Mount Jefferson is regarded as potentially active, and volcano hazards for the area are the same as those of any stratovolcano. Though eruption-related hazards (e.g., tephra fallout, pyroclastic flows) would affect a proximal radius of the MJA in the event of an explosive eruption, noneruption-related hazards (lahars, debris avalanches) are far more likely.

3 MAGMATIC EVOLUTION OF A FOUR MILLION YEAR VOLCANIC SYSTEM: GEOTHERMOMETRY, GEOBAROMETRY, AND RECONSTRUCTIONS OF EQUILIBRIUM COMPOSITION MAGMAS IN THE MOUNT JEFFERSON AREA

3.1 Introduction

Often in subduction zones, volcanic systems preferentially erupt rocks of andesitic composition (Anderson, 1976; Eichelberger, 1978; Rudnick, 1995; Reubi and Blundy, 2009, Kent et al., 2010). Andesite lavas, which play a crucial role in the formation and evolution of continental crust at convergent plate margins, are generally formed by the mixing between two distinct magmas (Newman et al., 1986; Bullen and Clyne, 1990; Conrey, 1991; Smith and Leeman, 1993; Clyne, 1999; Conrey et al., 2001; Kent et al., 2010). Usually the mixing components include a more primitive, mafic magma, and a more evolved, silicic magma. The abundance of andesite lavas in continental arcs suggests that eruption of intermediate composition magmas is preferential in subduction zone settings including the Cascade Range, a 1,200-km long volcanic arc resulting from subduction of the Juan de Fuca plate beneath North America.

Examples of mixing to produce andesite compositions in the Cascade arc were summarized for Mount Hood, in which homogenous (55-66 wt% SiO₂) andesite is produced through injection of mafic magmas into a shallow felsic reservoir (Kent et al., 2010; Koleszar et al., 2012; Cooper and Kent, 2014); Mount Lassen, where mixing between basaltic andesite and dacite initiated the 1915 eruption of hybrid andesite lavas (Clyne, 1999; Klemetti and Clyne, 2014); and Mount Shasta, in which the mixing of dacitic and basaltic magmas and entrainment of

ultramafic crystal material generated high Mg# (87) andesite compositions (**fig. 3.1**) (Streck et al., 2006).

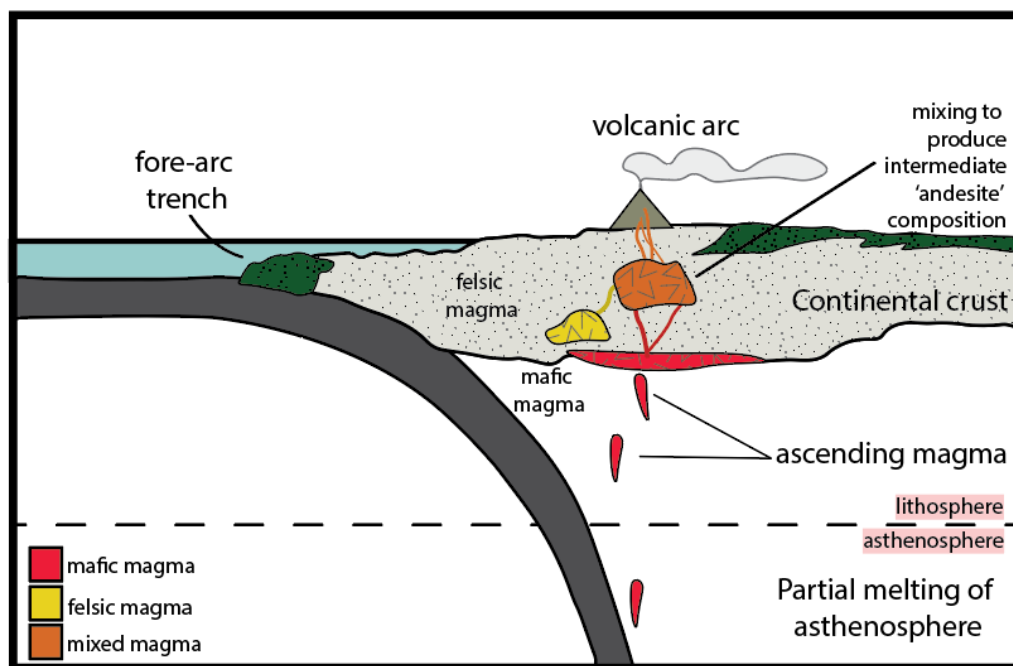


Figure 3.1. Generalized schematic of magma production. As shown, partial melting can occur at several crustal levels including the upper asthenosphere, middle, and upper crust. Magmatic storage typically occurs within a magmatic reservoir (granitic pluton upon cooling) in the upper crust

At other centers in the Cascade arc, diverse assemblages of mafic and intermediate rocks are extruded while dacite compositions remain relatively homogenous (Grove et al., 1988; Clynne, 1990; Bullen and Clynne, 1990; Bacon et al., 1994). Mount Jefferson, an andesite-dacite volcano of the central Oregon High Cascades, is perhaps the best example of this. Coupled geophysical models of Stanley et al. (1990) and trace element and isotopic studies of Conrey et al. (2001) propose the involvement of two types of intracrustal melting and an additional primitive magma to give three mixing endmembers, one basement source and two crustal

sources, to account for the substantial diversity of lavas (43.31-72 wt% SiO₂) observed at this volcanic system. The most likely mantle-derived magma in this scenario is a MORB-like basaltic magma (also known as the “low-K tholeiite” or “high-alumina olivine tholeiite”) associated with rifting of the High Cascades graben (Smith et al., 1989b; Hughes, 1990; Conrey et al., 1997). The two crustal endmembers are: (1) rhyodacite, generated through melting of amphibolite at 25-30 km depth and 850-900°C and (2) Sr-rich (>800 ppm) andesite, generated through partial melting of mafic granulite at 30-40 km depth and 1,050-1,100°C (**fig. 3.2**; Stanley et al., 1990; Conrey et al., 2001).

By this model, mixing of the three endmembers mostly occurs deep within the crust before reaching final placement in a small dacitic pluton residing approximately 10 km beneath the volcano. In the model, eruptions were likely initiated by the injection of the rhyodacite and Sr-rich andesite endmember into the shallow silicic reservoir (Conrey et al., 2001). Quenched mafic and intermediate inclusions within dacitic lavas, disequilibrium mineral assemblages, multiple phenocryst populations, the nearly ubiquitous presence of glomerocrysts in individual eruptive deposits, and as trace element ratios summarized in Conrey et al. (2001), indicate extensive mixing must have occurred to produce the erupted Mount Jefferson lava compositions.

Although it is accepted that mixing plays an important role in producing diverse lava compositions at volcanic arcs, several questions remain regarding the nature of the system in which mixing is occurring, including:

1. What are the physical conditions (pressure, temperature, depth) of the magma reservoir in which mixing occurs?

2. Is mixing confined to one shallow magma reservoir, as proposed by Conrey et al. (2001), or does mixing occur at several crustal levels?
3. Are erupted mafic and intermediate magmas (basaltic andesite) derived directly from deeper reservoirs than felsic (rhyodacite) magmas?

Here I employ the compositions of amphibole, plagioclase, orthopyroxene, and clinopyroxene phenocrysts from selected lavas across Mount Jefferson to estimate the temperatures and depths of crystallization and constrain the crustal residence history of erupted magmas, thereby testing the existing model of Stanley et al. (1990) and Conrey et al. (2001) for the magma plumbing system beneath Mount Jefferson.

An additional objective of this study is to reconstruct the range of melt compositions from which erupted compositions are derived by using the compositional record preserved in phenocrysts (e.g., Blundy and Wood, 1991; Bindeman et al., 1998). Plagioclase feldspar is ideally suited for this investigation as its composition is sensitive to melt composition and physical conditions in the magma chamber (Bowen, 1913; Johannes and Holtz, 1990; Househ and Luhr, 1991; Putirka, 2005; Blundy and Woody, 1991; Bindeman et al., 1998; Bindeman and Davis, 2002). Trace elements in plagioclase also have slow diffusion rates (Cherniak, 1994), incrementally records changes in melt composition during growth in the magma chamber (e.g., growth zones), and is a ubiquitous phase in the lavas selected for this study. Following the methods of Blundy and Wood (1991) and Bindeman et al. (1998), we glean temporal information about magmatic processes and test for evidence of the involvement of different magmatic endmembers, particularly the Sr-rich andesite discussed above.

In summary, the work presented in this study aims to accomplish two primary tasks:

- (1) Constrain the physical conditions (pressure, temperature, depth) at which magmas are stored and mixed prior to eruption, thereby better understanding the geologic processes that produce incremental volcanic eruptions of diverse lava compositions.
- (2) Reconstruct original melt compositions from which erupted compositions are derived using Sr and Ba concentrations in plagioclase phenocrysts, thereby validating the endmember compositions of Conrey (1991) and Conrey et al. (2001).

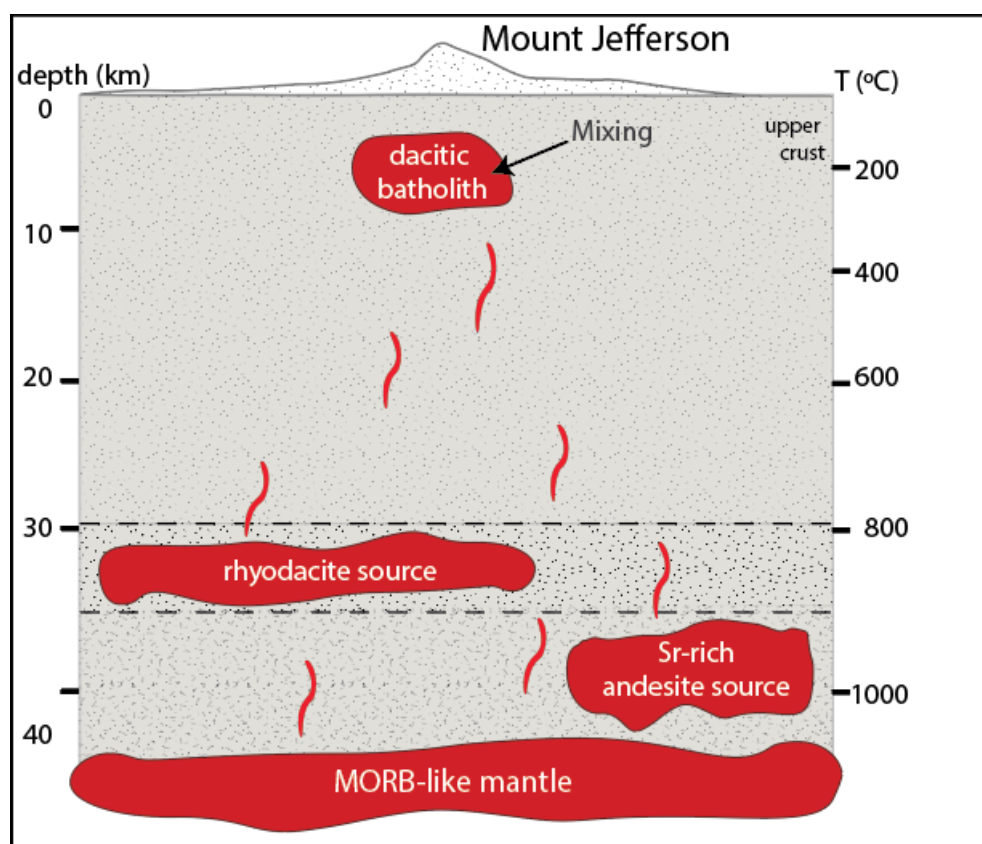


Figure 3.2. Model crustal cross section beneath MJA. Based on geophysical and geochemical model of Stanley et al. (1990) and Conrey et al. (2001). Modified from Conrey et al. (2001).

3.2 Study Area

The Mount Jefferson area is located along the High Cascade range of central Oregon. Within the MJA, the lavas of three units were selected for detailed study of the intensive parameters controlling eruptive behavior. These include the andesite of Whitewater Creek (*Qawc*), andesite of Park Butte (*Qapb*), which includes the compositions of dacite dikes (*Qdpb*), and the basaltic andesite of Whiskey Creek (*Qbawh*). The units are located in the northwest, north, and southern parts of the MJA, respectively (**fig. 3.3**).

Several faults and dikes cross cut the study area. Cinder cones of variable composition appear across the MJA, particularly to the north and south of the central stratocone. The area is also heavily dissected by rivers and streams, the physical record of three major glaciations advancing and receding since the early Wisconsin.

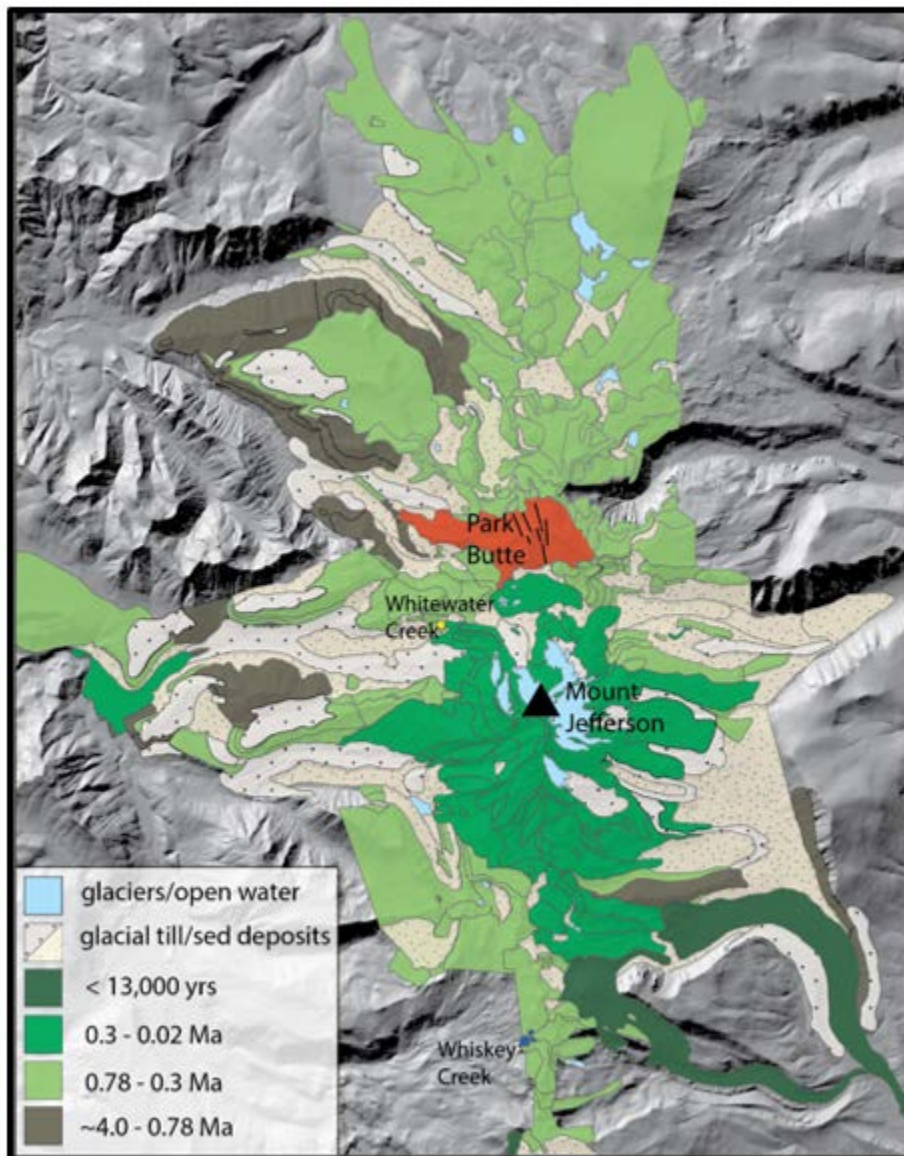


Figure 3.3. Study area, cut out from **figure 2.1** with addition geologic detail. Green fill denotes MJA. Warm Springs Reservation shown in dark tan. From north to south units are Q_{apb} (red), Q_{dpb} (black lines within Q_{apb}), Q_{awc} (small yellow polygon in middle of map), and Q_{bawh} (blue polygons at bottom of map). Red dashes indicate faults, black lines are dike, and white polygons with red dashes are vent deposits.

3.3 Summary of Geologic Units

3.3.1 Andesite of Whitewater Creek

The andesite of Whitewater Creek (*Qawc*) is an intermediate composition dome exposed near the headwall of the Whitewater Creek drainage about 4.5 km northwest of Mount Jefferson volcano (**fig. 3.3**). The 130-m-thick dome is mantled to the north and east by the andesite of Woodpecker Ridge and dacite lavas of Milk Creek and Whitewater Creek. Debris fan deposits and talus and colluvium frame the unit from the south and west. Chemically, *Qawc* is homogenous (61-62 wt% SiO₂), but texturally the unit is diverse; it varies from platy to massive conchoidal to polygonal in less than 10 m of outcrop distance. Glassy quench margins are observable at the base and midsection of the unit, and scoriaceous dikes appear to crosscut the other textures (**fig. 3.4**).

Mineralogically, the unit comprises plagioclase with amphibole and sparse ortho- and clinopyroxene arranged interstitially. Mafic inclusions are common. Textural evidence (e.g., glassy chilled margins, prismatic jointing) suggests that the dome was erupted on the floor of a glacial valley and sculpted by ice during eruption (refer to Evidence of Ice-Magma Interactions section for additional interpretation). Unit *Qawc* is likely correlative with andesite lavas erupted from the summit of Mount Jefferson (unit *Qaw*; **0.032±0.004 Ma**) on the basis of chemistry, plagioclase-rich phenocryst mineralogy, abundance of mafic inclusions, and degree of erosion (Conrey, 1991).

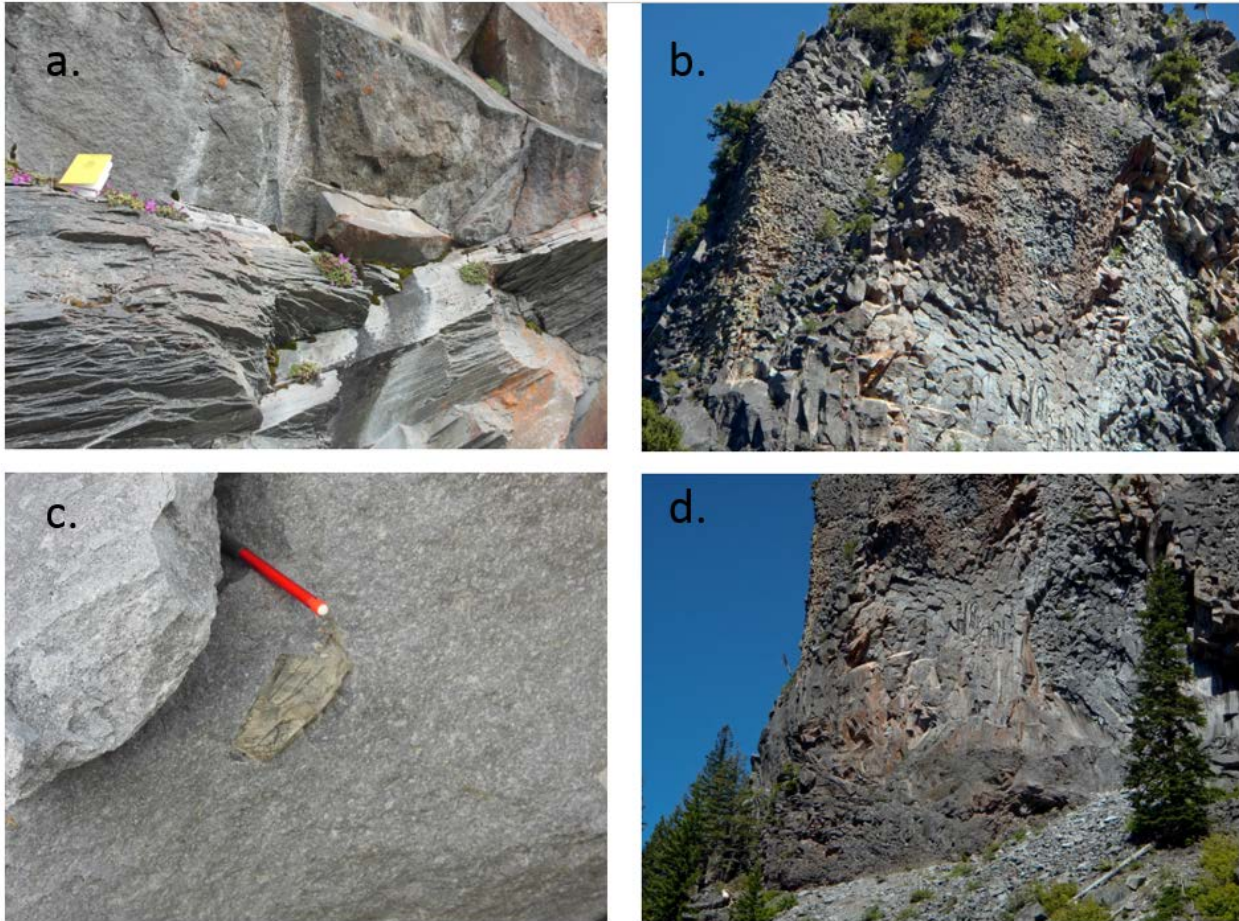


Figure 3.4. Photographs of andesite of Whitewater Creek (Qawc). a) platy andesite b) polygonal and hackly jointing c) inclusion d) polygonal jointing and basal quench zone.

3.3.2 Andesite of Park Butte

The 0.154 ± 0.028 Ma andesite of Park Butte (unit *Qapb*) is an aerielly extensive intermediate composition lava flow erupted from a vent centered at Park Butte, an eroded volcanic plug about 5 km north of Mount Jefferson volcano. At 6,851 ft, Park Butte provides exceptional views of the study area. To the south lie Jefferson Park and Mount Jefferson volcano (**fig. 3.5**). To the north, several dacite domes (Babe Lake, Campbell Butte, Pyramid Butte) dot the landscape, and to the east and west the Shitike and South Fork Breitenbush drainages expose volcanic stratigraphy. Basal pyroclastic deposits containing inclusions of

prismatically jointed blocks crop out on all sides of unit *Qapb* and are most commonly preserved in regions of low topographic relief. The ~70-130-m-thick lavas are geochemically variable (58.4-68.8 wt% SiO₂) over the unit's areal extent and several populations of mafic and rhyodacitic inclusions were identified within a drainage off the Pacific Crest National Scenic Trail (**fig. 3.6**). Bands of crystal-rich rhyodacite are common in basal flows. Mineralogically, unit *Qapb* comprises plagioclase, ortho- and clinopyroxene, and, rarely, olivine phenocrysts arranged in 1-2 mm glomerocrysts.

Unit *Qapb* is cut by a series of north-northwest-striking dacite dikes, including a feeder dike for the dacite dome of Park Butte (0.118±0.024 Ma). These dikes are amphibole-rich in composition and collectively referred to as the dacite of Park Butte (unit *Qdpb*, **fig. 3.7**). Unit *Qdpb* is geochemically variable (58.4-68.8 wt% SiO₂) but texturally simple (massive). Plagioclase and amphibole are the dominant phases, with only 1-2% ortho- and clinopyroxene combined. Mineral phases typically form independently within a glassy groundmass, but clusters of four to five plagioclase laths are common. Palagonitized basal scoria in unit *Qapb*, glassy, prismatic jointing in unit *Qdpb*, and marine oxygen isotope records indicating a cold stage between 100 and 200 ka suggest eruption of both Park Butte units occurred during a glacial epoch.



Figure 3.5. Jefferson Park and Mount Jefferson volcano looking south from Cascade crest. Whitewater Glacier (WG), Jefferson Park Glacier (JPG), Russell Glacier (RG), and Russell Creek drainage as shown.



Figure 3.6. Examples of inclusions in andesite of Park Butte. a, typical platy andesite, no inclusions visible; b-d, atypical inclusions.



Figure 3.7. Dacite of Park Butte (*Qdpb*) (left) and amphibole-rich phenocryst assemblage (right).

3.3.3 Basaltic andesite of Whiskey Creek

The Pleistocene age basaltic andesite of Whiskey Creek (*Qbawh*, **fig. 3.8**) consists of four ~50-100-m-high glassy domes located about 9.5 km south of Mount Jefferson volcano and 0.3 to 0.7 km west of the Pacific Crest Scenic Trail. This part of the Mount Jefferson area consists almost exclusively of basaltic andesite domes and lava flows (e.g., basaltic andesite of Forked Butte and Jefferson Lake Trail) that are Pleistocene to Holocene in age. Unit *Qbawh* lies between North and South Cinder Peaks. Similar to unit *Qawc*, the chemical variation of unit *Qbawh* is relatively limited (54.9-55.4 wt % SiO₂). Lithologically, the unit is more diverse and contains both sparsely porphyritic and highly porphyritic extrusions. The plagioclase, olivine, and ortho- and clinopyroxene phenocrysts commonly form glomerocrysts within a glassy groundmass. Similar chemistry, apparent ages, degree of erosion, and glassy character suggest the four domes are magmatically related and were erupted intraglacially.



Figure 3.8. Basaltic andesite of Whiskey Creek (*Qbawh*) tuya.

3.4 Methods

3.4.1 Field Work and Sample Selection:

Fieldwork was completed over three weeks during the summer of 2014. 38 samples were collected from lavas flows and domes of various ages (~150 to 30 ka) and compositions (54.12 - 64.84 wt% SiO₂). One basaltic andesite and two andesite lavas were sampled spanning the observed range of erupted compositions at the volcano, including the andesite of Whitewater

Glacier (*Qawc*), andesite of Park Butte (*Qapb*), and basaltic andesite of Whiskey Creek (*Qbawh*)

(fig. 3.3) Samples were also collected from dacite dikes intruding the andesite of Park Butte.

Emphasis was placed on sampling textural changes within units. Sample locations were noted on 1-10 m resolution orthoimagery and air photos and recorded using a Garmin eTrex 30. Transects crossed from peak to valley of unit *Qapb*, along the quenched interface of unit *Qawc*, and from all three domes of *Qbawh*. Sample locations and brief rock descriptions are provided in **digital appendix I**.

3.4.2 Analytical Approach:

3.4.2.1 *Petrographic thin section analysis*

Polished thin sections were prepared from 18 samples (**table 2.2**) representing the temporal, spatial, and compositional spectrum of the dataset at Spectrum Petrographic in Vancouver, WA. Variation in mineral assemblages and textures were photographed using a Nikon digital camera DXM1200 and an Epson Perfection 4990 Photo Scanner at 1200 dpi resolution in preparation for in-situ analyses.

3.4.2.2 *XRF and ICP-MS*

Major and trace element whole rock data were collected for 8 representative samples (**table 2.2**) using the ThermoARL Advant'XP sequential X-ray fluorescence spectrometer (XRF) and Agilent 7700 Inductively Coupled Plasma Mass Spectrometer (ICP-MS) at the Washington State University Geoanalytical Lab. Weathered, altered, and oxidized surfaces were removed prior to analysis. Analytical methods are detailed in Johnson et al. (1999) and Knaack et al. (1994).

3.4.2.3 Electron Microprobe Analysis

Major and trace element data were collected for individual plagioclase, amphibole, orthopyroxene, and clinopyroxene phenocrysts in selected samples. The majority of data presented in this paper were collected using electron microprobe analysis (EMPA) at Oregon State University equipped with five wavelength-dispersive spectrometers (WDS), one energy-dispersive spectrometer (EDS), and a high-speed backscattered (BSE) electron imaging system. A total of 763 chemical analyses were obtained from 214 phenocrysts from 11 representative samples (**table 2.3**). Of these, 102 plagioclase, 38 amphibole, 24 orthopyroxene, and 28 clinopyroxene phenocrysts were used in calibrating thermobarometry experiments. 5 to 20 step transects were completed on an additional 22 plagioclase grains to gauge variation in composition across crystals. All analyses were conducted using a spot size of 1 μm , beam intensity of 30 nA, and accelerating voltage of 15 keV. Analyses were calibrated using in-house LABR, KHOR, and KAUG standards for plagioclase, amphibole, and pyroxene, respectively. Compositional data and analytical uncertainties are shown in **digital appendix II**.

Table 2.2. Types of analysis completed on each sample in the MJA.

Sample	Unit	Thin-section	EMP	LA-ICP-MS	XRF/ICP-MS
Qawc-14	Andesite of Whitewater Creek	X	X		X
Qawc-16	Andesite of Whitewater Creek	X	X		
Qawc-17	Andesite of Whitewater Creek	X	X		X
Qawc-19-a	Andesite of Whitewater Creek	X	X		
Qawc-20-a	Andesite of Whitewater Creek	X	X	X	X
Qawc-22	Andesite of Whitewater Creek	X	X		
Qapb-10	Andesite of Park Butte	X	X	X	X
Qapb-12-a	Andesite of Park Butte	X			
Qapb-12-bi	Andesite of Park Butte	X			
Qapb-12-bii	Andesite of Park Butte	X			
Qapb-12-c	Andesite of Park Butte	X	X	X	X
Qapb-13-b	Andesite of Park Butte	X			
Qapb-14	Andesite of Park Butte	X			
Qdpb-5	Dacite of Park Butte	X	X	X	X
Qbawh-1	Basaltic andesite of Whiskey Creek	X			
Qbawh-2	Basaltic andesite of Whiskey Creek	X	X	X	X
Qbawh-3	Basaltic andesite of Whiskey Creek	X	X	X	X
Qbawh-4	Basaltic andesite of Whiskey Creek	X			

3.4.2.3.1 Determining Intensive Parameters from electron microprobe data

Intensive parameters were calculated from plagioclase, amphibole, clinopyroxene, and orthopyroxene using three independent methods. The first employs the Microsoft Excel Amp-TB spreadsheet (Ridolfi et al., 2010), which calculates pressure, temperature, water content of the melt, and oxygen fugacity (fO_2). The model was applied to amphibole composition of 38 phenocrysts. Though accurate to some extent, application of the algorithm is limited by the assumption that amphibole crystallized in equilibrium with a calc-alkaline melt and that small fluctuations in intensive parameters trigger re-equilibration of the crystallizing assemblage. Additionally, results are restricted to approximately 765 to 1065°C, ΔNNO between -0.3 and 2.5, and H₂O melt between 3.4 and 10.6 wt%, precluding use of this application for anhydrous and/or mafic compositions.

Together, the Holland and Blundy (1994) and Anderson and Smith (1995) calibrations define the second independent method of estimating intensive parameters. In this technique, 102

plagioclase and 38 amphibole crystals appearing to be in equilibrium were selected for analysis. Criterion for equilibrium assemblages includes touching pairs or, commonly, plagioclase inclusions inside amphibole. Crystals with large breakdown rims or dissolution cores were avoided. Errors are approximately $\pm 30^\circ \text{C}$ and 0.5 kbar for temperatures between 400 and 1000°C and pressures 1-15 kbar (Anderson and Smith, 1995; Bachmann and Dungan, 2002).

A third method, two-pyroxene thermobarometry, was also investigated by analysis of touching clinopyroxene-orthopyroxene pairs and using the revised calculations (equation 37) discussed in Putirka (2008). Pressure estimates are obtained using equation 39 of Putirka (2008). Equilibrium conditions for pyroxene pairs include adjacent crystals, orthopyroxene cores with clinopyroxene rims, and rarely, crystals not in direct contact but part of the same glomerocryst.

Eqn. 37:

$$\frac{10^4}{T(^{\circ}\text{C})} = 13.4 - 3.4 \ln\left(\frac{X_{EnFs}^{cpx}}{X_{EnFs}^{opx}}\right) + 5.59 \ln(X_{Mg}^{cpx}) - 8.8(Mg\#^{cpx}) + 23.85(X_{Mn}^{opx}) \\ + 6.48(X_{FmAl_2SiO_6}^{opx}) - 2.38(X_{Di}^{cpx}) - 0.044P(\text{kbar})$$

Eqn. 39:

$$P(\text{kbar}) = -94.25 + 0.045T(^{\circ}\text{C}) + 187.7(X_{Al(VI)}^{opx}) + 246.8(X_{Fm_2Si_2O_6}^{opx}) - 212.5(X_{En}^{opx}) \\ + 127.5(a_{En}^{opx}) - \frac{1.66}{K_f} - 69.4(X_{EnFs}^{cpx}) - 133.9(a_{Di}^{cpx})$$

3.4.2.4 Laser Ablation ICP-MS Analysis:

Trace element concentrations were measured in 76 plagioclase and 20 amphibole crystals from 6 samples (**table 2.2**) with LA-ICP-MS using a Photon Machines Analyte G2 193 nm ArF-

“fast”-Excimer laser system and Thermoscientific X Series 2 Quadrupole ICP-MS systems in the W.M. Keck Collaboratory for Plasma Mass Spectrometry at Oregon State University.

Compositional data and instrument parameters for samples are shown in **digital appendix III**.

Where possible, LA-ICP-MS points were picked adjacent to those analyzed on the EMPA.

3.4.2.4.1 Trace Element Inversions

Reconstruction of primary melt compositions of trace elements Sr and Ba in the liquidus phase are calculated for 39 plagioclase phenocrysts in four samples encompassing the four stratigraphic units in **table 3.1**. Plagioclase-melt partition coefficients were determined for Sr and Ba using models from Blundy and Wood (1991) and Bindeman et al. (1998). These models make the assumption that trace element partitioning is largely dependent upon anorthite content and, to a lesser degree, temperature and magma composition. Calculations follow equations 18 and 19 from Blundy and Wood (1991).

$$[18] \quad RT \ln D_{Sr} = 26,800 - 26,700 \cdot X_{An}$$

$$[19] \quad RT \ln D_{Ba} = 10,200 - 38,200 \cdot X_{An}$$

Where R is equal to the gas constant (8.314 J/K·mol), T is equal to temperature (K), D is the partition coefficient (J/mol) of a given trace element (Sr or Ba), and X_{An} is anorthite content (mol%). Temperature is estimated from amphibole (Ridolfi et al., 2010), plagioclase-amphibole (Holland and Blundy, 1994 and Anderson and Smith, 1995) and two-pyroxene (Putirka, 2008) geothermometry experiments. Anorthite content is measured from electron microprobe point analyses on plagioclase crystals. Equations 18 and 19 are rearranged to solve for partition coefficients of Sr (eqn 20) and Ba (eqn 21):

$$[20] \quad D_{Sr} = \frac{e^{(26,800 - 26,700 \cdot X_{An})}}{RT}$$

$$[21] \quad D_{Ba} = \frac{e^{(10,200 - 38,200 \cdot X_{An})}}{RT}$$

Equations 20 and 21 are then rearranged to solve for the concentration of Ba and Sr in the melt ($[Ba, Sr]_{melt}$) (eqns. 22 and 23).

$$[22] \quad D_{Sr} = \frac{[Sr]_{crystal}}{[Sr]_{melt}} \quad D_{Ba} = \frac{[Ba]_{crystal}}{[Ba]_{melt}}$$

$$[23] \quad [Sr]_{melt} = \frac{[Sr]_{crystal}}{D_{Sr}} \quad [Ba]_{melt} = \frac{[Ba]_{crystal}}{D_{Ba}}$$

3.5 Petrography

3.5.1 Andesite of Whitewater Creek

Thin sections were prepared for the six samples collected from the andesite of Whitewater Creek. Rocks of *Qawc* are approximately 50-55% phenocrysts and 45-50% groundmass; phenocryst proportions are 70-85 vol% plagioclase, ~10-15 vol% amphibole, 5-10 vol% orthopyroxene, and 2-10 vol% clinopyroxene. Glomerocrysts up to 5 mm are common, typically present as plagioclase + orthopyroxene + clinopyroxene. Clinopyroxene or orthopyroxene tends to compose the core of the glomerocrysts while plagioclase fills interstices and accretes to external grain boundaries. Amphibole is sparse in glomerocrysts. One sample (*Qawc-16*) exhibits pockets of brown glass appearing to preserve cooling lobes and an almost sandy texture.

Plagioclase phenocrysts have sizes of 0.1-1.8 mm and are divided into two groups on basis of size, morphology, and texture. Group 1 plagioclase grains are small (0.1-0.4 mm), euhedral elongate laths, and typically exhibit albite and synthetic twinning. Group 1 phenocrysts

are generally unaltered, though often fringe the edges of glomerocrysts or are enclosed as inclusions in other mineral phases. Mineral inclusions are rare in Group 1 crystals. Group 2 plagioclase grains are larger (0.4-1.8 mm), appear square to blocky, and often display serrated, tattered, or broken edges. Patchy to oscillatory zoning is common, and pervasive disequilibrium textures such as resorbed rims, sieved cores, and grain fragmentation, are evident. The largest crystals typically have sieved cores enclosed by an unaltered rim. Reverse sieves (sieved rim, undeformed cores) and undeformed crystals were also observed. Orthopyroxene and clinopyroxene inclusions are observed in ~5-10% of the large plagioclase grains, and melt inclusions are ubiquitous in both Groups 1 and 2 plagioclase. Melt inclusion morphology varies greatly from 10-20 μm spheres and squares to large (up to 500 μm) irregular-shaped globules and tubes.

Amphibole phenocrysts, largely undeformed and euhedral, range in size from ~0.2-1 mm, though some phenocrysts are as large as 2.5 mm (measured lengthwise). Subhedral morphologies vary from elongate and prismatic to tapered ovals to rhombohedral. Rhombohedral phenocrysts are often broken or embayed around a plagioclase crystal. Partially resorbed amphibole rims vary in width from about 20 to 100 μm . Amphibole rarely exists independently of other mineral phases, forming clusters with adjoining amphibole crystals or plagioclase. Plagioclase typically forms interstitially in amphibole clusters and is observed as inclusions in nearly all amphibole phenocrysts.

Orthopyroxene generally ranges from about 150 to 650 μm , with the largest phenocryst measured at 900 μm . Grains are euhedral to subhedral and usually squareish to slightly elongate. Edges are often rounded. No notable disequilibrium textures are observed, though fracture patterns perpendicular to cleavage planes and tattered edges are common. Mineral inclusions are

uncommon; however, holes in the orthopyroxene phenocrysts indicate inclusions may have been plucked at some point in the magmatic history. Melt inclusions are abundant, ranging from 20-30 μm to 200 μm . Orthopyroxene rarely forms solitary crystals; instead, it typically appears as slightly deformed cores within plagioclase \pm clinopyroxene \pm amphibole glomerocrysts.

Clinopyroxene phenocrysts are similar in size and abundance to orthopyroxene, with euhedral to anhedral grains ranging from \sim 200 to 900 μm . Crystals are predominantly subhedral to anhedral, fractured, and twinned. Surfaces are deformed, and morphology of original grain boundaries is often undiscernible due to tattered edges and incomplete crystal morphology. New clinopyroxene growth frequently replaces corroded plagioclase laths. Subophitic and ophitic textures are common. Petrographic microphotographs are shown in **figure 3.9** and Petrographic descriptions of all four stratigraphic units is detailed in **digital appendix IV**.

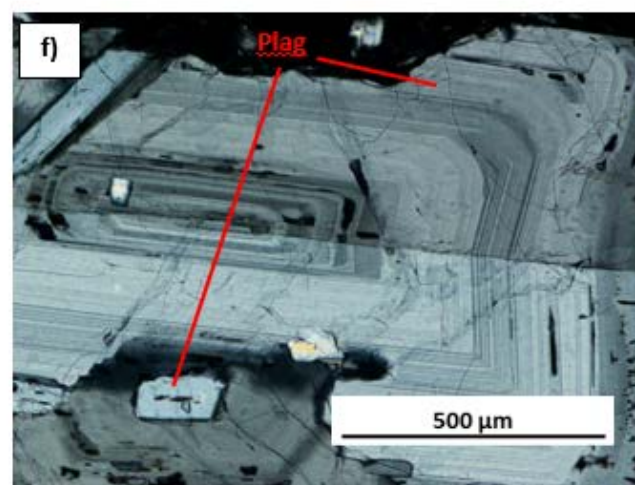
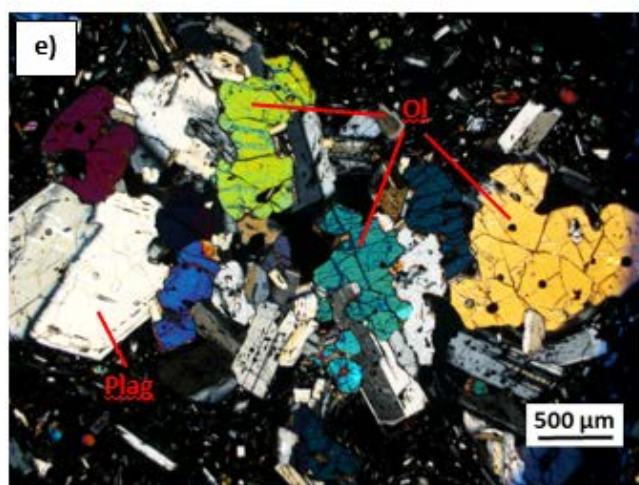
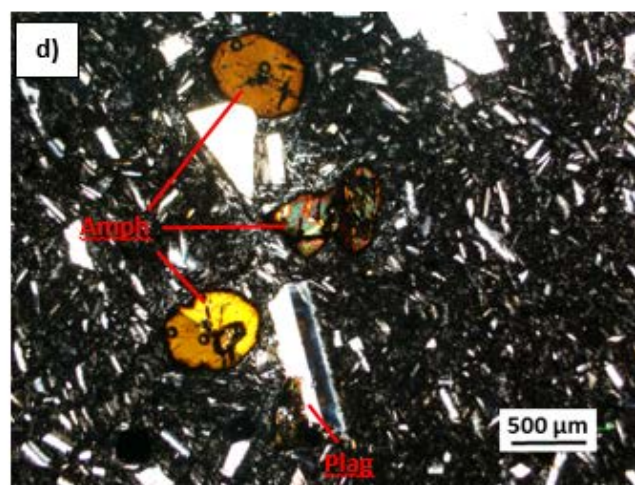
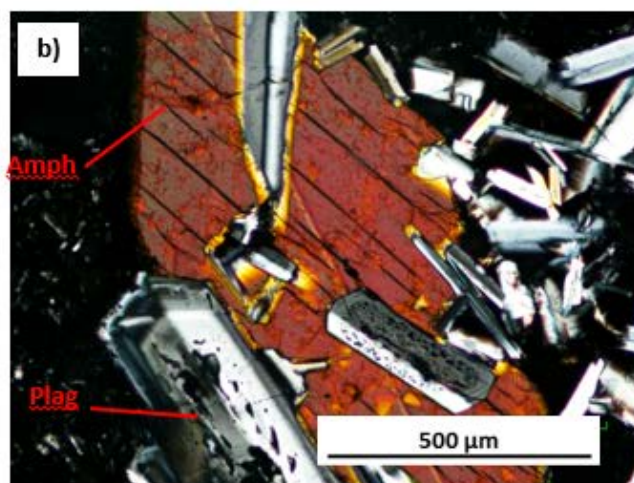
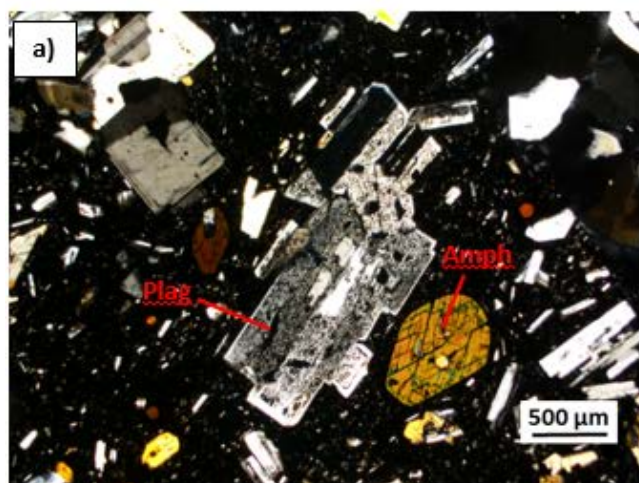


Figure 3.9. Photomicrographs of MJA thin-sections. a) Group 2 (400-1800 μm) plagioclase (Plag) phenocryst with sieved interior and equant amphibole in *Qawc-22*. Group 1 (125-400 μm) plagioclase is abundant in surrounding matrix. b) Amphibole (Amph) phenocryst with abundant plagioclase inclusions of variable morphology and textures in *Qawc-17*. c) Orthopyroxene (Opx) + plagioclase glomerocryst in *Qapb-14*. Note irregular grain boundaries and clinopyroxene (Cpx) mineral inclusions. d) Amphibole and plagioclase phenocrysts within fine-grained groundmass in *Qdpb-5*. Many of the amphiboles exhibit resorbed cores and reaction rims ~ 30 to $40 \mu\text{m}$ wide. e) $\sim 2,500 \mu\text{m}$ olivine (Ol) + plagioclase glomerocryst in *Qbawh-2*. Pervasive alteration to iddingsite is common along fracture planes or along rims of most phenocrysts. f) Complex, oscillatory zoned plagioclase phenocryst with fragmented grain boundaries and aggregated plagioclase inclusions along edges in *Qbawh-4*.

3.5.2 Andesite of Park Butte

Thin sections were prepared for six of the seven samples collected from the andesite of Park Butte. The samples are from a transect from the basal quench zone (early eruptive products) to the fresh crest (late eruptive products) of the unit, as well as a central dacite plug and are highly variable in mineralogy and texture. Several inclusions were sampled in thin-sections *Qapb-12-a*, *Qapb-12-b*, and *Qapb-12-c*. The groundmass forms 45 to 70 vol% of samples and varies from quenched glass with needle-like plagioclase microlites to a cryptocrystalline vesicular matrix. Phenocrysts range from 35 to 65 vol% and mineral assemblages are 65-80 vol% plagioclase, 10-20 vol% orthopyroxene, 5-10 vol% clinopyroxene, and <1 vol% olivine. Glomerocrysts of size ~1.2-1.7 mm are abundant as plagioclase clusters or resorbed accretions of plagioclase + orthopyroxene + clinopyroxene. A light-colored vesicular material is observed in *Qapb-12-b*; which includes ~200 µm phenocrysts of plagioclase, orthopyroxene, and brown glass.

Plagioclase crystals are generally 150-1,000 µm though can be as large as 2,100 µm. Plagioclase phenocrysts in unit *Qapb* display zoning patterns that range from simple monotonous to complex oscillatory and can be divided into Group 1 and Group 2 populations using the same criteria discussed in the above (*Qawc*) section. Group 1 phenocrysts are elongate laths, nearly always euhedral, and monotonous to lightly sieved. The Group 2 plagioclase population is subhedral to anhedral and square to tabular with fragmented grain boundaries or rounded edges that appear “eroded.” Complex disequilibrium textures are pervasive in Group 2 population including sieved to wormy textures affecting part or all of the crystal, deeply corroded cores, and resorbed rims. Alteration to sericite, a common alteration mineral of plagioclase, is observed in

sample *Qapb-12-bii*. Acicular to rounded melt inclusions are observed in nearly all plagioclase grains from both Group 1 and 2 with occasional orthopyroxene mineral inclusions.

Orthopyroxene and clinopyroxene phenocrysts often occur together and typically range in size from 150 to 625 μm . Phenocryst shapes range from euhedral grains prismatic, square, or blocky in appearance to anhedral grains which are fragmented with irregular to rounded crystal boundaries. Alterations products are common and plagioclase frequently replaces resorbed cores, particularly in clinopyroxene. Pyroxene crystals in several samples have melt inclusion-rich rims and occur as inclusions in other pyroxene grains, as coronas along the boundaries of plagioclase grains, and as a common vesicle-filling material in sample *Qapb-14*. 150-300 μm euhedral plagioclase is the most prevalent mineral inclusion in pyroxene crystals and occurs in ophitic and subophitic textures. Olivine is rare in unit *Qapb* and predominantly occurs as 250-300 μm grains in glomerocrysts or, less commonly, as isolated crystals in the groundmass. Crystals are predominantly euhedral to subhedral, exhibiting hexagonal to slightly deformed morphologies. Alteration to iddingsite is common along fractures, often paired with a corona of amorphous orthopyroxene around the rim. Plagioclase is the predominant mineral inclusion within olivine, and 10-20 μm melt inclusions are present in most crystals.

One sampled dacite is also discussed with the andesite of Park Butte. The dacite of Park Butte is composed of 88 vol% plagioclase, 10 vol% amphibole, and 2 vol% pyroxene (orthopyroxene and clinopyroxene) within a fine-grained matrix constituting 70 vol% of the sample. Plagioclase phenocrysts are 500-1300 μm , predominantly euhedral to subhedral, and have tabular, elongate, and blocky morphologies. Disequilibrium textures are less prevalent than in *Qapb*, and grains are mostly unaltered with the exception of slight resorption along grain boundaries. Mineral and melt inclusions are uncommon in plagioclase. Amphibole phenocrysts

have sizes of 500-750 μm , are predominantly euhedral to subhedral in form, and exhibit equant to elongate prisms or slightly rounded shapes. Crystals have partially to completely resorbed cores, 30-40 μm wide reaction rims, and ubiquitous plagioclase inclusions. Pyroxene phenocrysts are \sim 500 μm and subhedral. Crystal shapes are elongate with tapered to blocky crystal boundaries. Resorption textures and orthopyroxene mineral inclusions are common.

3.5.3 Basaltic Andesite of Whiskey Creek

Thin sections were prepared for the four samples collected from the basaltic andesite of Whiskey Creek. The rocks are composed of 65% phenocrysts within a fine-grained, plagioclase-rich, and occasionally glassy, groundmass. Of the phenocryst phases, 60-70 vol% are plagioclase, 15-35 vol% are olivine, and 5-10 vol% are ortho- and clinopyroxene. Plagioclase + olivine clusters 600-2,250 μm are the predominant glomerocryst assemblage followed by plagioclase + pyroxene.

Plagioclase phenocrysts range in size from about 150 to 1,250 μm and euhedral to subhedral. Morphologies are predominantly elongate laths. Secondary morphologies include equant blocks and rounded fragments. Zoning patterns vary from unzoned (monotonous) to patchy to oscillatory. As with the previous two units, two populations of plagioclase are observed within *Qbawh* samples and the criteria are discussed above. Sieving is observed to varying degrees within all plagioclase grains, from mild (little sieving and limited to core) in Group 1 crystals to severe (multiple sieve zones in concentrically zoned crystals and multiple areas in patchy zoned crystals) in Group 2 crystals. Resorption along grain boundaries is also a very common texture. Melt inclusions are prevalent. Mineral inclusions are less common, with the exception of partially intruding plagioclase and occasional pyroxene remineralizations where resorption has removed much of the original plagioclase mineral

Olivine grains typically range from 150 to 750 μm and can grow as large as 900 μm . Crystals are generally euhedral. Minimal to severe dissolution is exhibited in the cores of grains and pervasive alteration to iddingsite is common along fracture planes or along rims of most phenocrysts. Poikilitic inclusion of plagioclase and pyroxene is frequently observed across all samples. Olivine is found predominantly in clusters with other olivine grains of varying size.

Pyroxene is 400 to 1000 μm in size and generally subhedral. Crystal morphology varies greatly and includes equant prisms, rounded ovular forms, or fragmented grains predominant in glomerocrysts. Resorbed rims 10-20 μm wide are ubiquitous and patchy dissolution and complex dissolution cores form the interior of many crystals. Melt inclusions are rare; mineral inclusions are mostly limited to equant plagioclase 100 μm or smaller.

3.6 Geochemistry

3.6.1 Andesite of Whitewater Creek

The major element chemistry of the *Qawc* samples (**digital appendix V**) exhibits limited variation. All compositions plot within the andesite field on a TAS diagram (LeBas, 1986; **fig. 3.10**). Samples contain 24.9 to 31.4 wt% MgO and 61 to 62 wt% SiO₂ (**fig. 3.11**) Trace element chemistry (**digital appendix VI**) is limited as well, with Sr and Ba concentrations between 496 and 558 and 249 to 306 ppm, respectively (**fig. 3.12**). Plagioclase crystals analyzed using EMPA have mineral compositions of An₆₁₋₉₃, with a mean composition of An₈₀ (**fig. 3.13**). The compositions of MJA pyroxenes and amphiboles are shown in **figures 3.14** and **3.15**.

3.6.2 Andesite of Park Butte

The major element chemistry of the *Qapb* samples exhibit more variable compositions, though all compositions still plot within the andesite field of the TAS diagram. Samples range

from 30.5 to 41.8 wt% MgO and 56.7 to 59.3 wt% SiO₂. Trace element chemistry is more variable, with Sr concentrations varying between 269 and 761 ppm and Ba concentrations between 214 and 351 ppm. Plagioclase crystals analyzed using EMPA have mineral compositions of An₆₀₋₇₄ with a mean composition of An₆₉.

The major element chemistry of the *Qdpb* samples is extremely variable when compared to the unit it cross-cuts, *Qapb*. Plotted compositions fall between the dacite and rhyolite fields on the TAS diagram. Samples contain 10.5 to 41.8 wt% MgO and 58.4 to 68.8 wt% SiO₂. Sr concentrations vary from 522 to 573 ppm and Ba concentrations range from 483 to 556 ppm. Anorthite content of plagioclase crystals ranges from An₃₅₋₉₈ with a mean composition of An₆₁.

3.6.3 Basaltic Andesite of Whiskey Creek

Similar to unit *Qawc*, the major element chemistry of the *Qbawh* samples is relatively limited. Plotted compositions fall within the basaltic andesite field of the TAS diagram, with compositions spanning 46.5 to 56.1 wt% MgO and 54.9 to 55.4 wt% SiO₂. Sr and Ba concentrations are 573 to 594 and 218 to 259 ppm, respectively. Anorthite content ranges from An₈₁ to An₈₅, with an average composition of An₈₄.

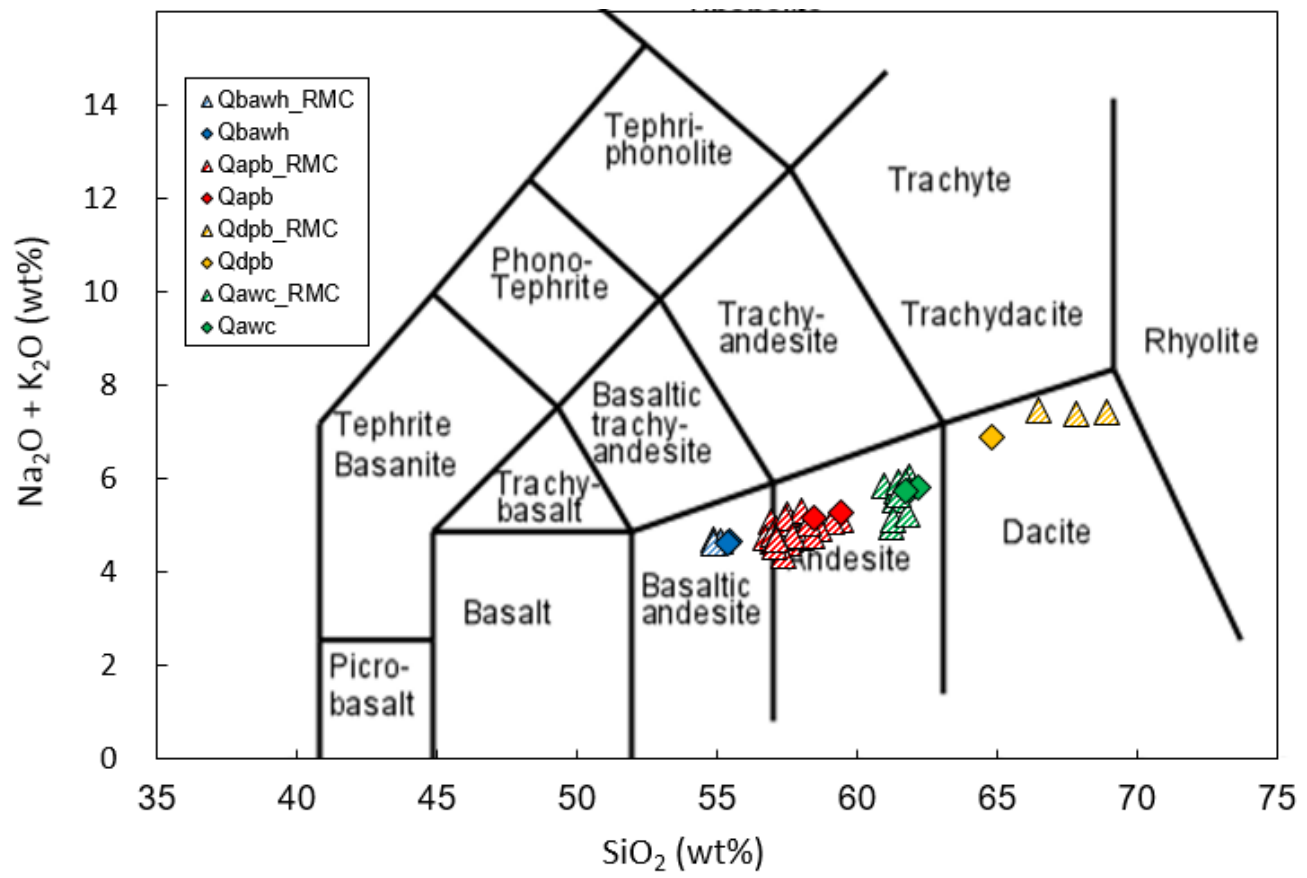


Figure 3.10. Total alkali vs. silica (TAS) diagram (LeBas, 1986) showing compositions of samples from *Qawc*, *Qapb*, and *Qbawh*.

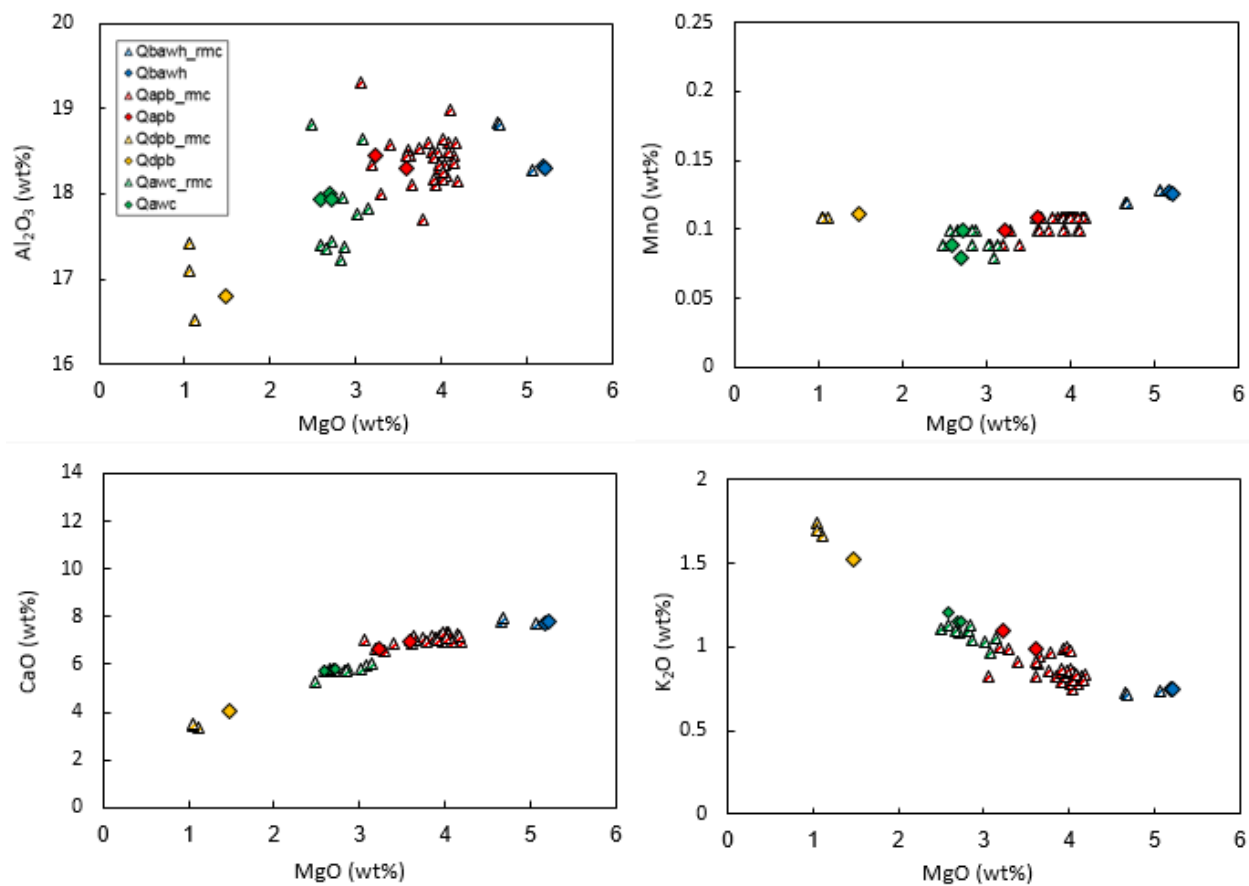


Figure 3.11. Major element variation diagrams from representative units in the MJA.

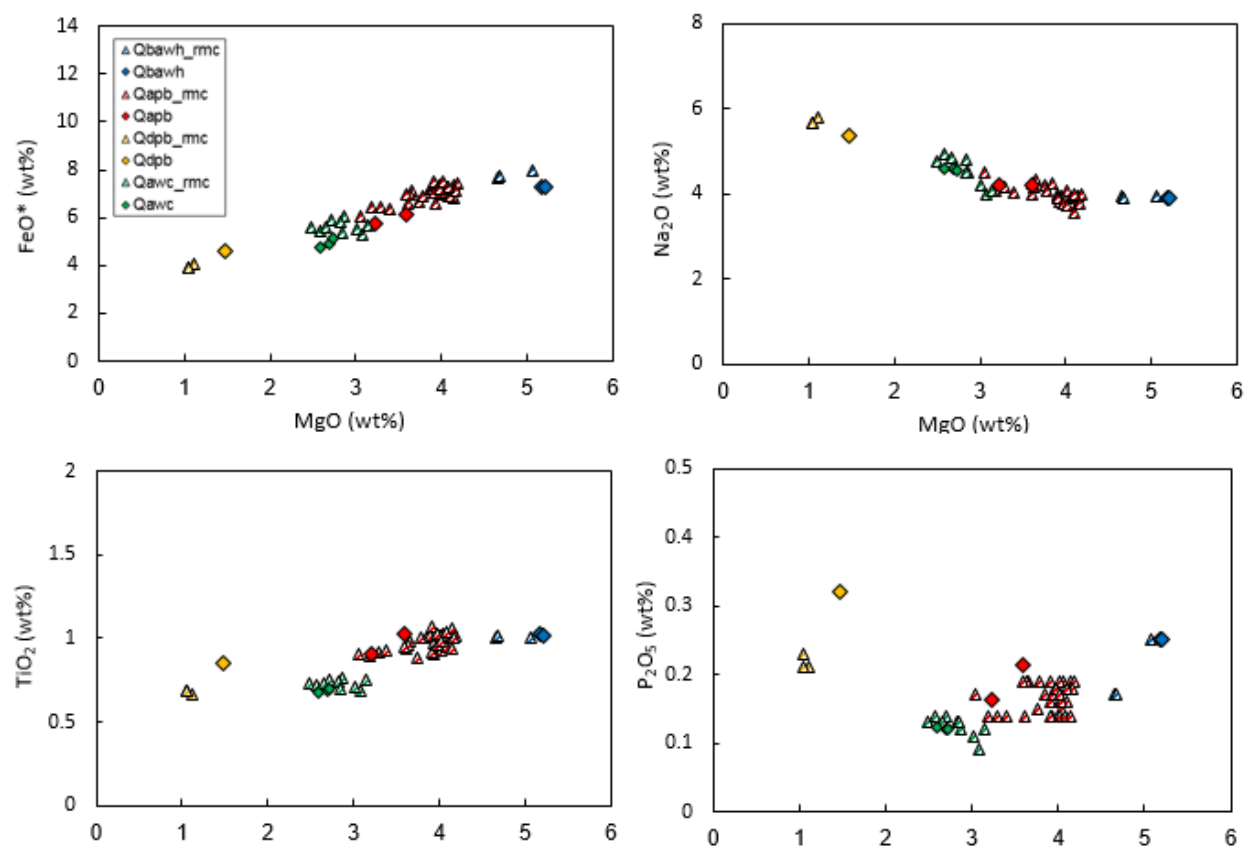


Figure 3.11 (Continued).

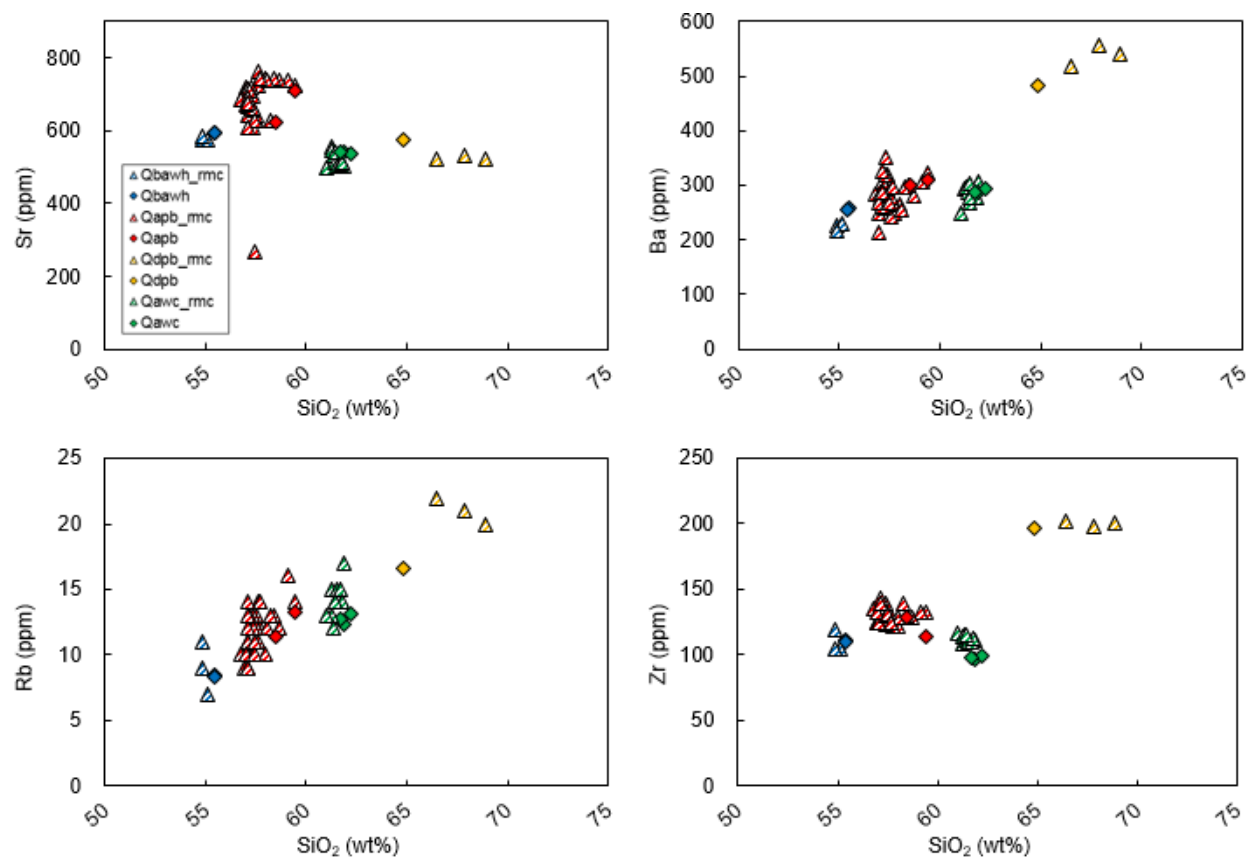


Figure 3.12. Trace element variation diagrams for representative units. Colors as before.

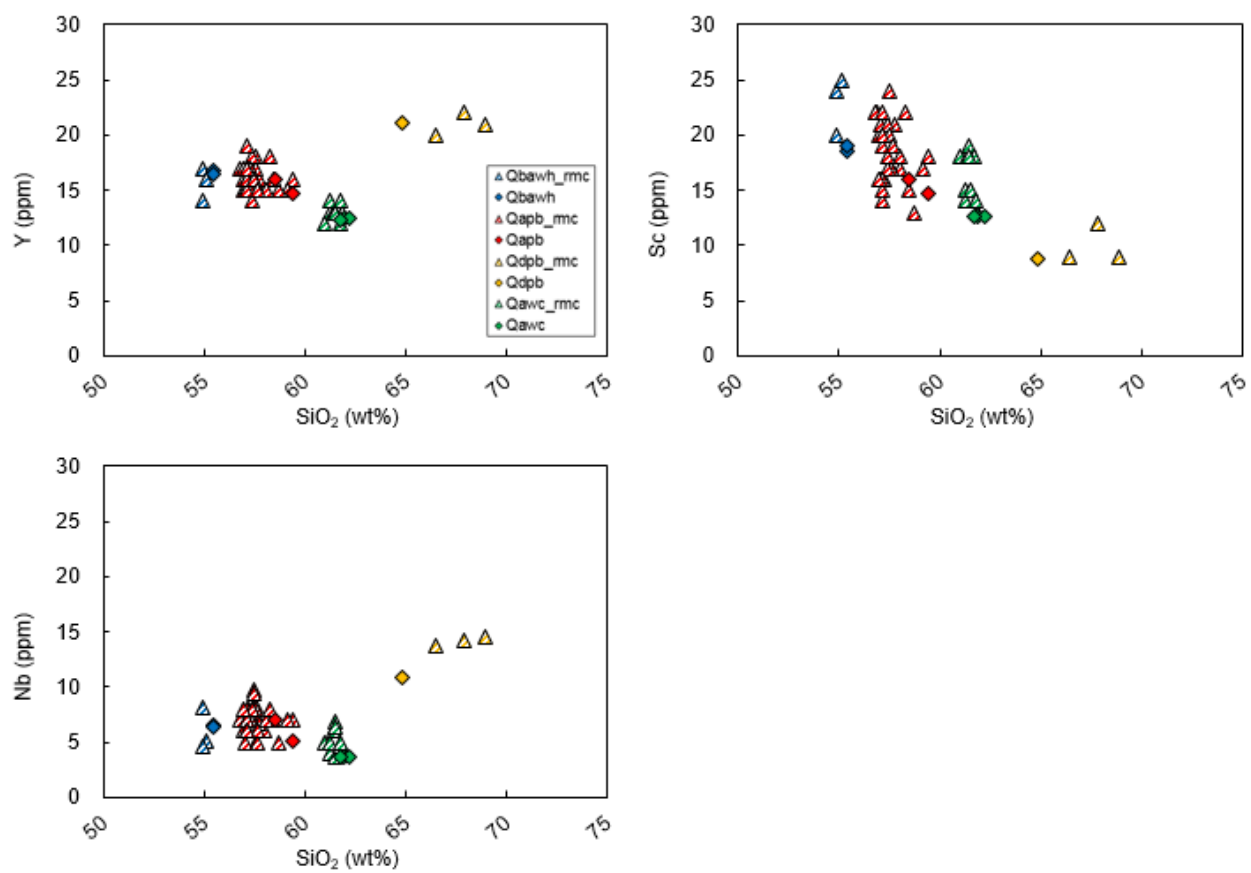


Figure 3.12. (continued).

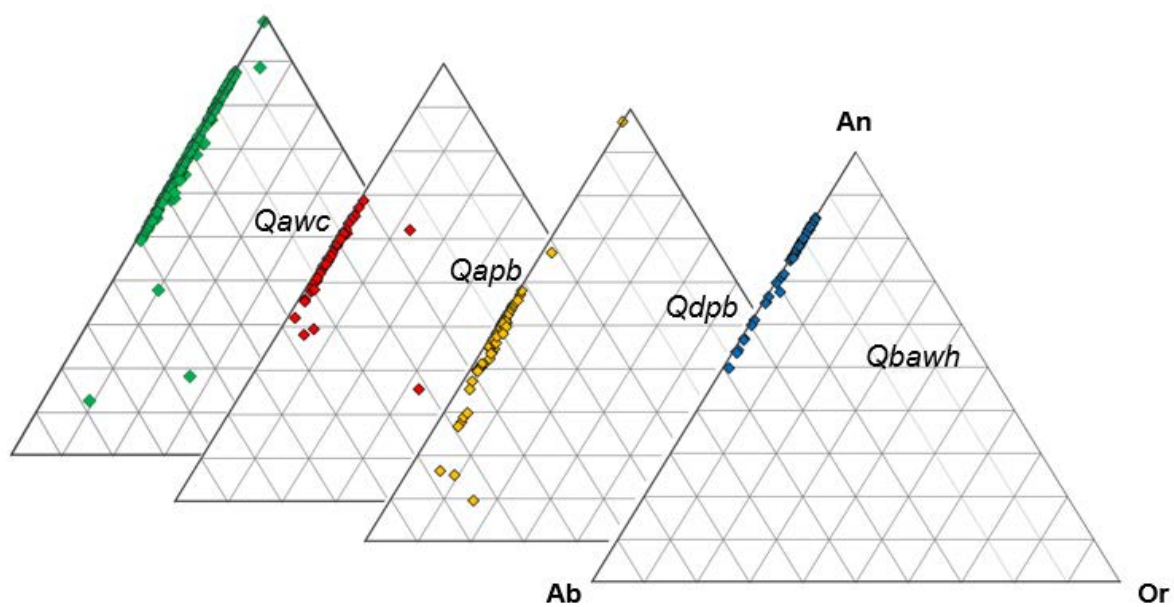


Figure 3.13. Compositions of feldspars from four stratigraphic units in the MJA. Green, unit *Qawc*, Red, *Qapb*, Yellow, *Qdpb*, Blue, *Qbawh*. Ab Albite, An Anorthite, Or Orthoclase.

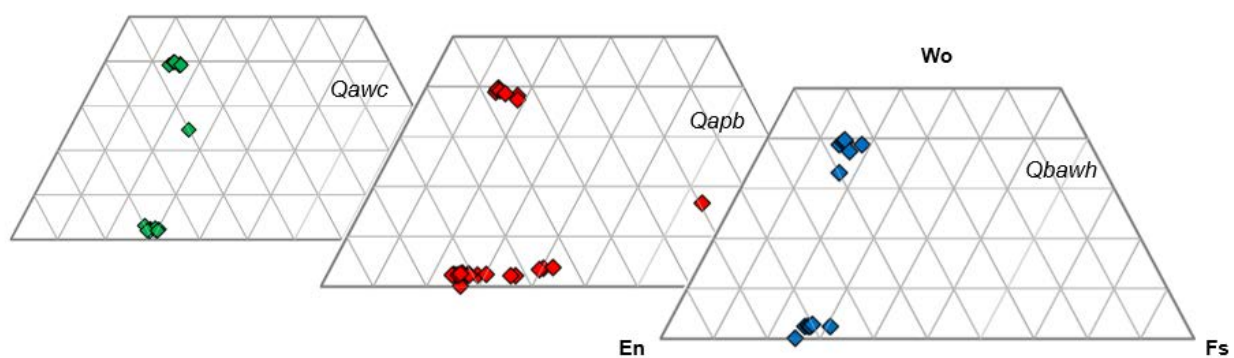


Figure 3.14. Compositions of pyroxenes from four stratigraphic units in the MJA. Green, unit *Qawc*, Red, *Qapb*, Blue, *Qbawh*. En Enstatite, Wo Wollastonite, Fs Ferrosilite.

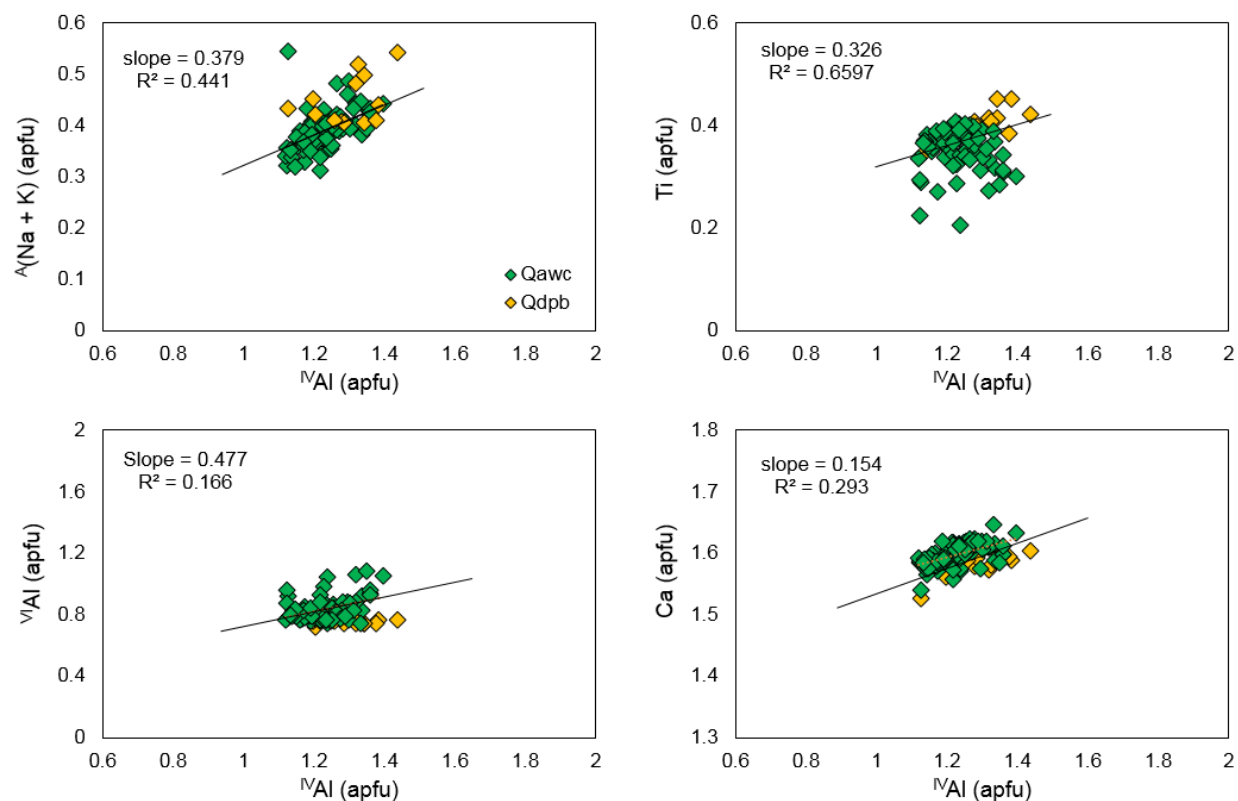


Figure 3.15. Compositions of amphiboles from four stratigraphic units in the MJA. Green, unit *Qawc*; yellow, unit *Qdpb*.

3.7 Thermobarometry

Pressure and temperature were estimated for amphibole, plagioclase, and pyroxene by applying thermobarometric calibrations from three techniques. The first technique utilizes the amphibole thermobarometer from Ridolfi et al. (2010) (hereafter: “Ridolfi model”). This model operates by reconstructing pre-eruptive conditions of amphibole-bearing calc-alkaline magmas residing <40 km depth (<10 kbar) in the earth’s crust. By making the assumption that calc-alkaline magmas crystallize at conditions near the stability boundary of amphibole, conditions may be estimated using the pressure- and temperature-dependent components (^{IV}Al and ^{VI}Al) of a single equilibrium phase. The Ridolfi model was applied to amphiboles from two units in the map area: *Qawc* and *Qdpb*. The overall range of amphibole temperature and pressure estimates is

874 to 973 °C and 1.3 to 4.6 kbar in unit *Qawc* and 832 to 965 °C and 0.9 to 3.5 kbar in unit *Qdpb* (**fig. 3.16**). Several samples from *Qawc* vary little in temperature and pressure, ranging less than 50 °C and 1 kbar (*Qawc*-16, -19, -22). Conversely, two samples (*Qawc*-14 and *Qawc*-17) span the full range of temperatures and pressures. In general, the distribution of pressure and temperature estimates is consistent with the number of analyses collected per sample (i.e., less scatter is observed in samples with fewer EMP analyses) (**digital appendix VI**).

The second technique utilizes the plagioclase-amphibole thermometer and barometer of Holland and Blundy (1994) and Anderson and Smith (1995) hereafter: “HBAS model”, so named after the authors of the model) (**fig. 3.17**). Temperature of the system is estimated by approximating amphibole thermodynamics with a regular solution model, accounting for non-ideality in the crystal structure. Pressure, conversely, is estimated using an Al-in-Hornblende expression which incorporates the effect of temperature on the system on the basis of Al content. As in the Ridolfi model, units *Qawc* and *Qdpb* were analyzed (**fig. 3.18**) to estimate the temperatures and pressures of crystallization. Using the HBAS calibration, the overall range of temperatures and pressures is 535 to 947 °C and 2.2 to 7.2 kbar in unit *Qawc* and 582 to 796 °C and 4.6 to 7.5 kbar in unit *Qdpb*. Temperature and pressure estimates using this technique lack correspondence to those obtained using the Ridolfi calibration: values of the Ridolfi model are consistently higher. In contrast, when the two pressure estimates of the two different models are compared, values of the Ridolfi model are consistently lower. When the two pressure-temperature models are compared side-by-side they are inversely related (**figs. 3.19, 3.20**). For the Ridolfi model, there is a smooth positive trend of pressure with temperature. For the HBAS model, there is a steady negative trend of pressure with temperature. The implications of this inverse relationship are investigated in the discussion.

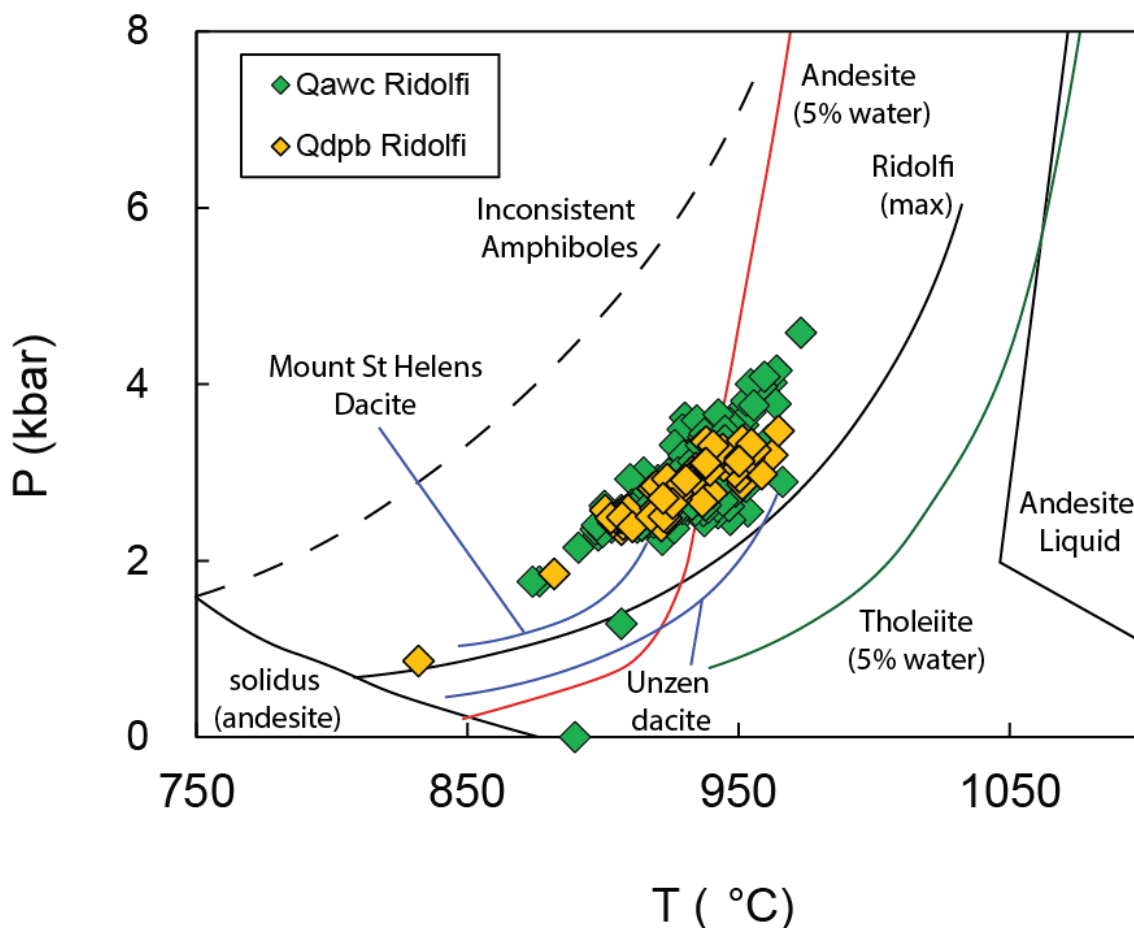


Figure 3.16. All crystallization pressures and temperatures of Mount Jefferson amphibole data as calculated from equations by Ridolfi et al. (2010). No “valid” amphiboles were rejected. The data plotted are the “maximum thermal stability” curve of Ridolfi et al. (2010) along with their line demarking “inconsistent” amphibole P-T conditions amphibole stability. Also shown are amphibole stability curves for tholeiite (from Green, 1982), andesite (Eggler and Burnham, 1973), Mount St. Helens dacite, and Unzen dacite. Note that many analyses yield a temperature higher than the amphibole stability for andesites at 5wt% H₂O. This discrepancy is likely attributable to the tendency of the equations of Ridolfi et al. (2010) to calculate P-Ts along “maximum amphibole stability,” rather than well inside the stability field.

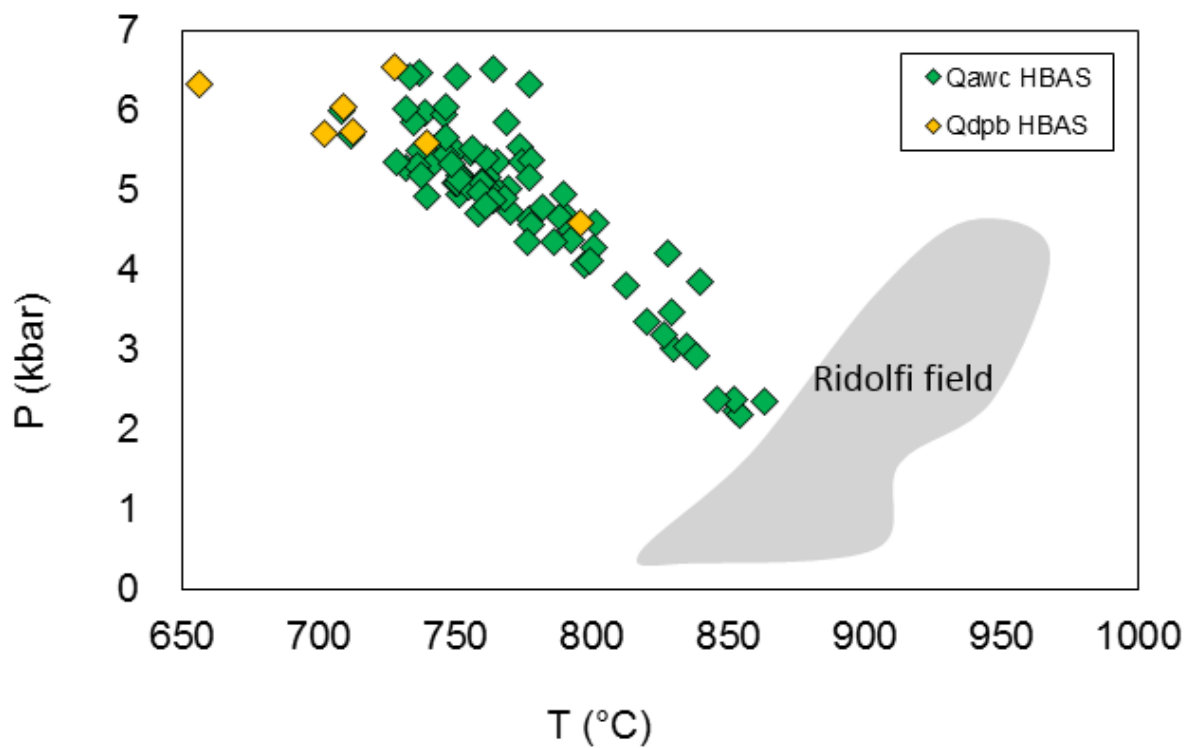


Figure 3.17. Pressure vs temperature as calculated using plagioclase-amphibole pairs. Ridolfi field (simplified from previous figure) shows generally lower pressures and higher temperatures than HBAS values.

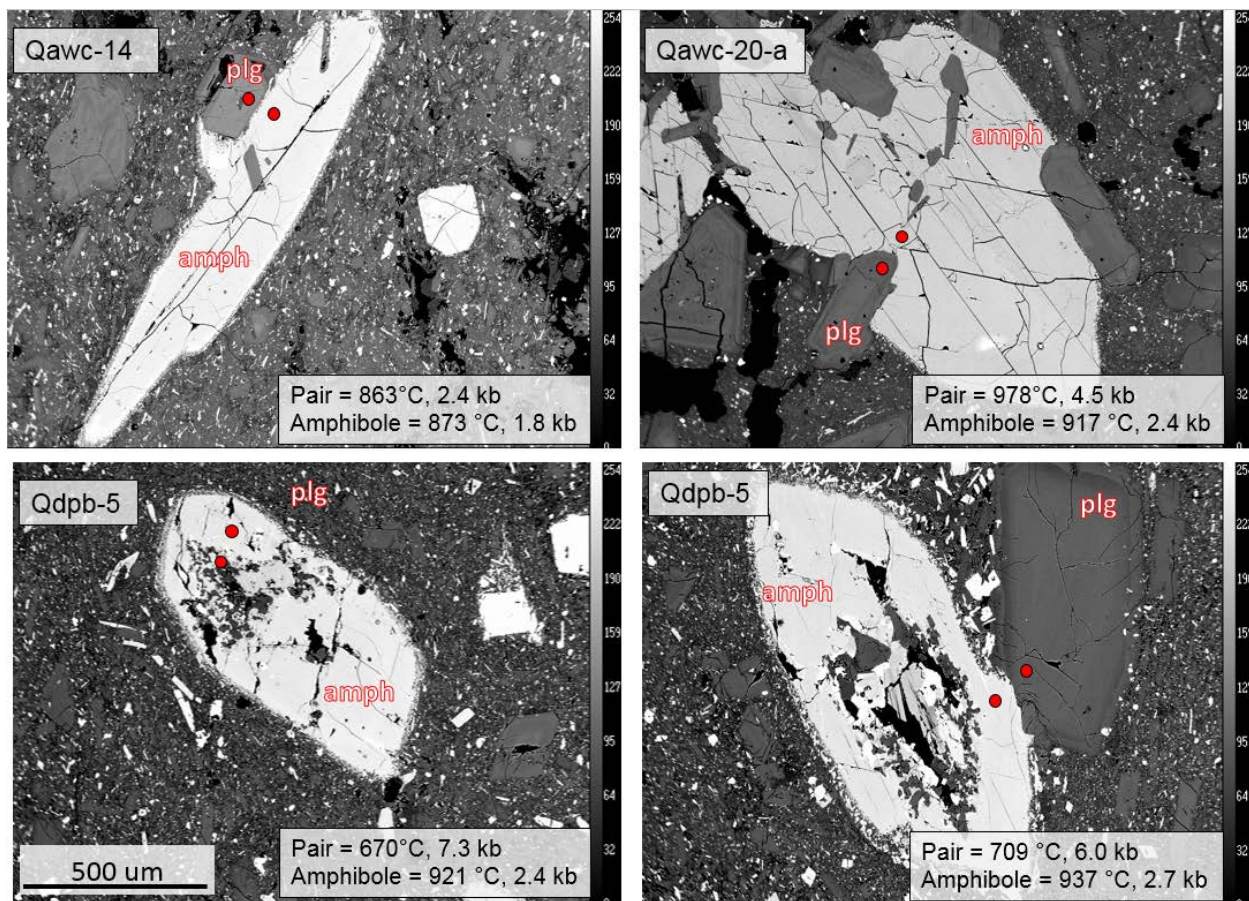


Figure 3.18. Backscattered electron images of selected plagioclase-amphibole pairs.

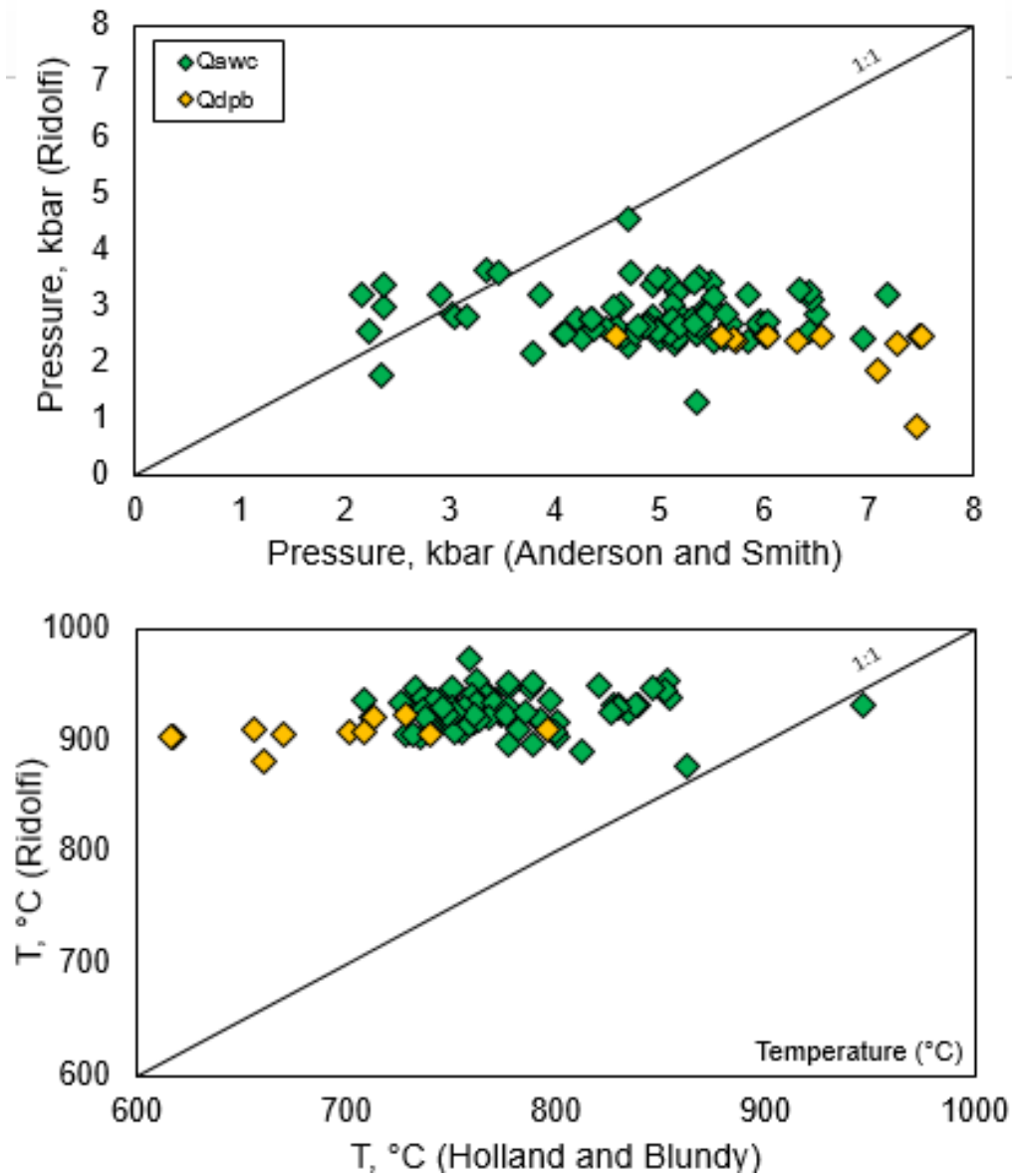


Figure 3.19. Pressure and temperature solutions calculated from Ridolfi et al. (2010) plotted against solutions calculated from Holland and Blundy (1994) and Anderson and Smith (1995).

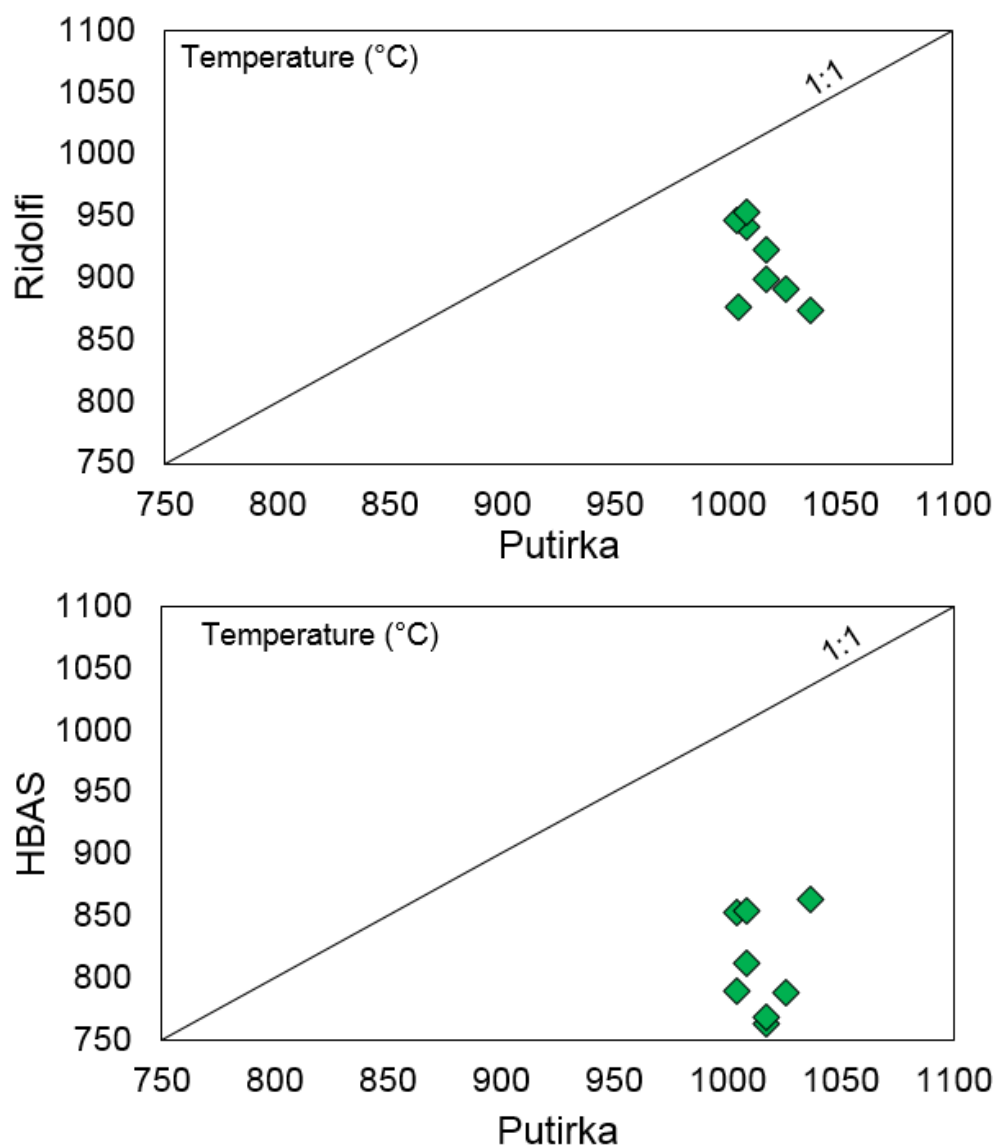


Figure 3.20. Temperature solutions calculated from the Ridolfi and HBAS models plotted against solutions calculated from Putirka (2008) for sample *Qawc-20-a*.

Temperatures and pressures were also obtained for clinopyroxene-orthopyroxene pairs (**fig. 3.21**) in units *Qawc*, *Qapb*, and *Qbawh* using the revised calculations of Putirka (2008) (hereafter: “Putirka model”). The Putirka model estimates pressures and temperatures based on the partitioning between enstatite and diopside, and equilibrium is tested for using Fe-Mg

exchange. Calculations from this model yield temperatures ranging from 1004 to 1036 °C and 1.1 to 7.7 kbar for *Qawc*, 928 to 1136 °C and 0.4 to 9.6 kbar for *Qapb*, and 1020 to 1078 °C and 3.3 to 5.6 kbar for *Qbawh*. Overall, temperatures calculated using the Putirka model are about 40-60 °C higher than the values of the Ridolfi calibration, and pressure calculations exceed the Ridolfi model by 2-3 kbar (**fig. 3.22**). In contrast, pressures calculated with the Putirka model are comparable to those of the HBAS field, but temperatures exceed the field by one to two hundred degrees (typically ranging between ~800 to 1,000 °C, **fig. 3.23**). A summary of the thermobarometric results is provided in **digital appendix VIII**.

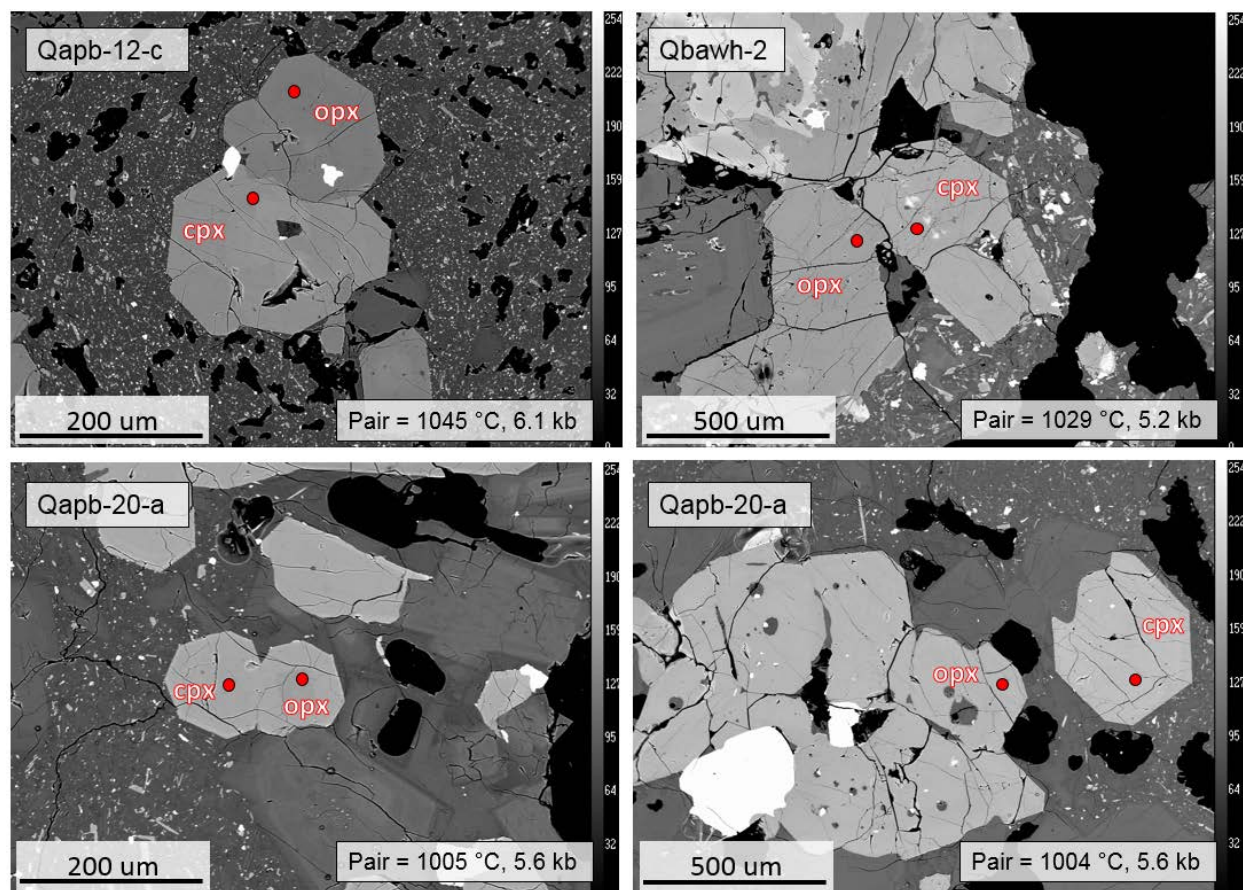


Figure 3.21. Backscattered electron images of selected 2-pyroxene pairs.

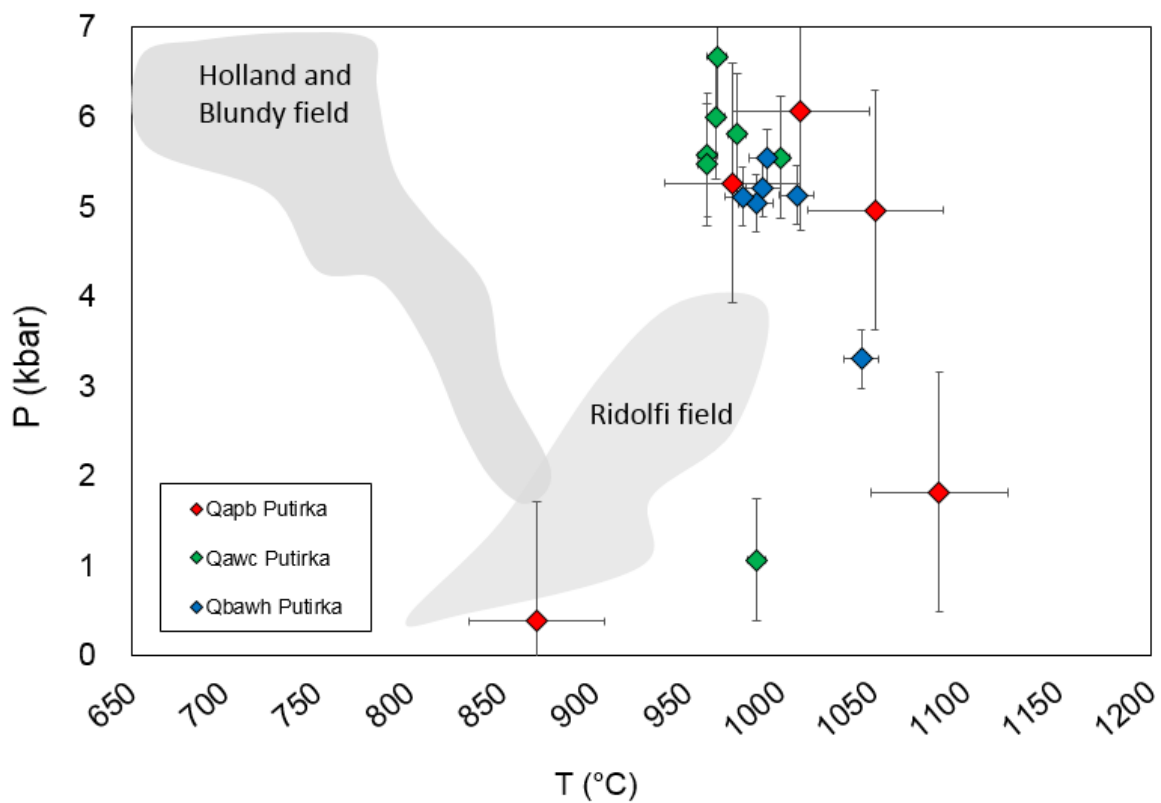


Figure 3.22. Pressure vs temperature calculated using two-pyroxene pairs and method of Putirka (2008). Simplified Holland and Blundy and Ridolfi fields from previous figures (4.16 and 4.17) shown.

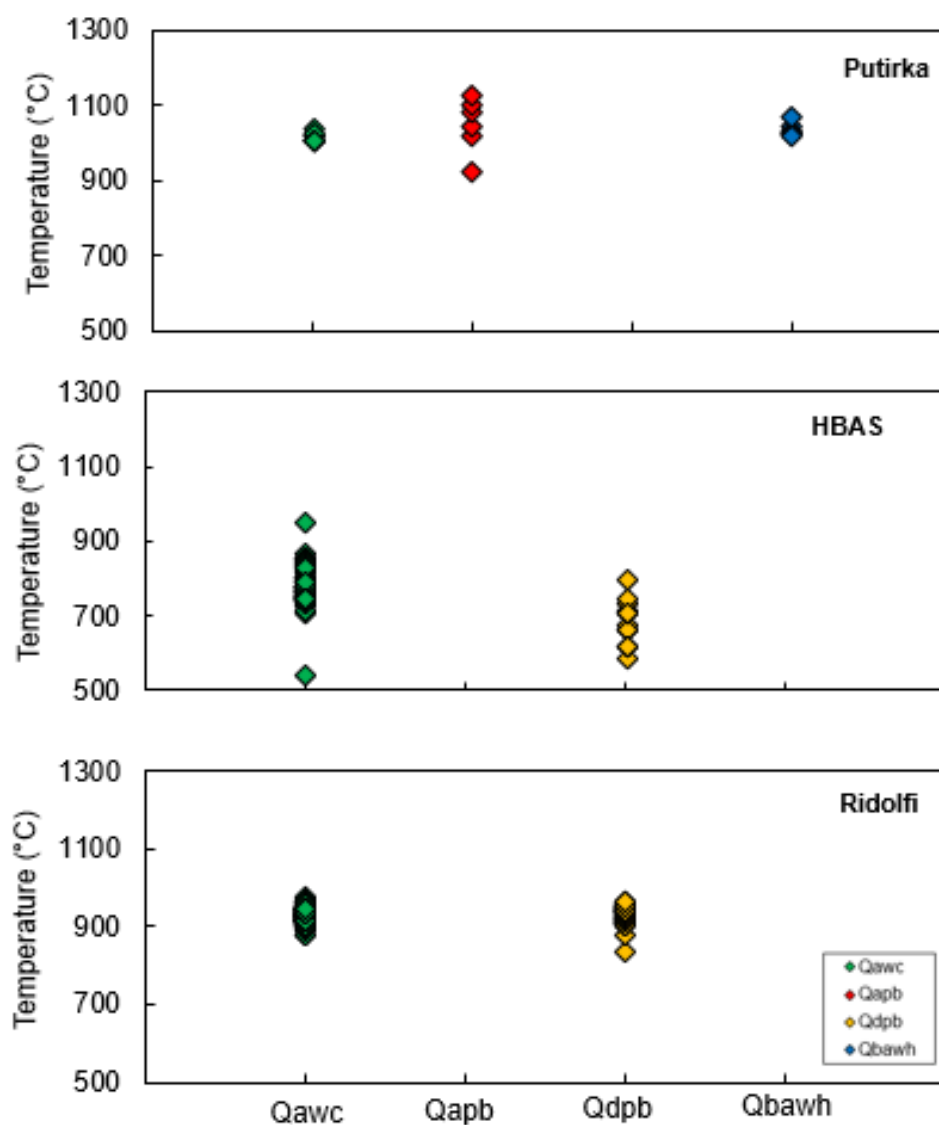


Figure 3.23. Mount Jefferson thermometry data for individual mineral systems. Each spot represents a single electron probe analysis.

3.8 Plagioclase-Melt Partitioning Model

Partitioning of trace elements between coexisting minerals and melts is widely used in geochemical and petrologic applications and is of considerable importance in modeling the trace element evolution of magmatic systems (Blundy and Wood, 1991; Bindeman et al., 1998). The partition coefficient (D) is the ratio of concentrations of an element between two phases (e.g.,

$D_{Sr} = \frac{[Sr]_{crystal}}{[Sr]_{melt}}$). The partitioning behavior of trace elements Sr and Ba between plagioclase feldspar and the coexisting melt are particularly well understood, making these elements helpful in reconstructing melt compositions from which the minerals were crystallized (e.g., Blundy and Wood, 1991; Bindeman et al., 1998; Dohmen and Blundy, 2014).

In this study, plagioclase-melt partition coefficients and coexisting melt compositions are calculated for Sr and Ba following the models of Blundy and Wood (1991) and Bindeman et al. (1998) (**digital appendix IX**). In these models, partitioning of trace elements between plagioclase and the melt is dependent upon anorthite content, temperature, and magma composition (Dohmen and Blundy, 2014; Bindeman et al., 1998). Anorthite content and trace element concentrations were measured in situ using EMP and LA-ICP-MS analytical techniques, and temperatures were calculated from thermometry experiments utilizing plagioclase, amphibole, and pyroxene thermometers (discussed above). In all cases, anorthite content and trace element concentrations were measured from the same mineral grains. Partition coefficients for Sr and Ba were calculated using maximum equilibrium temperature estimates of 1246, 1409, 1238, and 1346 K for units *Qawc*, *Qapb*, *Qdpb*, and *Qbawh*, respectively (**table 3.2**). Values were estimated with the Ridolfi model in units *Qawc* and *Qdpb*, and the Putirka model in units *Qapb* and *Qbawh*. As noted in Section 3.7, HBAS temperatures were determined to be artificially low as judged by the lack of agreement among the three models (**fig. 3.22**).

Measured Sr and Ba contents obtained from plagioclase feldspar ($[Sr]$, $[Ba]$), and calculated Sr and Ba concentrations of the coexisting melt ($[Sr]_{melt}$, $[Ba]_{melt}$) are shown in **figures 3.24** and **3.25**. There is some overlap between $[Sr]_{melt}$ and $[Ba]_{melt}$ and bulk rock Sr and Ba contents obtained from Conrey (1991). A bimodal Ba population is evident in unit *Qawc*, and calculated melt contents roughly overlap with bulk rock compositions in units *Qapb* and *Qbawh*

(**fig. 3.25**). Sr/Ba ratios of the primary melt ($[\text{Sr}/\text{Ba}]_{\text{melt}}$) were also calculated following plagioclase-melt partitioning models of Bindeman et al. (1998) (**fig. 3.26**). The $[\text{Sr}/\text{Ba}]_{\text{melt}}$ of plagioclase ranges from 0.8 to 7.6 across all the units. $[\text{Sr}/\text{Ba}]_{\text{melt}}$ values are tightly clustered in units *Qdpb* (0.8 to 2.1) and *Qapb* (1.4 to 2.2), more spread in unit *Qbawh* (1.1 to 3.0), and most variable in unit *Qawc* (0.9 to 7.6).

Table 3.2. Calculated plagioclase-melt partition coefficients.

Sample	T (K)	X_{An}	D_{Sr}	D_{Ba}
<i>Qawc</i> -20-a plag-1-spot-27	1246	0.70	2.18	0.20
<i>Qawc</i> -20-a plag-1-spot-28	1246	0.59	2.89	0.31
<i>Qawc</i> -20-a plag-2-spot-30	1246	0.77	1.82	0.16
<i>Qawc</i> -20-a plag-2-spot-31	1246	0.70	2.18	0.20
<i>Qawc</i> -20-a plag-3-spot-35	1246	0.75	1.90	0.17
<i>Qawc</i> -20-a plag-3-spot-36	1246	0.71	2.15	0.20
<i>Qawc</i> -20-a plag-5-spot-38	1246	0.85	1.50	0.12
<i>Qawc</i> -20-a plag-6-spot-39	1246	0.63	2.63	0.27
<i>Qapb</i> -10 plag-1-spot-1	1409	0.65	2.24	0.29
<i>Qapb</i> -10 plag-2-spot-3	1409	0.59	2.54	0.35
<i>Qapb</i> -10 plag-2-spot-4	1409	0.60	2.48	0.34
<i>Qapb</i> -10 plag-3-spot-7	1409	0.54	2.88	0.42
<i>Qapb</i> -10 plag-3-spot-8	1409	0.53	2.93	0.43
<i>Qapb</i> -10 plag-4-spot-6	1409	0.50	3.12	0.46
<i>Qapb</i> -10 plag-5-spot-9	1409	0.56	2.78	0.39
<i>Qapb</i> -10 plag-6-spot-11	1409	0.61	2.44	0.33
<i>Qapb</i> -10 plag-6-spot-12	1409	0.59	2.58	0.35
<i>Qdpb</i> -5 plag-1-spot-1	1238	0.41	4.68	0.60
<i>Qdpb</i> -5 plag-2-spot-4	1238	0.57	3.07	0.33
<i>Qdpb</i> -5 plag-2-spot-5	1238	0.58	3.00	0.32
<i>Qdpb</i> -5 plag-2-spot-6	1238	0.54	3.31	0.36
<i>Qdpb</i> -5 plag-3-spot-7	1238	0.50	3.73	0.43
<i>Qdpb</i> -5 plag-3-spot-8	1238	0.52	3.55	0.40
<i>Qdpb</i> -5 plag-4-spot-10	1238	0.45	4.23	0.51
<i>Qdpb</i> -5 plag-4-spot-9	1238	0.55	3.26	0.36
<i>Qdpb</i> -5 plag-5-spot-12	1238	0.46	4.05	0.48
<i>Qdpb</i> -5 plag-5-spot-13	1238	0.51	3.58	0.41
<i>Qdpb</i> -5 plag-5-spot-14	1238	0.42	4.51	0.56
<i>Qdpb</i> -5 plag-6-spot-15	1238	0.50	3.68	0.42
<i>Qdpb</i> -5 plag-6-spot-16	1238	0.51	3.58	0.41

<i>Qdpb-5</i> plag-8-spot-18	1238	0.27	6.75	1.00
<i>Qdpb-5</i> plag-9-spot-19	1238	0.51	3.64	0.42
<i>Qdpb-5</i> plag-9-spot-20	1238	0.50	3.72	0.43
<i>Qbawh-2</i> plag-1-spot-45	1346	0.76	1.79	0.19
<i>Qbawh-2</i> plag-1-spot-46	1346	0.67	2.19	0.25
<i>Qbawh-2</i> plag-2-spot-47	1346	0.77	1.76	0.18
<i>Qbawh-2</i> plag-3-spot-48	1346	0.82	1.55	0.15
<i>Qbawh-2</i> plag-4-spot-49	1346	0.82	1.56	0.16
<i>Qbawh-2</i> plag-5-spot-51	1346	0.75	1.82	0.19

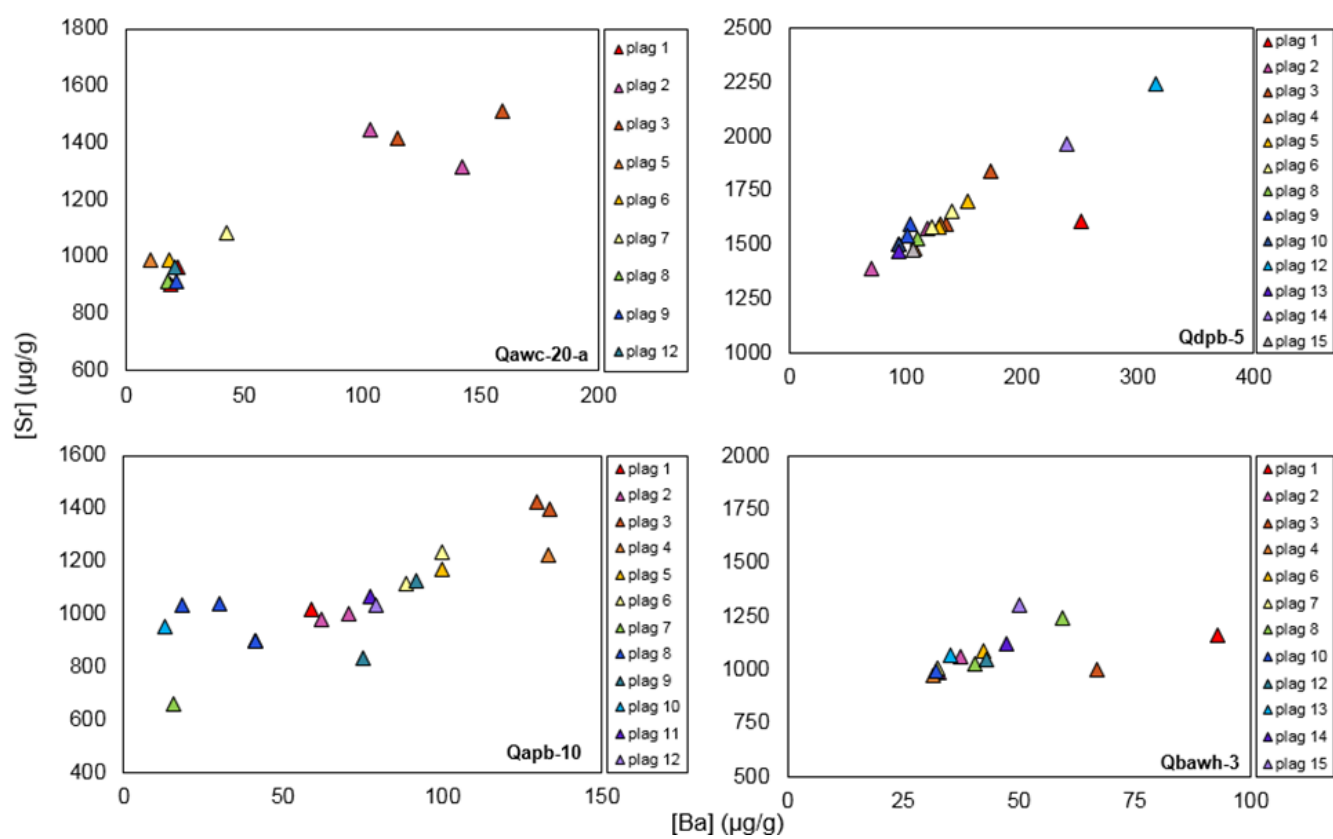


Figure 3.24. Measured trace element contents of Sr and Ba in the host feldspar phase ([Sr], [Ba]) for units *Qawc*, *Qapb*, *Qdpb*, and *Qbawh*. Each color symbol indicates an individual feldspar host within the sampled unit.

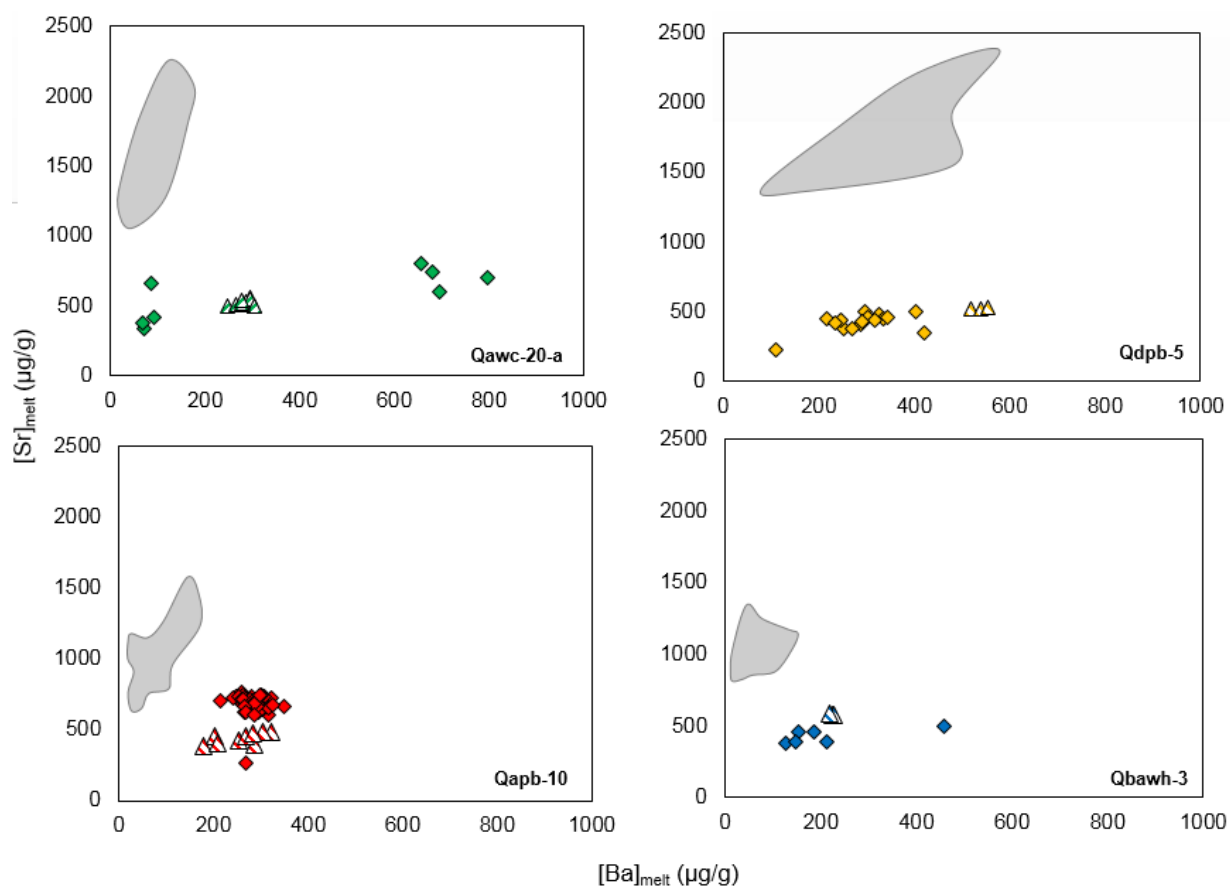


Figure 3.25. Calculated trace element contents of Sr and Ba in the primary melt ($[Sr]_{\text{melt}}$, $[Ba]_{\text{melt}}$) in units *Qawc*, *Qapb*, *Qdpb*, and *Qbawh*. Gray fields indicate Sr and Ba contents measured in situ from the host feldspar (previous figure). Solid diamonds indicate calculated concentrations from this study, striped triangles indicate bulk rock XRF analyses from previous studies (Conrey, 1991).

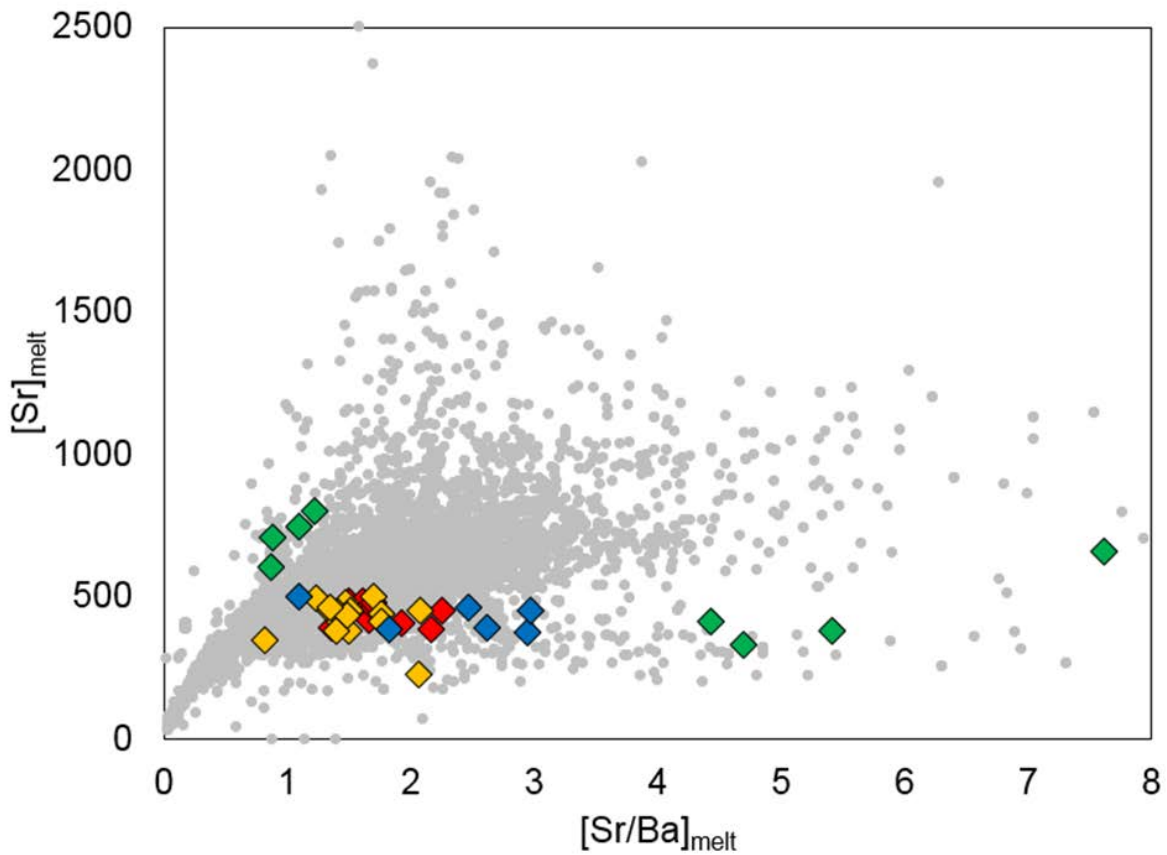


Figure 3.26. $[Sr]_{melt}$ versus $[Sr/Ba]_{melt}$ for units Qawc, Qapb, Qdpb, and Qbawh (colors and symbols as before). Gray circles are unprocessed (were not passed through thermobarometric equations for melt components) individual whole-rock analyses in the full Mount Jefferson dataset (Conrey, 1991; and R.M. Conrey, unpub. data).

3.9 Discussion

3.9.1 Thermobarometric Considerations

Here we evaluate the magma assembly and residence conditions under the MJA through comparison of three geothermometers and barometers: The single-phase Ridolfi model (amphibole), and the multi-phase HBAS (plagioclase-amphibole) and Putirka (orthopyroxene-clinopyroxene) models. The limitations of each model are discussed below.

3.9.1.1 Single-Phase Thermobarometers: The Ridolfi Model

Pressures and temperatures of MJA amphiboles calculated using the Ridolfi model yield values within the range of other intermediate magmas (Ridolfi et al., 2010), and all but two analyses fall within the amphibole stability with respect to andesitic (Eggler and Burnham 1973; Green, 1982) and dacitic (Rutherford and Devine, 2003, 2008; Holtz et al., 2005) magmas shown in **figure 3.16**. Because the Ridolfi model uses only amphibole to constrain pressure, temperatures, and water pressure, several assumptions are required when considering this model. The first assumption made is that all pressures and temperatures derived from amphiboles will lie close to the upper limit of amphibole stability (termed “Ridolfi max” in **fig. 3.16**). Consequently, this model cannot always yield realistic pressures and temperatures of the all amphiboles sampled; for example, amphiboles which crystallized during isobaric cooling.

Magma rejuvenation has been invoked by previous authors (Conrey, 1991; Conrey et al., 2001) as the most likely process accounting for the diversity of whole-rock trace element values in the MJA. The coexistence of distinct disequilibrium textures among amphiboles

within and between units (**fig. 3.18**) suggests that erupted lavas include crystals from different magma batches which mixed prior to eruption (Giles, 2009).

Variable Al contents in the amphiboles (**fig. 3.15**) further corroborates evidence that the lavas contain separate populations of amphibole which grew at variable pressures and temperatures. In general, the set of assumptions applied by Ridolfi et al. (2010) are probably valid for magmas in which amphiboles crystallize near the liquidus (i.e., volcanic conditions), as is the case with MJA magmas. The model is less robust for amphiboles crystallizing closer to solidus, or plutonic conditions (Walker et al., 2013).

3.9.1.2 Multi-Phase Thermobarometers: The HBAS and Putirka Models

Utilizing multi-phase thermobarometers demands fewer assumptions than single-phase geothermobarometers (e.g., Ridolfi model), but predicates that the phases be in equilibrium. Identification of equilibrium conditions can be difficult in volcanic rocks, in which phases from different source magmas are juxtaposed upon or within each other (**figs. 3.9, 3.18**). Identifying equilibrium phases may be particularly problematic in the plagioclase-amphibole geothermobarometer (HBAS model), as both phases are sensitive to small changes in pressure and temperature and commonly display complex disequilibrium textures (e.g., oscillatory zoning). In this study, only touching plagioclase-amphibole pairs of similar size were selected for analysis to diminish uncertainty. Even so, the HBAS model returns a considerable range of temperatures and pressures (~650-850 °C, 2-7 kbar) incongruent with results of the Ridolfi (~800-950 °C, 0.5-4 kbar) and Putirka (~950-1100 °C, 5-7 kbar) models. With respect to the two-pyroxene geothermobarometer (Putirka model), equilibrium

is tested for using Fe-Mg exchange, and data falling outside of 3σ are excluded from analysis (Putirka, 2008).

3.9.1.3 Comparison of Geothermobarometers

The geothermobarometers considered here employ four different phases (amphibole, plagioclase, orthopyroxene, clinopyroxene) and two phase pairs (plagioclase-amphibole, two-pyroxene) to estimate the pressures and temperatures at which phases in the MJA were crystallizing. Of the nine samples analyzed, only one single sample (*Qawc-20-a*) contained the phases necessary to employ all three geothermobarometers. Seven samples yielded amphibole and plagioclase-amphibole estimates, and two yielded only two-pyroxene estimates (**table 3.1**). As uncertainties are unavoidable in all geothermobarometric models (Putirka, 2008), agreement amongst our Ridolfi, HBAS, and Putirka models is assessed next.

Within samples, and for the dataset as a whole, the two-pyroxene geothermometer always yielded the highest temperatures, ranging from about 950 to 1100 °C. Unit *Qbawh* displayed the lowest amount of variation, followed by *Qawc*, then *Qapb*, though scatter was prevalent in all units tested with the Putirka model (**fig. 3.22**). The HBAS model always yielded the lowest temperatures of ~650-900 °C with ~150 °C variation for individual units, and Ridolfi temperatures fall in between HBAS and Putirka estimates (**figs. 3.16, 3.17, 3.22**). The hottest HBAS temperatures overlap with the coolest Putirka temperatures (~875 °C), and greatest temperature overlap is between the Ridolfi and Putirka temperatures at about 950-1,025 °C.

Pressure estimates are similarly variable amongst the three geobarometers. Pressures are highest in the HBAS and Putirka models, which also display the greatest amount of overlap between 2 and 7 kbar. Pressures are lowest in the Ridolfi model, never exceeding ~4 kbar.

Regardless of the aforementioned limitations, some overlap in the calculated crystallization temperatures and pressures is expected, as each phase crystallizes at a different stage in the cooling process (Bowen reaction series; Bowen, 1913). The diversity of textures and compositional populations in our study, as in many other studies of intermediate arc rocks, suggests that the crystals formed over a range of pressure and temperature conditions. Evidence includes the substantial overlap of mineral compositions from units *Qawc*, *Qapb*, *Qdpb*, and *Qbawh* and disequilibrium textures within samples.

Ridolfi pressure and temperature estimates are directly compared to HBAS estimates in **figure 3.20**. In general, agreement is best between the Ridolfi and HBAS geobarometers in unit *Qawc*, intersecting the 1:1 line. Agreement between geothermometers is best between Ridolfi and HBAS, moderate between Ridolfi and Putirka, and poorest between HBAS and Putirka (**figs. 3.20, 3.21**).

3.9.1.4 Equilibration, Mixing, and Eruption

The relative timing of crystallization of the mineral phases is less clear, though rough estimates can be made on the basis of equilibration rates. Re-equilibration rates for pyroxene in intermediate to mafic composition magmas are estimated to be on the order of tens of thousands of years (Brady and McAllister, 1983), while amphibole re-equilibration may take only days to weeks (Rutherford and Hill, 1993). The significant range of disequilibrium textures, from unaltered and euhedral to zoned and resorbed, preserved in crystals indicates

interaction between at least two distinct batches of magma, and a tumultuous petrologic history for the MJA.

On the basis of mineralogic (**secs. 3.5, 3.6**) and thermobarometric (**sec. 3.7**) results, we determined that the significant mineralogic heterogeneity in the MJA is the result of repeated magmatic rejuvenation and mixing in a crustal magmatic reservoir. Systematic variance in pressures and temperatures (**figs. 3.16, 3.19, 3.22**) and mineral compositions (**figs. 3.13, 3.14, 3.15**), coupled with different textures (**figs. 3.9, 3.18, 3.21**) among units suggests this is a reasonable postulation. Similar conditions were described for the Auchanquilcha Volcanic Cluster (AVC; Walker et al., 2013). However, unlike in the AVC, in which pyroxene mineral compositions displayed distinct bimodality, MJA pyroxenes display a more continuous spectrum of compositions (**figs. 3.13, 3.14, 3.15**). Pressure and temperature estimates in the MJA are more comparable to AVC, though exhibit less diversity of compositions in the low-pressure, low-temperature regions.

In the AVC, the authors envisioned a scenario in which phenocryst-rich magma grew at elevated pressure-temperature conditions deep in the earth's crust (~30-40 km) before sporadically injecting a shallower, cooler reservoir in the upper crust (~10-20 km). This scenario is supported by distinct crystal populations documenting a hot invading magma, a cool host magma, and the resultant hybrid magma. In contrast, rocks from the MJA have a more continuous blend of mineral compositions and pressure-temperature estimates in our dataset, so we propose an alternative model for the MJA.

In contrast to the AVC model, in which mixing is assumed to primarily occur within a large crustal reservoir, possibly a zoned batholith, (Walker et al., 2013), our model proposes

the involvement of several smaller reservoirs at variable levels within the mid- and -upper crust. The highest temperatures, recorded by pyroxenes with the Putirka model, represent a deep crustal source in which the crystals grew in equilibrium with the melt. This is evidenced by monotonous crystal gains and mostly euhedral crystal shape. Relatively large (up to 1,000 μm) phenocryst size indicates the pyroxenes spent the majority of time in the deep, mafic reservoir before injection into a shallower reservoir. In the samples containing two pyroxenes (**table 3.1**), groundmass is comparatively fine-grained and reaction textures are minimal, suggesting eruption was rapid following injection.

Table 3.1. Mount Jefferson samples used in this study.

Sample	Unit	Amph	Amph/plag pairs	2-px pairs
Qawc-14	Andesite of Whitewater Creek	96	31	-
Qawc-16	Andesite of Whitewater Creek	4	4	-
Qawc-17	Andesite of Whitewater Creek	72	22	-
Qawc-19-a	Andesite of Whitewater Creek	4	4	-
Qawc-20-a	Andesite of Whitewater Creek	59	19	9
Qawc-22	Andesite of Whitewater Creek	4	4	-
Qapb-12-c	Andesite of Park Butte	-	-	9
Qdpb-5	Dacite of Park Butte	76	16	-
Qbawh-2	Basaltic andesite of Whiskey Creek	-	-	6

Crystallization pressures and temperatures are less well-constrained for plagioclase and amphibole. The Ridolfi model gives estimates $\sim 800\text{-}950^\circ\text{C}$ and 0.5-4.5 kbar, whereas the HBAS model gives estimates of $650\text{-}800^\circ\text{C}$ and 2.5-7 kbar (**fig. 3.17**). As discussed previously, no thermobarometer is completely without error. In this case the Ridolfi model is likely a better representation of crystallization conditions than the HBAS model, as Ridolfi estimates are generally reliable for volcanic rocks and equilibrium assemblage plagioclase-amphibole pairs for

the HBAS method were often complexly zoned. The complex zoning probably resulted in erroneously high pressure estimates and perhaps contributed to the broad spread of pressure and temperature values as well.

3.9.2 Reconstructed Melt Composition Considerations

Here we used the partitioning behavior of Sr and Ba between plagioclase feldspar and the coexisting melt to reconstruct equilibrium melt compositions from which MJA mineral phases crystallized.

3.9.2.1 Reconstruction of Coexisting Melt Compositions

Reconstructions of partition coefficients (**table 3.2**) and trace element concentrations of Sr and Ba in the coexisting melt were calculated following the models of Blundy and Wood (1991) and Bindeman et al. (1998) (equations 20-24, discussed in **sec. 3.5.1**). To assess reliability of our partition coefficients, we plotted our calculated partition ($D_{\text{calculated}}$) to measured partition coefficients (D_{measured}) of Bindeman et al. (1998) and Dohmen and Blundy (2014).

In comparing our calculated D values to the measured D values (**fig. 3.27**), we found that our calculated partition coefficients are in better agreement with partition coefficients of Bindeman et al. (1998) in both Sr and Ba.

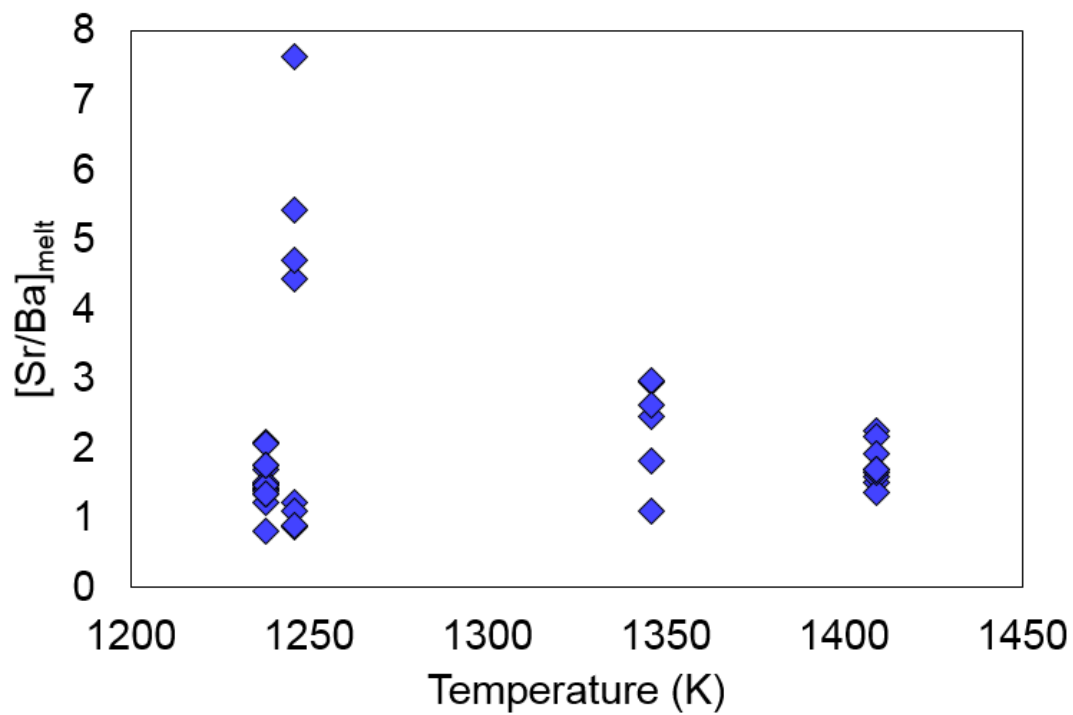


Figure 3.28. $[\text{Sr}/\text{Ba}]_{\text{melt}}$ versus temperature (in Kelvin). Note that higher $[\text{Sr}/\text{Ba}]_{\text{melt}}$ concentrations tend to correspond to lower temperatures.

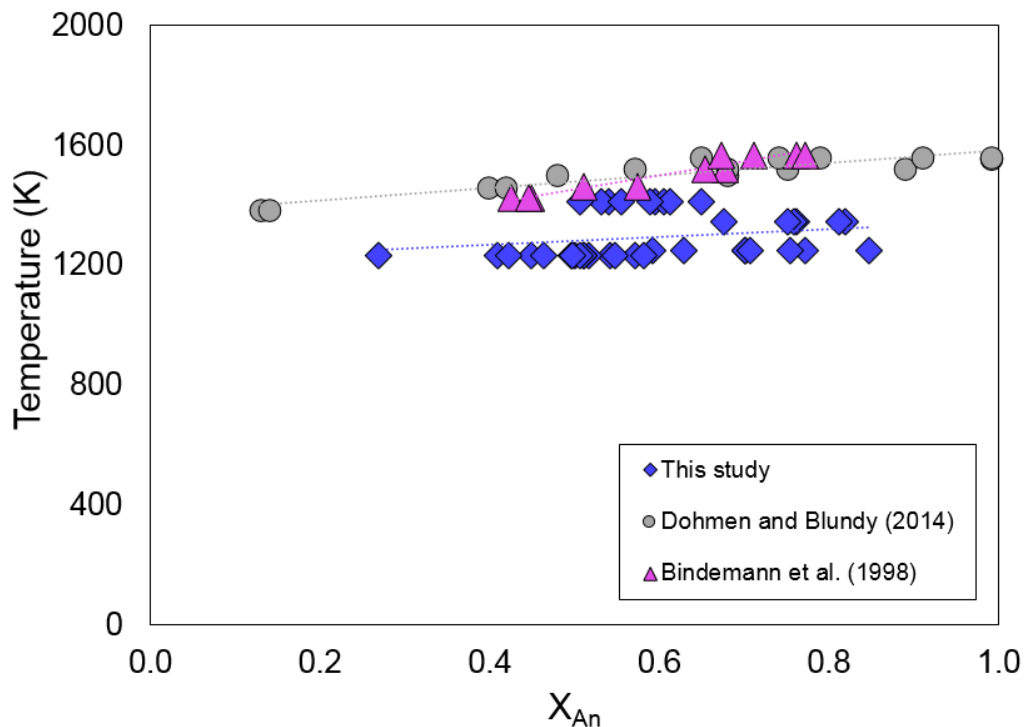


Figure 3.29. Temperature (Kelvin) versus anorthite content (X_{An}). Purple diamonds show results from this study, gray circles show the results of Dohmen and Blundy (2014), and pink triangles are the results from Bindeman et al. (1998). There is good overlap between results from Dohmen and Blundy (2014) and Bindeman et al. (1998), and between Bindeman et al. (1998) and higher temperature results of this study.

As previously mentioned (**sec. 3.8**), partition coefficients are heavily dependent upon anorthite content, temperature, and magma composition, and the disparity between our calculated partition coefficients and the measured coefficients of Dohmen et al. (2014) and Bindeman et al. (1998) is probably linked to a suite of artificially low temperatures measured in our thermobarometric experiments. On the basis of the set of observations discussed in **figures 3.27-3.29**, it seems that we were appropriate in selecting the Ridolfi and Putirka temperature estimates, instead of HBAS estimates, to apply to our melt reconstruction model.

3.9.1 Synthesis: Model for Diversity of MJA Magma Compositions

Reliable temperature estimates ranging between about 800 to 1100 °C, pressure gradients ranging from about 2 to 8 kbar, broad, continuous spectrums of mineral chemistry, and pervasive equilibrium textures in MJA lavas suggest that mixing occurred along a variable range of physical conditions between about 3 to 25 km depth. Systematic breaks in temperatures at ~850-900 °C and ~950-1125 °C (**figs. 3.28, 3.29**), the pressure gradient around 3-4 kbar, and bimodal pyroxene mineral compositions further corroborate evidence of two primary magma chambers at about 15 and 20-25 km depth.

According to the model of Conrey et al. (2001), a ~850-900 °C amphibolite source resides at 25-30 km and gives rise to a rhyodacite crustal endmember, and a ~1,050-1,100°C mafic granulite source resides at ~30-40 km and gives rise to a Sr-rich andesite crustal endmember. Primitive compositions are supplied by an underplated MORB-like basaltic magma residing ≥ 40 km depth. Magmas from each of these sources rise and mingle briefly in a small dacitic batholith between about 0 and 10 km before eruption. Agreement in temperature is excellent between our study and the estimates of Conrey et al. (2001). Agreement in depth is poor, however.

Evidence of the Sr-rich (>800 ppm) andesite endmember is also lacking in our study (fig. 3.30). In no instances do our reconstructed melt compositions ($[Sr]_{\text{melt}}$) exceed or even approach 800 ppm, except in unit *Qawc*, which gives a single $[Sr]_{\text{melt}}$ value of 799 ppm (**fig. 3.30**).

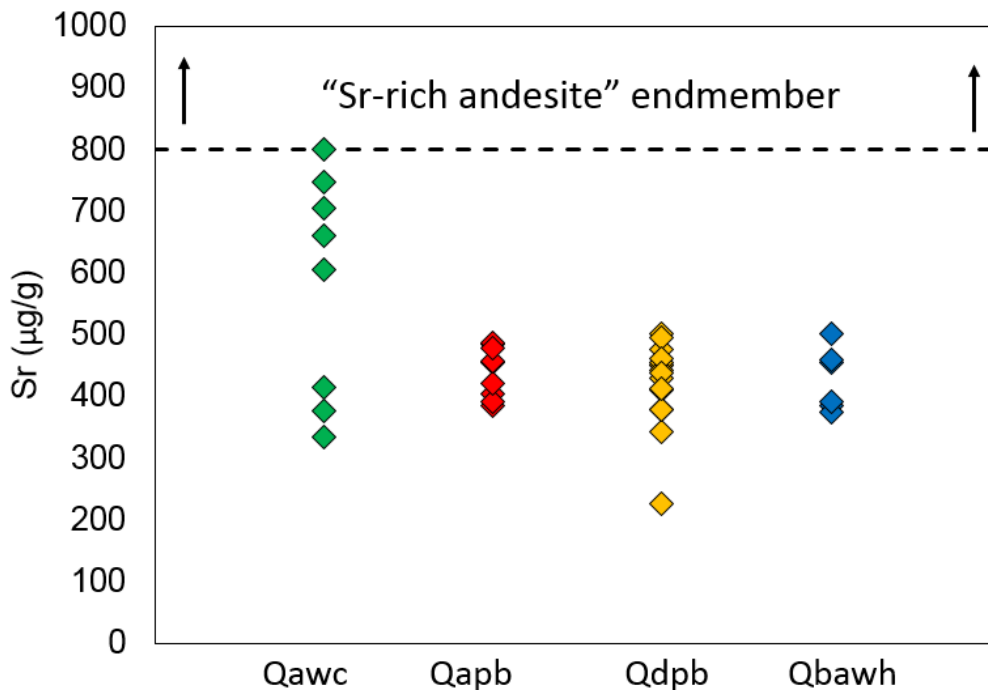


Figure 3.30. Sr concentrations in units *Qawc*, *Qapb*, *Qdpc*, and *Qbawh*. The “Sr-rich (>800 ppm Sr) andesite” endmember field of Conrey et al. (2001) is indicated above the dashed line.

Stark disagreement in $[Sr]_{\text{melt}}$ concentrations and pressures, coupled with the robust set of melt reconstruction and barometric experimentation carried out on MJA lavas in this study suggests that crustal magma storage conditions may be much shallower than initially proposed by Conrey (2001). We therefore recommend a modified crustal model for the MJA.

In our proposed model (**figure 3.31**), primitive magmas are supplied much as in the Conrey et al. (2001) model, in which MORB-like magma rises and interacts with the crustal reservoirs. However, the crustal reservoirs reside primarily at 15 and 20-25 km depth in the model presented here. Differentiation occurs in magmatic reservoirs at several levels within the 15 and 20-25 km range, thereby creating variable magma compositions predominantly andesitic to dacitic in

composition. More peripheral compositions, such as basaltic andesite or rhyodacite, are formed more singularly, the injected crystal cargo interacting with one or no magmatic reservoirs before eruption. In this scenario, basaltic andesite erupted compositions would be derived straight from a primitive source without any mixing interactions.

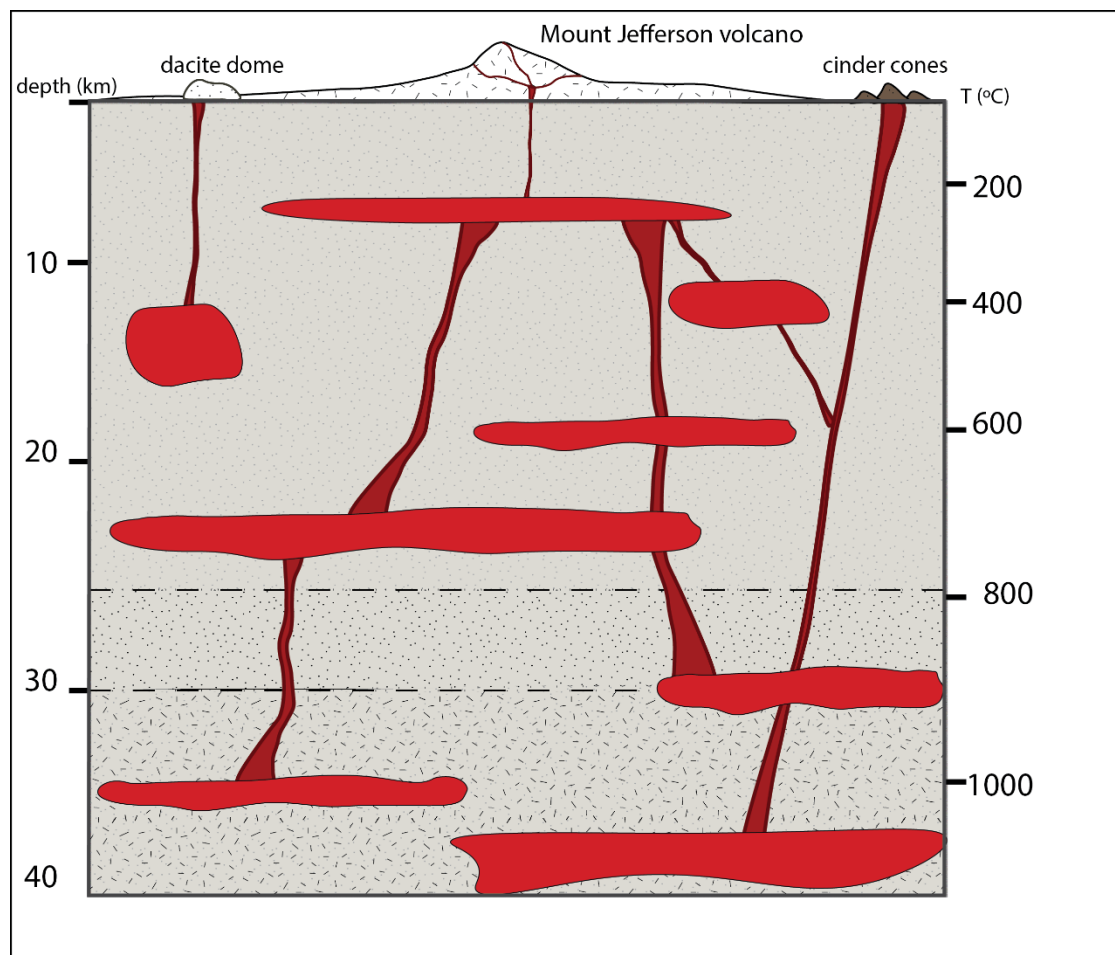


Figure 3.31. Synthesized depth model.

The overarching view that emerges from our data is that MJA lavas, by and large, display substantial compositional, textural, and geochemical diversity. The diversity of compositions

reflects a complex petrogenetic and crustal history which dominantly takes place at 15-25 km depth over temperatures of ~850 to 1100 °C.

3.10 Conclusion

The phenocryst assemblage of lavas of four stratigraphic units have been probed to assess pressure and temperature conditions of pre-eruptive magmas in the MJA, an example of a long-lived volcanic system. Crystallization is documented over about 8 kbar (~25 km) of pressure and 600 °C in the basaltic andesite, andesite, and dacite lavas sampled. The diversity of crystallization temperatures and pressures recorded by phases in the four individual MJA lavas suggests that erupting magma batches originated from several levels in the mid- and upper crust between, mostly between ~15 and 25 km. Complex disequilibrium textures and disparate mineral chemistry additionally suggests that, in many cases, magma evolution occurred in multiple phases.

Reconstructed melt compositions, ascertained from trace element concentrations of Sr and Ba reveal little evidence of the Sr-rich (>800 ppm) andesite endmember hypothesized by Conrey et al. (2001). $[Sr]_{\text{melt}}$ concentrations only exceed 600 ppm in unit *Qawc*, and are less than 500 ppm in units *Qapb*, *Qdpb*, and *Qbawh*. However, a more comprehensive sampling of the MJA is required to determine the true source of the Sr-rich lavas erupted throughout the MJA.

The diverse spread of data reported here indicate complex petrologic mixing processes and crustal evolution beneath the MJA. However, the physical finding of three peripheral vent and dome lavas cannot and should not represent the evolution of the MJA as a whole. We have several recommendations for future research, the most important of which include completing a comprehensive pressure-temperature investigation from representative units from the main

phases of volcanism across the MJA (**fig. 2.3**, Ch. 2). We also recommend analyzing units with well-constrained age relations, thereby allowing a time-transgressive study of the MJA as has been demonstrated in the Auchanquilcha volcanic cluster by Walker et al. (2013). Also exciting is the possibility of including glacially modified units in the investigation to determine if major glaciations affect the physical parameters of shallow magmatic reservoirs. The following recommendations would deliver a detailed and time-transgressive record of arc volcanism in a glacially-modified terrain.

4 GENERAL CONCLUSION

Widespread lava flows, glacial till, and morphologic features in the Mount Jefferson area document how the intimate interaction between volcanoes and ice has sculpted a complex geologic terrain spanning four million years of earth history. The quintessential stratocone shape of Mount Jefferson was only achieved in the past ~5% of the area's lifetime. At several points in the MJA's history, eruptions were accompanied by the ice sheets of major glacial advances, now recognizable by remnant moraines, cirques, and other glacial features scattered throughout the area. Modification of the erupted lavas themselves is common, identifiable by columnar jointing, perched lava flows, and anomalously glassy lava flows.

Erupted lavas of the MJA are diverse, ranging from basaltic andesite to rhyodacite. Bulk and mineral compositional trends of MJA lavas indicate that, after fractional crystallization, magma mixing is the dominant processes in generating the compositional diversity observed in any given eruptive phase.

The phenocryst assemblages of MJA lavas have been probed for various intensive parameters including pressure, temperature, and mineral and melt compositions. Crystallization of pyroxene, amphibole, and plagioclase is observed over ~8 kbar (~25 km) and ~650 – 1,100 °C in lavas from four sampled units. The diversity of crystallization temperatures and pressures recorded by phases in individual MJA lavas suggests that magma batches originated from several levels in the mid- and upper crust, mostly between 15 and 25 km.

[Sr]_{melt} compositions reconstructed in this study do not provide supporting evidence for the 1050 - 1100 °C, 35-40 km crustal melting hypothesis of Stanley et al. (1990) and Conrey et al. (2001), which addresses the unusually Sr-rich andesite composition lavas in the MJA.

However, lack of evidence of Sr-rich melt in four stratigraphic units does not singularly disprove the hypothesis, and additional data collection is required to determine the source of the evasive Sr-rich andesite.

The findings presented in this study contribute to understanding of pre-eruptive magmatic conditions and provide perspective on the evolution and organization of a long-lived volcanic system in the central Cascade Range.

REFERENCES

- Anderson, A.T., 1976, Magma mixing: Petrological process and volcanological tool: *Journal of Volcanology and Geothermal Research*, v. 1, p. 3-33.
- Anderson, J.L., and Smith, D.R., 1995, The effects of temperature and fO₂ on the Al-in-hornblende barometer: *American Mineralogist*, v. 80, p. 549-559.
- Armstrong, R.L., Taylor, E.M., Hales, P.O., and Parker, D.J., 1975, K-Ar dates for volcanic rocks, central Cascade Range of Oregon: *Isochron/West*, no. 13, p. 5-10.
- Atwater, B.F., Satoko, M.-R., Satake, K., Tsuji, Y., Ueda, K., and Yamaguchi, D.K., 2005, The Orphan Tsunami of 1700—Japanese clues to a parent earthquake in North America: U.S. Geological Survey Professional Paper 1707, 133 p.
- Bachmann, O., Dungan, M.A., and Lipman, P. W., 2002, The Fish Canyon magma body, San Juan volcanic field, Colorado: Rejuvenation and eruption of an upper-crustal batholith: *Journal of Petrology*, v. 43(8), p. 1469-1503.
- Bachmann, O. and Bergantz, G., 2008, The magma reservoirs that feed supereruptions: *Elements*, v. 4, p. 17-21.
- Bachmann, O., Dungan, M. A., 2002, Temperature-induced Al-zoning in hornblendes of the Fish Canyon magma, Colorado: *American Mineralogist*, v. 87(8-9), p. 1062-1076.
- Bacon, C.R., Gunn, S.H., Lanphere, M.A., Wooden, J.L., 1994, Multiple isotopic components in Quaternary volcanic rocks of the Cascade arc near Crater Lake, Oregon: *Journal of Petrology*, v. 35, p. 1521-1556.
- Bindeman I.N., Davis, A.M., 2002, Convection and redistribution of Alkalis and Trace elements during the mingling of basaltic and rhyolitic melts: *Journal of Petrology*, v. 7, p. 11-101.
- Bindeman, I.N., Davis, A.M., and Drake, M.J., 1998, Ion microprobe study of plagioclase-basalt partition experiments at natural concentration level of trace elements: *Geochimica et Cosmochimica Acta*, v. 62(7), p. 1175-1193.
- Blackwell, D.D., Steele, J.L., Frohme, M.K., Murphey, C.F., Priest, G.R., and Black, G.L., 1990, Heat flow in the Oregon Cascade Range and its correlation with regional gravity, Curie point depths, and geology: *Journal of Geophysical Research*, v. 95, p. 19.
- Blong, R. J., 1996, Volcanic hazards risk assessment: Monitoring and mitigation of volcano hazards, Springer Berlin Heidelberg, p. 675-698.

- Blundy, J.D., Wood, B.J., 1991, Crystal-chemical controls on the partitioning of Sr and Ba between plagioclase feldspar, silicate melts, and hydrothermal solutions: *Geochimica et Cosmochimica Acta*, v. 55(1), p. 193–209.
- Bowen, N. L., 1913, The melting phenomenon of the plagioclase feldspars: *American Journal of Science*, 4th Series, v. 35, p. 577–599.
- Brady, J.B. and McCallister, R.H., 1983, Diffusion data for clinopyroxenes from homogenization and self-diffusion experiments: *American Mineralogist*, v. 68, p. 95–105. Brown, D.E., McLean, G.D., Priest, G.R.,
- Bullen, T. D. and Clynne, M. A., 1990, Trace element and isotopic constraints on magmatic evolution at Lassen volcanic center: *Journal of Geophysical Research*, v. 95, p. 19671–19691.
- Cherniak, D. J., 1995, Diffusion of lead in plagioclase and K-feldspar: an investigation using Rutherford backscattering and resonant nuclear reaction analysis: *Contributions to Mineralogy and Petrology*, v. 120(3-4), p. 358-371.
- Clynne, M. A., 1990, Stratigraphic, lithologic, and major element geochemical constraints on magmatic evolution at Lassen volcanic center, California: *Journal of Geophysical Research*, v. 95, p. 19651–19669.
- Clynne, M.A., 1999, A complex magma mixing origin for rocks erupted in 1915, Lassen Peak, California: *Journal of Petrology*, v. 40, p. 105–132.
- Colman, S.M., and Pierce, K.L., 1981, Weathering rinds on andesitic and basaltic stones as a Quaternary age indicator, western United States: *U.S. Geological Survey Professional Paper 1210*, 56 p.
- Conrey, R.M., 1985, Volcanic stratigraphy of the Deschutes Formation, Green Ridge to Fly Creek, north-central Oregon: Corvallis, Oregon State University, M.S. thesis, 349 p.
- Conrey, R.M., 1991, Geology and petrology of the Mt. Jefferson area, High Cascade Range, Oregon: Pullman, Washington State University, Ph.D. diss., 374 p.
- Conrey, R.M., Hooper, P.R., Larson, P.B., Chesley, J., Ruiz, J., 2001, Trace element and isotopic evidence for two types of crustal melting beneath a High Cascade volcanic center, Mt. Jefferson, Oregon: *Contributions to Mineralogy and Petrology*, v. 141(6), p. 710-732.
- Conrey, R.M., Taylor, E.M., Donnelly-Nolan, J.M., and Sherrod, D.R., 2002, North-central Oregon Cascades: Exploring petrologic and tectonic intimacy in a propagating intra-arc rift, *in* Moore, G.W., ed., *Field guide*

to geologic processes in Cascadia: Oregon Department of Geology and Mineral Industries Special Paper 36, p. 47-90.

Conrey, R.M., Grunder, A.L., and Schmidt, M.E., 2004, SOTA Field trip guide—State of the Cascade arc: Stratocone persistence, mafic lava shields, and pyroclastic volcanism associated with intra-arc rift propagation: Oregon Department of Geology and Mineral Industries Open-File Report O-04-04, 40 p.

Couch, R.W., and Riddihough, R.P., 1989, The crustal structure of the western continental margin of North America, in Pakiser, L.C., and Mooney, W.D., eds., Geophysical framework of the continental United States: Boulder, Colo., Geological Society of America Memoir 172, p. 103–128.

Cooper, K.M., and Kent, A.J.R., 2014, Rapid remobilization of magmatic crystals kept in cold storage, *Nature*, v. 506, p. 480-483.

Crandell, D.R., 1969, Surficial geology of Mt. Rainier National Park, Washington: U.S. Geological Survey Bulletin 1288, 41 p.

Darr, C. M., 2006, Magma chamber processes over the past 475,000 years at Mount Hood, Oregon: Insights from crystal zoning and crystal size distribution studies. M.S. thesis, Corvallis, Oregon, Oregon State University.

Dicken, S.N., 1965, Oregon geography: the people, the place, and the time, 4th ed.: Ann Arbor, Michigan, Edwards Brothers, 147 p.

Dohmen, R. and Blundy, J., 2014, A predictive thermodynamic model for element partitioning between plagioclase and melt and a function of pressure, temperature, and composition: *American Journal of Science*, v. 314, p. 1319-1372.

Donnelly-Nolan, J. L., and Hildreth, W., 1997, Primitive magmas at five Cascades volcanic fields: Melts from hot, heterogeneous sub-arc mantle: *Canadian Mineralogist*, v. 35, p. 397–423.

Easterbrook, D.J., 1986, Stratigraphy and chronology of Quaternary deposits of the Puget Lowland and Olympic Mountains of Washington and the Cascade Mountains of Washington and Oregon, in Sibrava, V., Bowen, D.Q., and Richmond, G.M., eds., Quaternary glaciations in the northern hemisphere: Oxford, Pergamon Press, p. 145–159.

Eggler, D.H., and Burnham, C.W., 1973, Crystallization and fractionation trends in the system andesite-H₂O-CO₂-O₂ at pressures to 10 kb: *Geological Society of America Bulletin*, v. 84(8), p. 2517-2532.

- Eichelberger, J. C., 1978, Andesitic volcanism and crustal evolution: *Nature*, v. 275, p. 21–27.
- Girard, G., and Stix, J., 2009, Magma recharge and crystal mush rejuvenation associated with early postcollapse Upper Basin Member rhyolites, Yellowstone Caldera, Wyoming: *Journal of Petrology*: p. 1–31.
- Green, J.C., 1982, Geology of Keweenaw an extrusive rocks: *Geological Society of America Memoirs, Memoir 156*, p. 47-56.
- Grove, T.L., Kinzler, R.J., Baker, M.B., Donnelly-Nolan, J.M., and Leshner, C.E., 1988, Assimilation of granite by basaltic magma at Burnt Lava flow, Medicine Lake volcano, northern California: decoupling of heat and mass transfer: *Contributions to Mineralogy and Petrology*, v. 99, p. 320-343.
- Grunder A.L., Klemetti E.W., Feeley T.C., and McKee C.M., 2008, Eleven million years of arc volcanism at the Aucanquilcha Volcanic Cluster, northern Chilean Andes: Implications for the life span and emplacement of plutons: *Transactions of the Royal Society of Edinburgh: Earth Sciences*, v. 97, p. 415–436.
- Hildreth, W., 1981, Gradients in silicic magma chambers: Implications for lithospheric magmatism: *Journal of Geophysical Research, Solid Earth*, v. 86(B11), p. 10153-10192.
- Hildreth, W. and Moorbath, S., 1988, Crustal contributions to arc magmatism in the Andes of central Chile: *Contributions to Mineralogy and Petrology*, v. 98, p. 455-489.
- Hildreth W., 2004, Volcanological perspectives on Long Valley, Mammoth Mountain, and Mono Craters: Several contiguous but discrete systems: *Journal of Volcanology and Geothermal Research*, v. 136, p. 169-198
- Hildreth, W., Fierstein, J., and Calvert, A.T., 2012, Geologic map of the Three Sisters volcanic cluster, Cascade Range, Oregon: U.S. Geological Survey Scientific Investigations Map 3186, scale 1:24,000.
- Holland T.J.B., and Blundy J.D., 1994, Non-ideal interactions in calcic amphiboles and their bearing on amphibole-plagioclase thermometry. *Contributions to Mineralogy and Petrology*, v. 116, p. 433–447.
- Househ, T.B. and Luhr, J.F., 1991, Plagioclase-melt equilibria in hydrous systems: *American Mineralogist*, v. 76, p. 477–492.
- Hughes, S.S., and Taylor, E.M., 1986, Geochemistry, petrogenesis, and tectonic implications of central High Cascade mafic platform lavas: *Geological Society of America Bulletin*, v. 97, p. 1024–1036.
- Hughes, S.S., 1990, Mafic magmatism and associated tectonism of the central High Cascade Range, Oregon: *Journal of Geophysics*, v. 95, 15 p.

- Johannes, W. and Holtz, F., 1990, Formation and composition of H₂O-undersaturated granitic melts *in* High-temperature Metamorphism and Crustal Anatexis. (J.R. Ashworth and M. Brown, eds.) London, Allen and Unwin, p. 87-104.
- Johnson, D. M., Hooper, P.R., and Conrey, R.M., 1999, XRF analysis of rocks and minerals for major and trace elements on a single low dilution Li-tetraborate fused bead: *Advances in X-ray Analysis*, v. 41, p. 843-867.
- Jones, C.H., Unruh, J.R., and Sonder, L.J., 1996, The role of gravitational potential energy in active deformation in the southwestern United States: *Nature*, v. 381, p. 37-41.
- Kelsey, H.M., 1990, Late Quaternary deformation of marine terraces on the Cascadia subduction zone near Cape Blanco, Oregon: *Tectonics*, v. 9, p. 983-1014.
- Kent, A.J.R., Darr, C., Koleszar, A.M., Salisbury, M.J., and Cooper, K.M., 2010, Preferential eruption of andesitic magmas through recharge filtering: *Nature Geoscience*, v. 3, p. 631-636.
- Klemetti, E.W., and Clynne, M.A., 2014, Localized rejuvenation of a crystal mush recorded *in* zircon temporal and compositional variation at the Lassen volcanic center, northern California. *PIOS ONE*, v. 9(12), 22 p.
- Knaack, C., Cornelius, S., and Hooper, P.R., 1994, Trace element analyses of rocks and minerals by ICP-MS. Open File Report. Department of Geology, Washington State University, Pullman, USA.
- Koleszar A.M., Kent A.J.R., Wallace P.J., and Scott W.E., 2012, Controls on long-term low explosivity at andesitic arc volcanoes: Insights from Mount Hood, Oregon. *Journal of Volcanology and Geothermal Research*, v. 219-220, p. 1-14
- Leaver, D.S., Mooney, W.D., Kohler, W.M., 1984, A seismic refraction study of the Oregon Cascades: *Journal of Geophysical Research*, v. 89, p. 3121-3134.
- Lisiecki, L.E., and Raymo, M.E., 2005, A Pliocene-Pleistocene stack of 57 globally distributed $\delta^{18}\text{O}$ records: *Paleoceanography*, v. 20, PA1003, 17 p., doi:10.1029/2004PA001071.
- Luhr, J.F., 1992, Slab-derived fluids and partial melting in subduction zones: Insights from two contrasting Mexican volcanoes (Colima and Ceboruco) *Journal of Volcanology and Geothermal Research*, v. 54, p.1-18.
- Lux, D.R., 1982, K-Ar and ⁴⁰Ar-³⁹Ar ages of mid-Tertiary volcanic rocks from the western Cascade Range, Oregon: *Isochron/West*, v. 37, p. 3-60.

- Magill, J.R., and Cox, A., 1980, Tectonic rotation of the Oregon Western Cascades: Oregon Department of Geology and Mineral Industries Special Paper 10, 67 p.
- Marsh, B.D., 1981, On the crystallinity, probability of occurrence, and rheology of lava and magma: Contributions to Mineralogy and Petrology, v. 78: p. 85-98.
- McCaffrey, R., Qamar, A.I., King, R.W., Wells, R., Khazaradze, G., Williams, C.A., Stevens, C.W., Vollick, J.J., and Zwick, P.C., 2007, Fault locking, block rotation and crustal deformation in the Pacific Northwest: Geophysical Journal International, v. 169, p. 1,315–1,340.
- McCaffrey, R., King, R.W., Payne, S.J., and Lancaster, M., 2013, Active tectonics of northwestern U.S. inferred from GPS-derived surface velocities: Journal of Geophysical Research, Solid Earth, v. 118(2), p. 709-723.
- Memeti, V., Paterson, S., Matzel, J., Mundil, R., Okaya, D., 2010, Magmatic lobes as “snapshots” of magma chamber growth and evolution in large, composite batholiths: An example from the Tuolumne intrusion, Sierra Nevada, California: Geological Society of America Bulletin, v. 122, p. 1912–1931.
- Mitchell, C.E., Vincent, P., Weldon, R.J., and Richards, M.A., 1994, Present-day vertical deformation of the Cascadia margin, Pacific Northwest, United States: Journal of Geophysical Research, v. 99, p. 12257-12277.
- Myers, B., Brantley, S.R., Stauffer, P., and Hendley, J.W., 1997 (revised 1998), What are volcano hazards?: U.S. Geological Survey Fact Sheet 002-97, 2 p.
- Newman, S., Macdougall, J.D., and Finkel, R.C., 1986, Petrogenesis and ^{230}Th – ^{238}U disequilibrium at Mt. Shasta, California, and in the Cascades: Contributions to Mineralogy and Petrology, v. 93, p. 195–206.
- Paterson, S.R., 2009, Magmatic tubes, pipes, troughs, diapirs, and plumes: Late-stage convective instabilities resulting in compositional diversity and permeable networks in crystal-rich magmas of the Tuolumne batholith, Sierra Nevada, California: Geosphere, v. 5, p. 496–527.
- Peck, D.L., Griggs, A.B., Schlicker, H.G., Wells, F.G., Dole, H.M., 1964, Geology of the central and northern parts of the western Cascade Range in Oregon: U.S. Geological Survey Professional Paper 449, 56 p.
- Pezzopane, S.K., and Weldon, R.H., II, 1993, Tectonic role of active faulting in central Oregon: Tectonics, v. 12, p. 1140–1169.
- Porter, S.C., Pierce, K.L., and Hamilton, T.D., 1983, Late Wisconsin mountain glaciation *in* the western United States, in Porter, S.C., ed., The late Pleistocene, v. 1 of Late Quaternary environments of the United States: Minneapolis, University of Minnesota Press, p. 71–111.

- Priest, G.R., 1990, Volcanic and tectonic evolution of the Cascade volcanic arc, central Oregon: *Journal of Geophysical Research*, v. 95, no. B12, p. 19583–19599, doi:10.1029/JB095iB12p19583.
- Priest, G.R., Woller, N.M., Black, G.L., and Evans, S.H., 1983, Overview of the geology of the central Oregon Cascade Range, *in* Priest, G.R., and Vogt, B.F., eds., *Geology and geothermal resources of the central Oregon Cascade Range*: Oregon Department of Geology and Mineral Industries Special Paper 15, p. 3–28.
- Priest, G.R., Woller, N.M., and Ferns, M.L., 1987, Geologic map of the Breitenbush River area, Linn and Marion Counties, Oregon: Oregon Department of Geology and Mineral Industries Geological Map Series GMS-46, scale 1:62,500.
- Putirka K.D., 2005, Igneous thermometers and barometers based on plagioclase + liquid equilibria: Tests of some existing models and new calibrations: *American Mineralogist*, v. 90, p. 336–346
- Putirka K.D., 2008, Thermometers and barometers for volcanic systems: *Reviews in Mineralogy and Geochemistry*, v. 69, p. 61–120
- Rasmussen, J., and Humphreys, E., 1988, Tomographic image of the Juan de Fuca Plate beneath Washington and western Oregon using teleseismic P-wave travel times: *Geophysical Research Letters*, v. 15, p. 1417–1420.
- Reubi, O. and Blundy, J.D.A., 2009, A dearth of intermediate melts at subduction zone volcanoes and the petrogenesis of arc andesites: *Nature*, v. 461, p. 1269–1273.
- Ridolfi F., Renzulli A., and Puerini M., 2010, Stability and chemical equilibrium of amphibole in calc-alkaline magmas: An overview, new thermobarometric formulations and application to subduction-related volcanoes: *Contributions to Mineralogy and Petrology*, v. 160, p. 45-66.
- Rubin, M., and Alexander, C., 1960, U.S. Geological Survey radiocarbon dates V: *American Journal of Science Radiocarbon Supplement*, v. 2, p. 129–185.
- Rudnick, R.L., 1995, Making continental crust: *Nature*, v. 378(6557), p. 571-577.
- Rutherford, M.J. and Devine, J.D., 2008, Magmatic conditions and processes in the storage zone of the 2004–2006 Mount St. Helens dacite: *U.S. Geological Survey Professional Paper 1750*, p. 703-725.
- Rutherford, M.J., and Hill, P.M., 1993, Magma ascent rates from amphibole breakdown: An experimental study applied to the 1980–1986 Mount St. Helens eruptions: *Journal of Geophysical Research, Solid Earth*, v. 98(B11), p. 19667-19685.

- Schmidt, M.E., and Grunder, A.L., 2009, The evolution of North Sister: A volcano shaped by extension and ice in the central Oregon Cascade arc: *Geological Society of America Bulletin*, v. 121, p. 643–662.
- Schmidt, M.E., Grunder, A.L., and Rowe, M.C., 2008, Segmentation of the Cascade Arc as indicated by Sr and Nd isotopic variation among diverse primitive basalts: *Earth and Planetary Science Letters*, v. 266, p. 166–181.
- Scott, W.E., 1977, Quaternary glaciation and volcanism, Metolius River area, Oregon: *Geological Society of America Bulletin*, v. 88, p. 113–124.
- Scott, W.E., 1990, Temporal relations between eruptions of the Mount Bachelor volcanic chain and fluctuations of late Quaternary glaciers, Oregon: *Oregon Geology*, v. 52: p. 114–117.
- Scott, W.E., and Gardner, C.A., 1992, Geologic map of Mount Bachelor volcanic chain and surrounding area, Cascade Range, Oregon: U.S. Geological Survey Miscellaneous Investigations Series Map I-1967, scale 1:50,000.
- Scott, W.E., Gardner, C.A., and Johnston, D.A., 1990, Field trip guide to the central Oregon High Cascades, Part 1: Mount Bachelor-South Sister area: *Oregon Geology*, v. 52, p. 99–140.
- Sherrod, D.R., and Conrey, R.M., 1988, Geologic setting of the Breitenbush-Austin Hot Springs area, Cascade Range, north-central Oregon, *in* Sherrod, D.R., ed., *Geothermal resources of the Breitenbush-Austin Hot Springs area, Clackamas and Marion Counties, Oregon*: Oregon Department of Geology and Mineral Industries Open-File Report O-88-5, p. 1–14.
- Sherrod, D.R., and Smith, J.G., 2000, Geologic map of Upper Eocene to Holocene volcanic and related rocks of the Cascade Range, Oregon: U.S. Geological Survey Geologic Investigations Series Map I-2569, scale 1:500,000, pamphlet 17 p., available at <http://pubs.usgs.gov/imap/i-2569/>.
- Sherrod, D.R., Taylor, E.M., Ferns, M.L., Scott, W.E., Conrey, R.M., and Smith, G.A., 2004, Geologic map of the Bend 30- x 60-minute quadrangle, central Oregon: U.S. Geological Survey Geologic Investigations Series Map I-2683, scale 1:100,000, pamphlet 48 p., available at <http://pubs.usgs.gov/imap/i2683/>.
- Silver, E.A., 1971, Small plate tectonics in the northeastern Pacific Ocean: *Geological Society of America Bulletin*, v. 82, p. 3491–3496.

- Smith, G.A., 1986, Stratigraphy, sedimentology, and petrology of Neogene rocks in the Deschutes basin, central Oregon, a record of continental-margin volcanism and its influence on fluvial sedimentation in an arc-adjacent basin: Corvallis, Oregon State University, Ph.D. thesis, 467 p.
- Smith, G.A., and Taylor, E.M., 1983, The central Oregon High Cascade graben: What? Where? When?: Transactions of Geothermal Resource Council, v. 7, p. 309–314.
- Smith, J.G., 1987, New compilation geological map of the Cascade Range in Washington: Geothermal Resource Council, v. 40, p. 309-314.
- Smith, G.A., Shafiqullah, M., Campbell, N.P., and Deacon, M.W., 1989a,b, Geochronology of the Ellensburg Formation—Constraints on Neogene volcanism and stratigraphic relationships in central Washington: Isochron/West, v. 53, p. 28–32.
- Smith, D.R., and Leeman, W.P., 1993, The origin of Mount St. Helens andesites: Journal of Volcanology and Geothermal Research, v. 55, p. 271-303.
- Streck, M.J., Leeman, W.P., and Chesley, J., 2006, High-magnesian andesite from Mount Shasta: A product of magma mixing and contamination, not a primitive mantle melt: Geology, v. 35, p. 351-354.
- Stanley, W.D., Mooney, W.D., and Fuis, G.S., 1990, Deep crustal structure of the Cascade Range and surrounding regions from seismic refraction and magnetotelluric data: Journal of Geophysical Research, v. 95, p. 19,419-19,438.
- Sutter, J.F., 1978, K-Ar ages of Cenozoic volcanic rocks from the Oregon Cascades west of 121°30': Isochron/West, v. 21, p. 15-21.
- Taylor, E.M., 1981, Central High Cascade roadside geology, Bend, Sisters, McKenzie Pass, and Santiam Pass, Oregon, in Johnston, D.A., and Donnelly-Nolan, J., eds., Guides to some volcanic terranes *in* Washington, Idaho, Oregon, and northern California: U.S. Geological Survey Circular 838, p. 55–58.
- Taylor, E.M., 1990, Volcanic history and tectonic development of the central High Cascade Range, Oregon: Journal of Geophysical Research, v. 95, no. B12, p. 19611–19622.
- Tilling, R.I., ed., 1989, Volcanic hazards: Short course in geology, vol. 1, American Geophysical Union, Washington, D.C., 123 p.

- Trehu, A.M., Asudeh, T.M., Brocher, J.H., Luetgert, W.D., Mooney, J.L., Nabelek, J.L., and Nakamura, Y., 1994, Crustal architecture of the Cascadia forearc: *Science*, v. 266, p. 237–243.
- Trench, D., Meigs, A., and Grunder, A., 2012, Termination of the northwestern Basin and Range province into a clockwise rotating region of transtension and volcanism, southeast Oregon: *Journal of Structural Geology*, v. 39, p. 52–65, doi:10.1016/j.jsg.2012.03.007.
- Vazquez, J.A., and Reid, M.E., 2004, Probing the accumulation history of voluminous Toba magma: *Science*, v. 305, p. 991–994.
- Verplanck, E.P., and Duncan, R.A., 1987, Temporal variations in plate convergence and eruption rates in the Western Cascades, Oregon: *Tectonics*, v. 6, p. 197–209.
- Walder, J.S., Gardner, C.A., Conrey, R.M., Fisher, B.J., and Schilling, S.P., 1999, Volcano hazards in the Mount Jefferson region, Oregon: U.S. Geological Survey Open-File Report 99-24, 13 p.
- Walker, G.W., and Duncan, R.A., 1988, Geologic map of the Salem 1° by 2° quadrangle, Oregon: U.S. Geological Survey Miscellaneous Investigations Map I-1893, scale 1:250,000.
- Walker, B.J., Miller, C.F., Claiborne, L.L., Wooden, J.L., and Miller, J.S., 2007, Geology and geochronology of the Spirit Mountain batholith, southern Nevada: Implications for timescales and physical processes of batholith construction: *Journal of Volcanology and Geothermal Research*, v. 167, p. 239–262.
- Walker, B.J., Klemetti, E.K., Grunder, A.L., Dilles, J.H., Tepley, F.J.T., Giles, D., 2013, Crystal rearing during the assembly, maturation, and waning of an eleven-million-year crustal cycle: thermobarometry of the Aucanquilcha Volcanic Cluster: *Contributions to Mineral Petrology*, v. 165, p. 663–682.
- Watts, K.E., Bindeman, I.N., and Schmitt, A.K., 2012, Crystal scale anatomy of a dying supervolcano: An isotope and geochronology study of individual phenocrysts from voluminous rhyolites of the Yellowstone caldera: *Contributions to Mineralogy and Petrology*, v. 164, p. 45–67.
- Wells, R.E., Engebretson, D.C., Snively, P.D., Jr., and Coe, R.S., 1984, Cenozoic plate motions and the volcano-tectonic evolution of western Oregon and Washington: *Tectonics*, v. 3, p. 275–294.
- Wells, R.E., Weaver, C.S., and Blakely, R.J., 1998, Forearc migration in Cascadia and its neotectonic significance: *Geology*, v. 26, p. 759–762.

- Wells, R., Bukry, D., Friedman, R., Pyle, D., Duncan, R., Haeussler, P., and Wooden, J., 2014, Geologic history of Siletzia, a large igneous province in the Oregon and Washington Coast Range: Correlation to the geomagnetic polarity time scale and implications for a long-lived Yellowstone hotspot: *Geosphere*, v. 10(4), p. 692-719.
- West, D. O., and McCrumb, D. R., 1988, Coastline uplift in Oregon and Washington and the nature of Cascadia subduction-zone tectonics: *Geology*, v. 16(2), p. 169-172.
- White, C.M., 1980, *Geology of the Breitenbush Hot Springs quadrangle, Oregon*: Oregon Department of Geology and Mineral Industries Special Paper 9, 26 p.
- Yogodzinski, G.M., 1985, *The Deschutes Formation-High Cascade transition in the Whitewater River area, Jefferson County, Oregon*: Corvallis, Oregon State University M.S. thesis, 165 p.

